

Secondary mitral valve regurgitation: hemodynamic and numerical insights towards a patient-tailored approach.

To be submitted to obtain the degree of Doctor in Medical Sciences

Philippe B. Bertrand, MD, MSc

Promotor: Prof. Dr. Pieter Vandervoort | UHasselt

Co-promotors: Prof. Dr. ir. Pascal Verdonck | UGent

Prof. Dr. Piet Claus | KULeuven

TABLE OF CONTENTS

TABLE OF CONTENTS	1
LIST OF ABBREVIATIONS	3
GENERAL INTRODUCTION	7
The mitral valve: a gatekeeper in the heart	7
Secondary mitral valve regurgitation	8
Unresolved issues in secondary MR management	9
Research objectives	12
PART I: EXERCISE HEMODYNAMICS IN SECONDARY MITRAL REGURGITATION	13
Chapter 1 The Dynamics of Secondary Mitral Regurgitation: Pathophysiology and Therapeutic Implications	15
Chapter 2 Functional impact of transmitral gradients at rest and during exercise after restrictive annuloplasty for ischemic mitral regurgitation	47
Chapter 3 Mitral Valve Area During Exercise After Restrictive Annuloplasty: Importance of Diastolic Anterior Leaflet Tethering.	61
Chapter 4 Effective Orifice Area During Exercise After Mechanical Valve Replacement.	83
Chapter 5 Mechanism of symptomatic improvement after MitraClip therapy for secondary mitral regurgitation: the role of improved resting and exercise hemodynamics	101
Epilogue 'Surgical treatment of moderate ischemic MR'	121
PART II: PATIENT-SPECIFIC FINITE ELEMENT MODELING OF THE MITRAL VALVE APPARATUS	123

Chapter 6 Clinical validity of numerical mitral valve modeling: towards a patient-tailored approach in secondary mitral regurgitation	125
PART III: IN VITRO SET-UP AND HEMODYNAMIC STUDIES	151
Chapter 7 Influence of left ventricular outflow tract size on discrepancies in aortic stenosis grading: in vitro study and clinical relevance.	153
GENERAL DISCUSSION	179
Exercise dynamics in secondary MR	179
Numerical mitral valve modeling	182
In vitro steady state flow model	183
Future work	184
CURRICULUM VITAE	188
Scientific achievements	189
Awards	192
Grants	193
REFERENCES	194

LIST OF ABBREVIATIONS

AL	anterior (mitral) leaflet
AR	aortic regurgitation
AS	aortic stenosis
AVA	aortic valve area
CABG	coronary artery bypass grafting
Cc	coefficient of contraction
Cp	pressure recovery coefficient
CRT	Cardiac Resynchronization Therapy
EDV	end-diastolic volume
ESV	end-systolic volume
EOA	effective orifice area
EOAi	indexed effective orifice area
EROA	effective regurgitant orifice area
GOA	geometric orifice area
HF	heart failure
LV	left ventricle
LVOT	left ventricular outflow tract
MR	mitral regurgitation
MVR	mitral valve replacement
NYHA	New York Heart Association
RMA	restrictive mitral valve annuloplasty
sPAP	systolic pulmonary artery pressure

TAVR	transcatheter aortic valve replacement
TMG	transmitral pressure gradient
TTE	transthoracic echocardiography
VO ₂ max	maximal oxygen uptake

Gatekeeper

/'get,ki:pə/

- 1. a person who has charge of a gate and controls who may pass through it*
- 2. any of several Eurasian butterflies of the genus *Pyronia*, esp *P. tithonus*, having brown-bordered orange wings with a black-and-white eyespot on each forewing: family *Satyridae**
- 3. a manager in a large organization who controls the flow of information, esp to parent and subsidiary companies*

From: Collins English Dictionary - Complete & Unabridged 2012 Digital Edition

GENERAL INTRODUCTION

'The problem is to know what the problem is.'

The mitral valve: a gatekeeper in the heart

The mitral valve is a complex yet finely tuned apparatus that controls the passage of blood between the heart's left atrium and left ventricle. Much more than just a pair of leaflets, the mitral valve is composed of multiple components that are ingeniously designed to work together in 'sealing' the passage from the left ventricle to the left atrium during systolic contraction. The most essential components are the mitral annulus, the anterior and posterior mitral valve leaflets, the chordae tendineae, the anterolateral and posteromedial papillary muscles and the adjacent left ventricular wall¹⁻⁵; together they constitute the "mitral valve apparatus" (Figure 1-A). While preventing backflow towards the left atrium and pulmonary system during systole, an unrestricted inflow of blood from left atrium to ventricle must be provided during diastole. To accomplish such important tasks, several mechanisms interplay during the cardiac cycle: (1) a systolic contraction and diastolic dilation of the mitral annulus, (2) left ventricular systolic wall motion causing inward displacement of the papillary muscles facilitating leaflet coaptation while minimizing leaflet stress, and (3) a measured systolic contraction of the papillary muscles to keep tension on the chordae and avoid leaflet prolapse. A delicate balance is maintained between the tethering forces that prevent prolapse (transmitted via the chordae tendineae), and valve closing forces (left ventricular pressure, i.e. a combination of contractility, synchronicity, and mitral annular systolic contraction). Disruption in any of these mechanisms, either from organic or functional etiology, may unsettle the force balance and result in mitral regurgitation (MR)⁶⁻⁹.

Secondary mitral valve regurgitation

Secondary MR, also called 'functional' MR, results from a *functional* imbalance between increased tethering forces and decreased closing forces, in the presence of a structurally normal valve. The imbalance typically occurs in patients with prior myocardial infarction (ischemic cardiomyopathy), or with dilated heart disease (non-ischemic cardiomyopathy), causing the papillary muscles to be displaced and/or to move dyssynchronous while also the closing force is generally impaired. As a result, increased traction on the mitral valve leaflets occurs during systole (i.e. tethering), resulting in incomplete leaflet coaptation and MR (Figure 1-B).

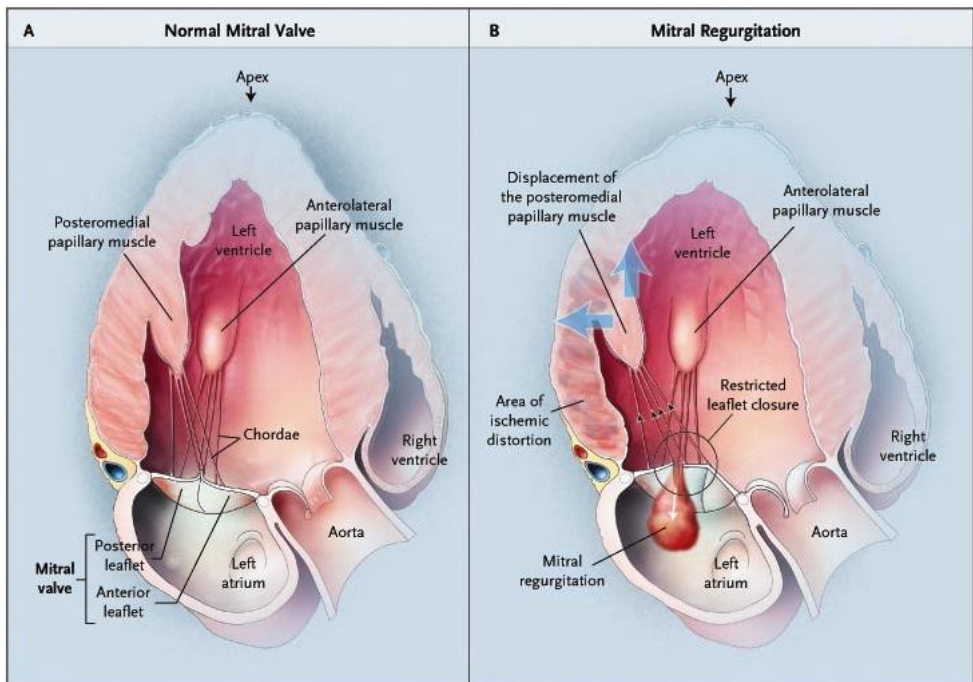


Figure 1 – The mitral valve as gatekeeper between left ventricle and atrium. Panel A shows a normal mitral valve function, with adequate leaflet coaptation during systolic contraction. Panel B displays functional mitral regurgitation, in which the leaflets cannot close effectively due to dilation of the left ventricle with outward displacement of the papillary muscles. Adopted with permission from Levine R.A. et al¹⁰ (N Engl J Med, 2004;351:1681-1684)

The prevalence of secondary MR is high, occurring in 20 to 25% of patients after myocardial infarction¹¹⁻¹⁴, and in roughly 50% of patients with congestive heart failure^{15, 16}. Furthermore, secondary MR is associated with poor clinical outcome^{17, 18}, and impaired exercise capacity¹⁹.

In contrast to patients with primary (organic) MR, that are known to benefit from timely surgical valve repair or replacement²⁰⁻²², the management of patients with secondary MR remains within the scope of controversy and paradox²³⁻²⁵. Surgical valve repair by means of an undersized prosthetic ring (restrictive mitral annuloplasty) has traditionally been preferred based on good short- and mid-term data from observational studies demonstrating significant reverse left ventricular remodeling and improved systolic function^{26, 27}. However, to date, no survival benefit could be demonstrated of performing mitral valve surgery in secondary MR patients^{28, 29}. As a result, the level of evidence in guideline recommendations remains low^{21, 22} and the optimal approach still is a matter of debate.

Unresolved issues in secondary MR management

Two unresolved issues are of particular importance when exploring the lack of clinical benefit of the current mitral valve interventions for secondary MR: (1) the inherent dynamic behavior of secondary MR that is generally underappreciated, and (2) the high MR recurrence rate after mitral valve interventions for severe secondary MR.

Issue #1 - The exercise dynamics of secondary MR

Secondary MR is characteristically dynamic in nature and highly sensitive to changes in ventricular geometry and loading conditions. Very often only mild MR at rest can swiftly increase to moderate or severe MR during dynamic exercise. Exercise-induced increase in secondary MR is highly prevalent, and is associated with impaired exercise capacity and

increased mortality. However, current treatment approaches for secondary MR are mainly focused on resting conditions. It remains unclear whether the dynamic lesion is reduced as well after a specific therapy, or whether severe exercise-induced MR persists, explaining the lack of clinical benefit in such patients. Furthermore, the impact of mitral valve interventions (valve repair, valve replacement, percutaneous approaches) on the respective exercise hemodynamics (even in case of adequate MR reduction) remain ill-understood. Recently, it was suggested that the undersized ring annuloplasty causes some degree of functional mitral stenosis during exercise that is associated with worse functional capacity even after adequate correction of secondary MR³⁰⁻³³. The underlying mechanisms however, and whether similar hemodynamic issues occur with other treatment approaches for secondary MR, remains to be explored.

Issue #2 – MR recurrence following mitral valve procedures

After a restrictive mitral annuloplasty, recurrence of secondary MR in up to 30% after 1 year is well recognized^{34, 35}. The pathophysiological mechanisms of MR recurrence relate to ongoing adverse left ventricular remodeling and subvalvular tethering, usually in patients with already severely dilated left ventricle and pronounced leaflet tethering at the time of surgery³⁶⁻³⁸. It has become increasingly clear that in this subset of (severely tethered) patients annuloplasty alone is unable to overcome the tethering imposed by the subvalvular apparatus and that add-on therapies that specifically target the subvalvular apparatus are critically needed. A number of surgical and percutaneous techniques targeting the chordae and/or papillary muscles are therefore emerging at fast pace. Examples of these techniques comprise papillary muscle relocation^{39, 40}, chordal cutting⁴¹, application of a papillary muscle sling⁴², application of external constraint device^{43, 44}, showing good short-term results in animal studies and promising results in a limited number of small patient series. However, none of these subvalvular approaches has gained clinical acceptance yet^{45, 46}; the reason

being that the underlying mechanisms causing the leaflet tethering are highly individual (ranging from global LV dilatation to very localized regional wall motion abnormalities; from synchronous to dyssynchronous papillary muscle movement, etc.), and a “one-size-fits-all” approach is destined to fail. In other words: *the problem is to know what the underlying problem is... in the specific patient.*

A patient-specific three-dimensional analysis of the individual valve dynamics and leaflet geometry could provide such delicate insights, and might even allow pre-intervention simulation of different approaches (e.g. papillary muscle relocation: in what direction? to what extent?) while evaluating the respective impact on the individualized mitral valve dynamics, leaflet tenting and coaptation. This kind of innovative approach could enable a truly tailored therapy adapted to the patient’s needs. With the current high quality three-dimensional (3D) imaging modalities (e.g. 3D echocardiography), the exponential increase in computational power these last years and the availability of dedicated software packages for numerical modelling (finite element modelling) of complex structural problems, such innovative three-dimensional patient-specific mitral valve analysis might in fact be possible.

Research objectives

This PhD thesis focuses on three main objectives to further explore the final frontiers in the approach of the patient with secondary MR, aiming at a more thorough understanding of the dynamics of the disease and providing a framework towards a patient-tailored evaluation and approach for this important pathology.

OBJECTIVE 1 – To explore the exercise dynamics of secondary MR, and the impact of current treatment approaches on the exercise-induced MR component and on exercise hemodynamics in particular (Part I).

OBJECTIVE 2 – To develop a patient-specific numerical model of the mitral valve apparatus based on three-dimensional echocardiography and validate its clinical potential in normal mitral valves as well as in secondary MR valves (Part II).

OBJECTIVE 3 – To design and build a computer-controlled steady state in vitro flow model for accurate fluid dynamic simulations in order to explore relationships between geometry and flow dynamics (Part III).

PART I:
EXERCISE HEMODYNAMICS IN
SECONDARY MITRAL REGURGITATION

Chapter 1

The Dynamics of Secondary Mitral Regurgitation: Pathophysiology and Therapeutic Implications

Bertrand PB, Schwammenthal E, Levine RA, Vandervoort PM

Status of the manuscript:

Under review

J Am Coll Cardiol (IF 16.5)

Abstract

Secondary mitral valve regurgitation (MR) remains a challenging problem in the diagnostic work-up and treatment of heart failure patients. Although secondary MR is characteristically dynamic in nature and sensitive to changes in ventricular geometry and loading, current therapy is mainly focused on resting conditions. Exercise-induced increase in secondary MR, however, is associated with impaired exercise capacity and increased mortality. In an era where a multitude of percutaneous solutions are emerging for the treatment of HF patients it becomes increasingly pressing to address the dynamic component of secondary MR during exercise as well. A critical reappraisal of the underlying disease mechanisms, and in particular of the dynamic component during exercise is of timely importance. This review summarizes the pathophysiologic mechanisms involved in the dynamic augmentation of secondary MR during exercise, its functional and prognostic impact, and the way current treatment options affect the dynamic lesion and exercise hemodynamics in general.

Introduction

Secondary mitral valve regurgitation (MR) is a challenging problem in the diagnostic work-up and treatment of heart failure (HF). It occurs in 11 to 59% of patients after a myocardial infarction^{11, 12, 14} and is present in more than half of patients with dilated cardiomyopathy^{15, 16, 23}. Despite this high prevalence, the optimal approach to secondary MR remains a matter of debate, and the level of evidence for guideline recommendations is disappointingly low^{22, 47}. A particularly controversial question remains whether moderate and mild-moderate MR should be regarded as treatment targets: It is well known that outcomes and exercise capacity are impaired in secondary MR, even when only mild^{18, 48-50}. This association may simply reflect the fact the occurrence of MR, even if only mild, is a marker of more advanced disease. However, it could also be rooted in the characteristically dynamic behavior of secondary MR, often becoming more severe during exercise or with changing loading conditions⁵¹. To date, our knowledge of exercise dynamics in secondary MR is insufficient: Does relief of the dynamic lesion result in better outcome? Is the prognosis of severe exercise-induced MR (mild resting MR) comparable to severe resting MR? Should such patients be referred for surgical treatment? Do we even know the potential impact of the available therapies for secondary MR on the respective exercise hemodynamics? In an era where a multitude of percutaneous solutions are emerging for the treatment of HF patients it becomes increasingly pressing to understand who may or may not benefit from a specific therapy. A critical reappraisal of our knowledge of the underlying disease mechanisms, and in particular of the dynamic component of secondary MR during exercise, is therefore of timely importance.

This review summarizes pathophysiological mechanisms involved in the dynamic augmentation of secondary MR, its functional and prognostic impact, and the manner in

which current treatment options affect dynamic MR and exercise hemodynamics in general. Finally, potential targets for future research are highlighted.

Pathophysiology

The mitral valvular apparatus

More than just a pair of leaflets, the mitral valve is an intricate apparatus comprised of multiple components – the mitral annulus, anterior and posterior leaflets, chordae tendineae, anterolateral and posteromedial papillary muscles and adjacent left ventricular wall – finely tuned to work together in ‘sealing off’ the passage of blood from the left ventricle to the left atrium in systole while enabling unrestricted inflow during diastole⁶. Several mechanisms interact during systole: (1) annular contraction and (2) left ventricular wall motion causing inward displacement of the papillary muscles, to facilitate leaflet coaptation while minimizing leaflet stress, and (3) contraction of the papillary muscles adapted to avoid leaflet prolapse. A delicate balance is maintained between tethering forces (transmitted via the left ventricular wall, papillary muscles and chordae tendineae system influenced by annular/leaflet dimensions) and valve closing forces (left ventricular contractility and synchrony, mitral annular systolic contraction). Disruption in any of these mechanisms may unsettle the force balance and result in MR⁸.

A mechanistic insight into secondary MR

Secondary MR results from a *functional* imbalance between increased tethering forces (annular and/or left ventricular dilation, segmental or global left ventricular dysfunction with papillary muscle displacement/dysfunction) and decreased closing forces (reduced left ventricular contractility or synchrony) acting on the mitral valve. As a result, increased traction of the mitral valve leaflets – tethering – occurs during systole, resulting in incomplete coaptation and MR (Figure 1.1). This balance of forces creates a lesion that is evidently dynamic even within each cardiac cycle: Schwammenthal et al⁵² demonstrated a

typical decrease in MR during ventricular contraction with a minimum in mid-systole (at the time of peak orifice velocity and peak systolic pressure) and an increase again during ventricular relaxation, suggesting a decisive impact of the instantaneous left ventricular-to-atrial pressure difference on leaflet coaptation. While a mid-systolic decrease in annular area could also contribute to this phenomenon it was subsequently shown that variation in annular area in patients with left ventricular dysfunction is minor and insufficient to explain the degree of observed MR orifice area variation⁵³. In addition, it was shown that an acute rise in closing force due to acute activation of cardiac resynchronization therapy (CRT) in patients with dilated hearts and secondary MR also reduces the degree of MR significantly⁵⁴. However, an impaired closing force is not the primary cause of secondary MR in HF. Numerous studies, both *in vitro*⁵⁵ and *in vivo*^{56, 57}, have demonstrated that increased tethering is a prerequisite for occurrence of secondary MR, and geometric disturbances of the left ventricle are key in the dynamic imbalance between closing and tethering forces⁵⁸. In an animal model of left ventricular systolic dysfunction without ventricular dilation, only trace MR was observed and tenting depth was the only predictor of MR, in contrast to ejection fraction or dP/dt ⁵⁶. Hence tethering (geometry) sets the stage for secondary MR, while closing force merely modulates its severity. More recent studies have confirmed the position and dynamics of the papillary muscles, not left ventricular dimensions *per se*, are major determinants of secondary MR⁵⁹⁻⁶². In a normal-sized left ventricle with regional wall motion abnormalities causing one or both PMs to be displaced or move asymmetrically^{60, 61} or dyssynchronously^{62, 63}, tethering forces increase, disrupting the force balance and causing secondary MR. A dilated mitral annulus further augments these effects and increases MR⁶⁰, but isolated annular dilation without subvalvular tethering does usually not cause more than moderate MR⁶⁴. Finally, inter-individual differences in mitral valve geometry, such as the inborn relative position of basal chordae tendineae insertion sites, modulate the individual susceptibility to development of (severe) secondary MR⁶⁵.

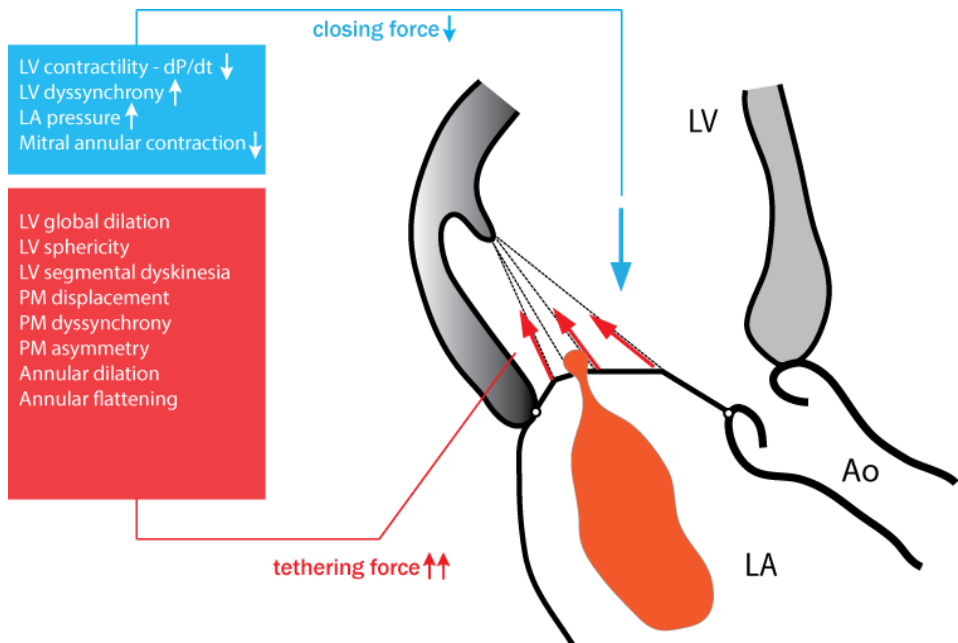


Figure 1.1 - Secondary mitral regurgitation results from functional disruption in the force balance between tethering and closing forces, inhibiting normal mitral leaflet coaptation.

The normal cardiovascular response to exercise

exercise, the cardiovascular system adapts to meet increased oxygen demands of peripheral muscles⁶⁶. Stimulation of the sympathetic system and withdrawal of vagal tone increase heart rate and myocardial contractility and decrease systemic vascular resistance, thus increasing cardiac output⁶⁷. The dynamic response of the left ventricle depends on the type of exercise performed, which can be either dynamic (isotonic), static (isometric), or a combination of both. In dynamic exercises (e.g. running, cycling, swimming), multiple muscle groups contract in order to achieve joint movement. Such activity is associated with profound vasodilation in the muscular vasculature causing a significant reduction in systemic vascular resistance to almost half its value at rest⁶⁶, and a substantial increase in venous return due to the skeletal muscle pump. The decreased afterload, increased contractility, and increased venous return significantly increase stroke volume. Increased cardiac output is therefore mediated by increased stroke volume, with heart rate becoming the dominant determinant as stroke volume reaches its plateau⁶⁷. In static exercise on the other hand (e.g. weightlifting, handgrip), systemic vascular resistance is not decreased and might even be increased. In the absence of afterload reduction, stroke volume remains largely unchanged and the rise in cardiac output is determined mainly by the increase in heart rate. Hence, static exercise imposes a pressure load on the left ventricle, whereas dynamic exercise constitutes a volume load⁶⁷. These differential loading conditions translate into different left ventricular geometric changes during exercise, as has been studied with radionuclide angiography⁶⁸⁻⁷⁰, echocardiography^{71, 72} and cardiac magnetic resonance imaging⁷³. In healthy subjects, dynamic exercise is associated with no increase (or a transient increase at mild-to-moderate exercise⁷¹) of the end-diastolic volume (EDV), while a concomitant decrease in end-systolic volume (ESV) is observed. This substantially increases stroke volume and ejection fraction (Figure 1.2). In contrast, during static exercise, no significant changes in either ESV or EDV occur^{74, 75}.

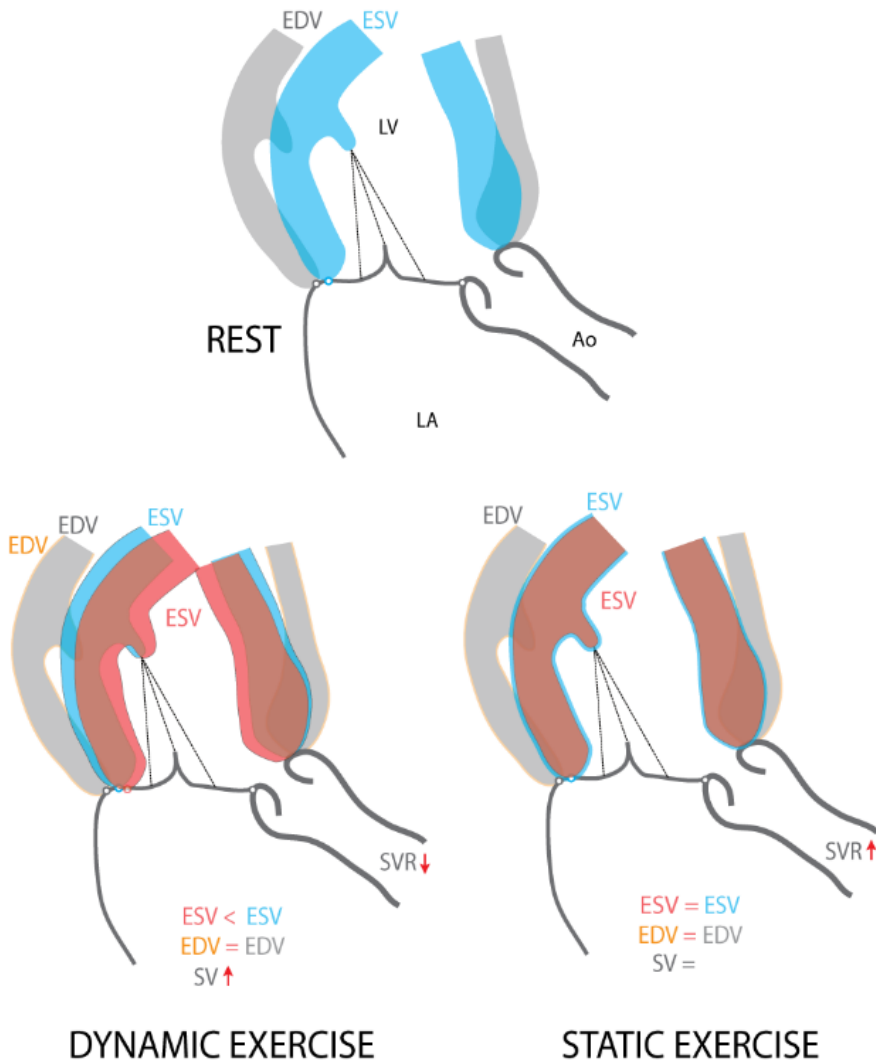


Figure 1.2 - The normal left ventricular response to exercise in healthy patients. EDV, end-diastolic volume; ESV, end-systolic volume; LV, left ventricle; LA, left atrium; SV, stroke volume; SVR, systemic vascular resistance; Ao, aorta.

Secondary MR during exercise

Left ventricular geometry

In patients with ischemic or idiopathic cardiomyopathy the left ventricular volumetric response to dynamic or static exercise may differ significantly from that observed in normal subjects^{70, 76, 77}. In general, both volume loading in dynamic exercise and pressure loading in static exercise result in exercise-induced ventricular dilation (EDV and ESV both tend to increase), while ejection fraction typically remains unchanged. The increase in left ventricular EDV during exercise is reported to be greater in ischemic (than in idiopathic dilated) cardiomyopathy⁷⁶, which may be directly related to the extent of myocardial scar⁷⁸, a finding of particular importance for the exercise dynamics of secondary MR. In addition, exercise may result in dyssynchronous contraction of the left ventricle in HF with (rate-dependent) conduction delay⁷⁹. While the acute rise in blood pressure during static exercise increases the mitral closing force, this is completely outweighed by increased mitral tethering resulting from the impact of the rise in afterload on left ventricular geometry. Consequently, significant increases in secondary MR have been observed during static exercise⁷⁷. Significant increases in systemic venous resistance are generally not observed during dynamic exercise in patients with cardiomyopathy. However, failure of adequate arterial dilatation during exercise occurs^{80, 81} and, in the presence of an increased volume load, contributes to exercise-induced ventricular dilatation. Dynamic exercise studies therefore demonstrate increases in secondary MR in >75% of HF patients, both with ischemic⁸²⁻⁸⁴ and non-ischemic etiology⁸⁵⁻⁸⁷. Table 1 summarizes the current literature on determinants of increasing secondary MR during exercise in HF. Interestingly, neither left ventricular volume nor ejection fraction at rest or during exercise are reliable predictors of exercise-induced MR deterioration. In fact, with respect to exercise-induced left ventricular dilatation, changes in shape (local remodeling) may count more than changes in the actual

volume⁸². An increase in left ventricular sphericity, which correlates with greater papillary muscle distance, may have a pronounced effect on mitral geometry even without a significant change in volume. On the other hand, an increase in left ventricular volume will have no effect on mitral valve geometry if brought about by apical dilatation of the cavity (which does not involve the mitral valve apparatus). It is therefore not surprising that, when looking at resting predictors of worsening MR during exercise, left ventricular sphericity and papillary muscle dyssynchrony are more useful, as is mitral valve tenting which reveals an already strained balance between closing and tethering forces. In addition, progressive annular dilation during exercise may be implicated as a contributor to exercise-induced MR in a majority of cases and is most predictive in non-ischemic cardiomyopathy⁸⁸.

Left ventricular scar

Especially in ischemic cardiomyopathy, the extent and localization of scar plays an important mechanistic role in dynamic MR deterioration (Figure 1.3)⁷⁸. Following an anterior wall myocardial infarction extending to the apical segments of the inferior wall, patients show more apically tethered mitral leaflets, with coaptation depth being a determinant of exercise-induced MR deterioration^{82, 83}. In patients with inferior wall infarction on the other hand, regional wall motion abnormalities during exercise tether the mitral valve more posteriorly, in particular restricting the posterior leaflet, and increase the annular dimension (in particular around P2-P3), thereby aggravating MR in a somewhat different way. Interestingly, significant contractile reserve of the inferoposterior wall in the latter group is related to an exercise-induced *decrease* in secondary MR, as tethering forces are reduced and the mitral annulus less distorted⁸². Large infarctions (which are frequently more anterior) or multiple infarctions leading to severe remodeling lead to more spherical ventricles with greater papillary muscle separation exerting traction on the mitral valve from opposite ends.

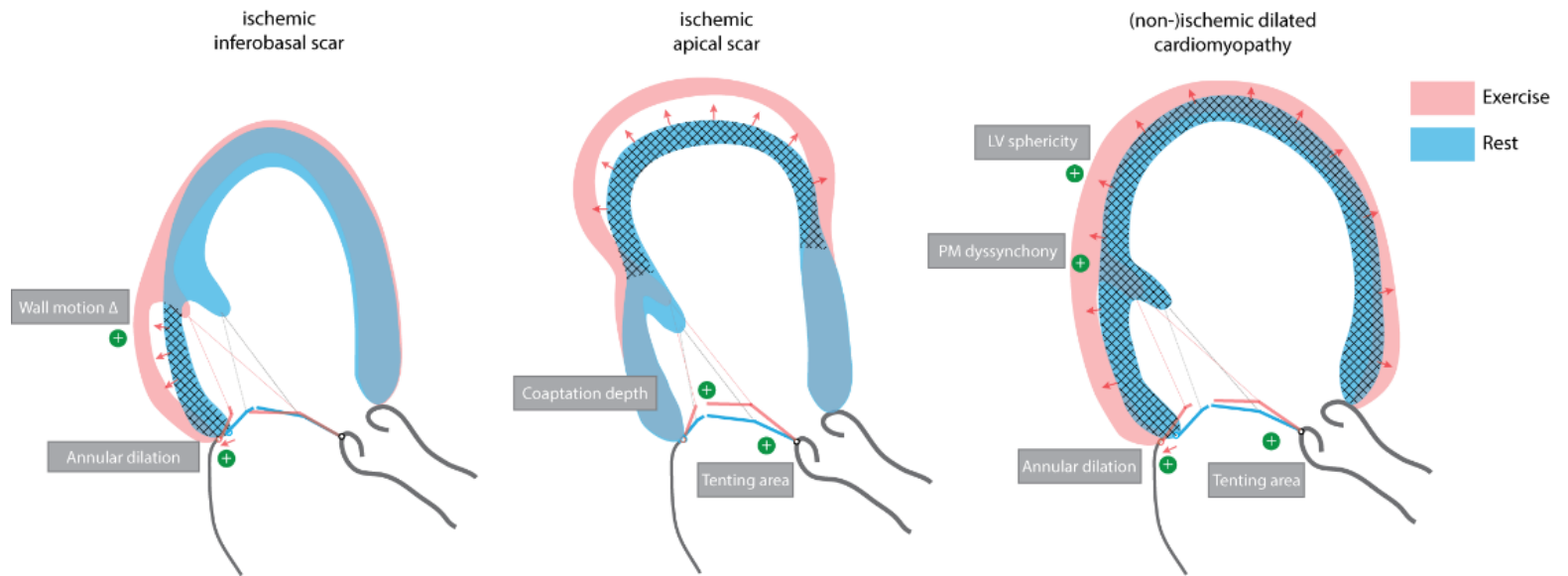


Figure 1.3 - The differential left ventricular response to exercise in cardiomyopathy based on the underlying etiology and location of the scar. Dominant predictors of worsening secondary MR during exercise are highlighted for each situation.

Closing versus tethering forces during exercise

Intriguingly, predictors of increasing MR during exercise (Table 1) are all related to left ventricular geometry^{82,83}, indicating that in the failing ventricle increases in tethering during exercise by far outweigh increases in closing force. This is supported by the observation that although onset of CRT causes an early decrease in secondary MR at rest (due to an immediate increase in closing forces⁵⁴), this effect is not maintained during exercise. Indeed, early after CRT, secondary MR often deteriorates to pre-CRT severity during dynamic exercise, despite an acute reduction in resting MR⁸⁹. Only after reverse left ventricular remodeling has taken place (resulting in reduced tethering forces), significant reductions in exercise-induced MR are observed (Figure 1.4)(52).

Of note, induction of myocardial ischemia during exercise in coronary artery disease associated with reversible wall motion abnormalities and a decrease in ejection fraction can also result in a subsequent increase in MR^{90,91}. This type of MR, however, is not discussed here, since the underlying mechanisms (inducible reversible ischemia) and treatment approaches (revascularization) are different from the topic of this review. The term 'ischemic MR' in this review refers exclusively to post myocardial infarction MR in patients with stable coronary heart disease. In these patients, it is the scar tissue and ventricular remodeling that truly determine the dynamic deterioration of MR during exercise⁹².

Table 1.1 – Geometric determinants of increasing secondary mitral valve regurgitation during exercise.

Author, Year, Ref.	n	IMR	Regression	LVEDD		LVEF		LV sphericity		LV dyssynchrony		Annular dilatation		Tenting area		Coaptation depth		WMSI	
				rest	Δ	rest	Δ	rest	Δ	rest	Δ	rest	Δ	rest	Δ	rest	Δ	rest	Δ
Keren et al., 1989 ⁷⁷	17	50%	UV		–														
Lapu-Bula et al., 2002 ¹⁹	25	50%	UV		–				+				–				+		
Lancellotti et al., 2003 ⁸²	70	100%	UV MV		–		–						+		+		+		+
Giga et al., 2005 ⁸³	40	100%	UV MV	–	–	–	–	–	+			–	+	–	+	–	+	–	+
Lancellotti et al., 2005 ⁸⁴	35	100%	UV MV		–		–			+	+				+				
Ennezat et al., 2006 ⁸⁸	70	50%	UV MV	+		–				+			+						
Takano et al., 2006 ⁸⁶	17	5/17	UV			–													
D'Andrea et al., 2007 ⁸⁵	60	0%	UV MV		–		–				+				+				
Yamano et al., 2008 ⁹³	32	0%	UV	–	–	–	–	+	–			–	–	+	+	–	+		
Izumo et al., 2009 ⁸⁷	50	16/50	UV MV	–	–	–	–	+	+	–	+	–	+	–	+	–	+		

Only studies without inducible ischemia were included. UV, univariate; MV, multivariate; Δ = changes during exercise; LV, left ventricle; LVEDD, left ventricular end diastolic dimension, LVEF, left ventricular ejection fraction; WMSI, wall motion score index; IMR, ischemic mitral regurgitation. † inferior myocardial infarction only; *anterior myocardial infarction only.

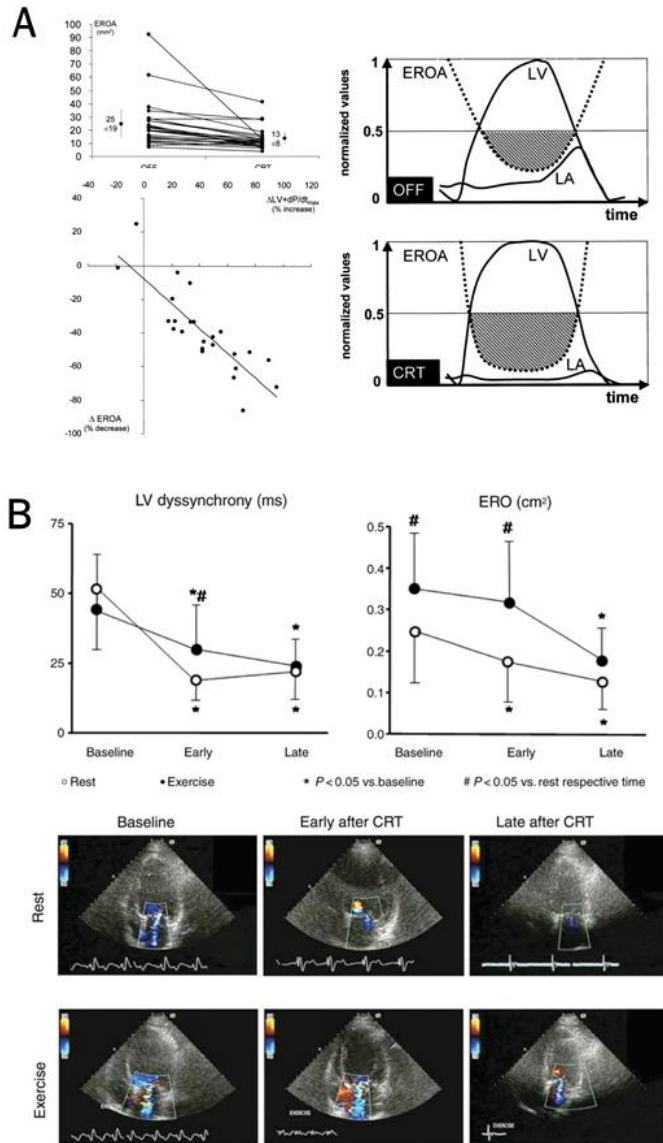


Figure 1.4 - Impact of cardiac resynchronization therapy (CRT) on secondary mitral valve regurgitation (MR) at rest and during exercise. (A) The acute effect of CRT on secondary MR at rest: the immediate decreased effective regurgitant orifice (ERO) relates to the increase in closing force (dP/dt) and longer relative duration of maximal closing force. Adapted from Breithart et al⁵⁴, with permission. (B) During exercise immediately after CRT implantation, no decrease in ERO is observed. Only after 3 months when reverse remodeling has occurred, a significant reduction in exercise-induced MR is observed. Adapted with permission from Madaric et al⁸⁹.

Prognostic impact of the dynamic lesion of mitral valve regurgitation

Exercise-induced increase in secondary MR is associated with poor exercise capacity^{19, 93-95} and outcomes^{48, 96, 97}. In a mixed cohort of ischemic and non-ischemic cardiomyopathy, Lapu-Bula et al¹⁹ were the first to demonstrate a significant negative impact of exercise-induced MR deterioration on exercise capacity, even though MR was only mild-to-moderate at rest. Piérard and Lancellotti⁹⁸ further showed that exercise-induced MR deterioration, by augmenting backward flow, can cause exercise pulmonary hypertension and may thus contribute to the development of acute pulmonary edema, but also impairs forward stroke volume during exercise. Importantly, a significant increase in effective regurgitant orifice area (EROA) during exercise (defined as an increase $>13\text{mm}^2$) is observed in 30% of HF patients and associated with increased mortality as well as readmissions^{48, 96}. Furthermore, all-cause mortality in HF patients with secondary MR follows a graded relationship with respect to MR severity, with EROA $>20\text{mm}^2$ already implying poor outcome^{17, 18}. This contrasts to the 40mm^2 cut-off that is traditionally used in primary MR (Figure 1.5). Although occurrence of secondary MR is also a marker of underlying heart disease, the lower EROA threshold in secondary MR could also be rooted in the typically dynamic nature of secondary MR, which is frequently underestimated at rest. Therapies for secondary MR aiming at improved exercise capacity and outcomes should therefore not only focus on resting status, but also reduce the dynamic component of MR.

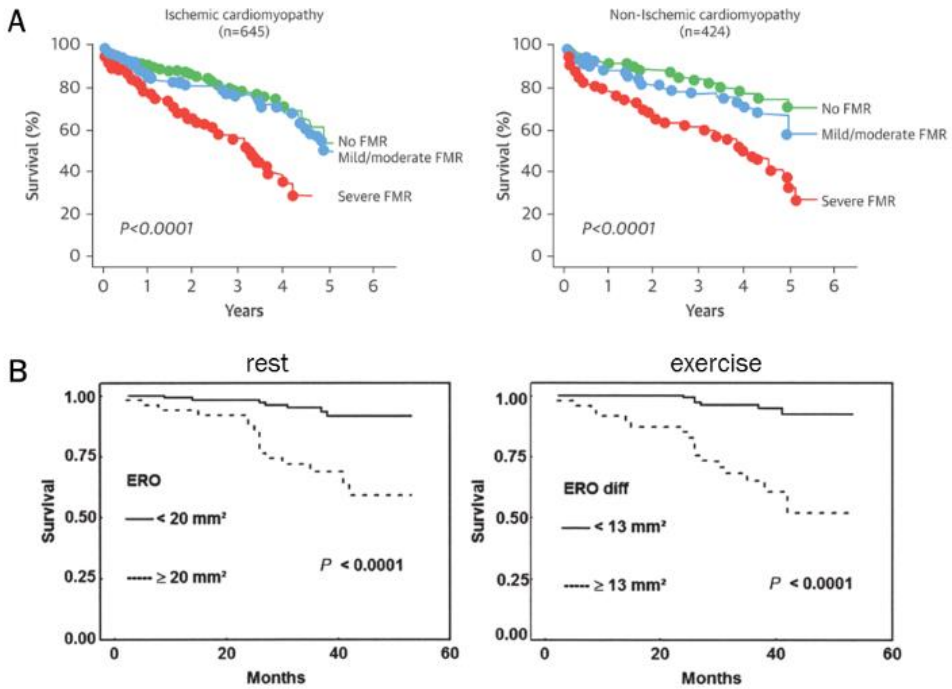
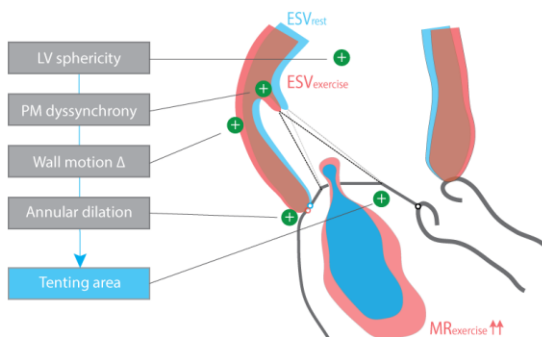


Figure 1.5 - Prognostic impact of secondary mitral valve regurgitation (MR) at rest and during exercise (A) Mortality in heart failure patients with secondary MR at rest follows a graded relationship with respect to MR severity. Severe MR ($\text{ERO} > 20 \text{ mm}^2$) already implies worse outcome for both ischemic and non-ischemic cardiomyopathy. Adapted from Rossi et al¹⁷, with permission. (B) Mortality in patients with deteriorating secondary MR during exercise ($\text{ERO increase} > 13 \text{ mm}^2$), is increased and similar to patients with severe secondary MR at rest. Adapted from Lancellotti et al⁴⁸, with permission.

Impact of treatment approaches for secondary MR on exercise dynamics

A complete and detailed overview of the evidence for the various therapeutic approaches for secondary MR, comprising guideline-directed HF medication, CRT, revascularization when appropriate, as well as mitral valve surgery and transcatheter interventions²⁴, is beyond the scope of this review. Instead, a critical evaluation of the (potential) impact of these therapies on the dynamic lesion in secondary MR is made based on the underlying determinants causing exercise-induced MR aggravation (**Central Illustration**).



	LV sphericity	PM dyssynchrony	Wall motion Δ	Annular dilation	Tenting area
Medical therapy	+	+/-		+	+
Cardiac Resynchronization Therapy	+	+	+	+	+
Revascularization	+		+	+	+
Restrictive annuloplasty	+			+	+
Ventricular approach	+			+	+
Subvalvular approach	?			?	+
MitraClip	+			+	+

CENTRAL ILLUSTRATION - Determinants and mechanisms of exercise-induced secondary mitral regurgitation, and the impact of current treatment approaches on the respective determinants.

Medical therapy

Medical therapy remains a cornerstone in the treatment of chronic HF and secondary MR. Adequate decongestion should be pursued at all times and patients should take the maximally tolerated guideline-recommended⁹⁹ target doses of neurohumoral blocker therapies. Adherence to neurohumoral blocker therapy reverses adverse left ventricular remodeling¹⁰⁰⁻¹⁰³, although a reduction in secondary MR has only been reported in non-randomized small-sample series¹⁰⁴⁻¹⁰⁶.

In order to understand the potential effect of a drug on the severity of secondary MR it is helpful to view it in terms of the underlying lesion mechanism: the tug of war between mitral closing and tethering forces (Figure 1.1). Table 1.2 summarizes the effects of the most frequently used HF medications²³. Preload-reducing medications, such as diuretics and nitrates, may significantly decrease the tethering forces, thus reducing EROA. These medications may also enhance mitral closing forces, as they tend to decrease left atrial pressure (reduce the size of V-waves) more than systolic left ventricular pressure, in particular in the presence of high left ventricular end-diastolic pressures. Since the failing heart operates on the flat portion of the cardiac function curve a significant reduction in left ventricular end-diastolic pressure will not affect cardiac output and systolic blood pressure significantly. Afterload-reducing drugs can also relieve tethering significantly in left ventricular dysfunction by decreasing left ventricular size and improving its shape.

Whether such potential effects of medical therapy translate in attenuated exercise dynamics in secondary MR remain largely unknown. Most of the literature on this topic predates the era of neurohumoral blocker treatment in HF. Nevertheless, some interesting observations deserve attention: (1) nitrates (nitroglycerin, isosorbide dinitrate), mainly by reducing cardiac preload, offer a consistent and sustained reduction in left ventricular EDV as well as ESV at rest and during exercise in healthy subjects and patients with coronary artery

disease¹⁰⁷. Because they unload the heart, significant benefits on left ventricular performance (i.e., increased stroke volume and decreased pulmonary arterial wedge pressure) are observed during exercise in HF patients treated with digoxin and diuretics¹⁰⁸. In this context, a significant reduction in dynamic secondary MR was also observed¹⁰⁹; (2) combined pre- and afterload reduction with nitroprusside and diuretics significantly reduces left ventricular EDV during upright bicycle exercise, thereby significantly decreasing secondary MR and increasing forward stroke volume in advanced HF¹¹⁰; (3) arteriolar vasodilation (hydralazine) and venodilation (nitroglycerin) offer a synergistic reduction in pulmonary arterial wedge pressure and V-wave amplitude during static exercise in patients with chronic MR¹¹¹; (4) intensive medical unloading of the heart in acute decompensation results in a significant decrease in intraventricular dyssynchrony, even in the absence of CRT¹¹².

Table 1.2 – Potential effects of common HF drugs on the balance of forces acting on the mitral valve lesion in secondary MR

Drug	Preload	Afterload	Closing Force (LV-LA Pressure)	Tethering Force (PM-Displacement)	Net Effect (ERO)
Diuretic	↓ ↓	↔	↑	↓	↓ ↓
Nitrate	↓ ↓	↓	↑	↓	↓ ↓
ACE-I/ARB	↓	↓ ↓	↑ ↔	↓	↓
Hydralazine	↔	↓ ↓ ↓	↑ ↔	↓	↓ ↓
Chonic BB	↓	↓	↓ ↔	↓	↓

ACE-I= ACE-inhibitor, ARB = Angiotensin Receptor Blocker, BB = Beta blocker. Although arterial vasodilators reduce systolic ventricular pressure they may nevertheless increase closing force, if the reduction in MR they induce through a relief in tethering decreases left atrial pressure sufficiently. Please note that the assessment of the individual effects of hydralazine is theoretic insofar as the drug is typically administered together with diuretics and/or nitrates.

Cardiac Resynchronization Therapy

CRT reduces secondary MR¹¹³ and improves outcomes in patients with symptomatic HF with reduced ejection fraction and intraventricular conduction delay^{114, 115}. The mechanism by which CRT reduces secondary MR is three-fold, comprising both acute and chronic effects that optimize the force balance¹¹⁶: (1) an acute rise in – and longer duration of – the systolic closing force (dP/dt) immediately after onset of CRT^{54, 117}; (2) an immediately improved coordinated mechanical contraction of the papillary muscles, which reduces tethering¹¹⁸⁻¹²⁰; and (3) long-term reverse left ventricular remodeling with significant reductions in EDV and ESV, which further lessens tethering forces^{113, 120, 121}, and is probably the clinically most important effect.

The dynamic component of secondary MR during exercise is attenuated by CRT as well^{122, 123}, resulting in increased forward stroke volume during exercise¹²⁴ and improved exercise capacity¹²⁵. However, dynamic worsening of MR during exercise is not entirely prevented by CRT¹²². The mechanism of MR reduction during exercise does not seem to be related to the acute effects, but probably relies on longer term reverse left ventricular remodeling and reduced dyssynchrony (Figure 1.4)^{89, 126}. Of note, the extent of reverse remodeling after CRT is most favorable in non-ischemic etiologies of HF¹¹³. The acute effects of CRT on the force-balance relationship are reversible, as cessation of biventricular pacing for 72h immediately causes a drop in dP/dt and an increase in secondary MR¹²⁷. Furthermore, acute withdrawal of biventricular pacing after 6 months in patients with papillary muscle dyssynchrony results in recurrent dyssynchrony and abrupt reappearance of secondary MR¹¹⁹.

CRT is considered a valid and less invasive alternative to surgery in eligible⁹⁹ patients with moderate-to-severe secondary MR and reduced ejection fraction as well as broad QRS complex, based on a long-term survival benefit in this particular population^{128, 129}. The

indication for CRT remains unclear in case of narrow QRS complex but dynamic worsening of dyssynchrony, causing prognostically important exercise-induced MR deterioration^{85, 130}. Finally, even after CRT, 37-50% of patients show no ≥ 1 grade improvement in MR^{120, 128}. In such patients, additional interventions should be considered.

Revascularization

In patients with ischemic cardiomyopathy and (moderate) secondary MR, revascularization can recruit viable myocardial segments and enhance reverse left ventricular remodeling, thereby reducing the degree of secondary MR in a majority of patients¹³¹. Whether this strategy is effective in reducing the dynamic component of MR during exercise is unknown. Secondary MR improvement at 1 year after isolated coronary artery bypass grafting (CABG) was predicted by ≥ 5 viable segments of myocardium (16 segment model) and absence of PM dyssynchrony in the prospective study of Penicka et al¹³². This observation has important implications with respect to exercise: (1) viability post-infarction; i.e. preserved contractile reserve during exercise, has been shown to decrease exercise-induced MR^{82, 83}, especially when inferior (basal) segments are involved; (2) papillary muscle dyssynchrony is implicated as an independent determinant of exercise-increased MR (**Central Illustration**). Hypothetically, based on these findings, coronary artery disease patients with worsening of secondary MR during exercise (not associated with evidence of inducible ischemia) are less likely to show improvement of MR following revascularization, and may therefore benefit from adjunctive therapy or intervention. However, this should certainly be subject to further study and exploration.

In the only prospectively randomized study to date that employed postoperative exercise echocardiography when comparing CABG versus CABG with mitral valve annuloplasty for moderate secondary MR, the dynamic (exercise-induced) MR component remained highly prevalent in the isolated CABG arm, but not after adjunctive mitral valve annuloplasty

(Figure 1.7-A)¹³³. Furthermore, in the Randomized Ischemic Mitral Evaluation (RIME) trial a greater improvement in exercise capacity after 1 year was observed in the combined CABG with mitral valve annuloplasty arm than in the isolated CABG group, likely due to improved dynamic MR during exercise. In contrast, the moderate ischemic MR trial of the CardioThoracic Surgical trials Network (CTSN), comparing 151 patients with moderate ischemic MR undergoing CABG alone with 150 receiving concomitant mitral valve annuloplasty, did not demonstrate a difference in left ventricular remodeling (primary endpoint), functional capacity, or clinical outcome after 1 year. However, in contrast to the RIME trial¹³⁴ and the randomized trial by Fattouch et al¹³³, exercise dynamics were not taken into account¹³⁵.

Mitral valve surgery

The surgical management of secondary MR remains challenging and controversial^{24, 25}. Not only the optimal surgical strategy but also indications for surgery remain highly debated, especially in case of moderate (possibly dynamic) secondary MR. Prospective randomized data to help decision-making are scarce, and the definition of moderate and severe secondary MR in the guidelines (severe = EROA $\geq 20\text{mm}^2$ instead of $\geq 40\text{mm}^2$) is not unchallenged^{136, 137}. Figure 1.6 summarizes the inclusion criteria of the prospectively randomized clinical trials on mitral valve surgery for secondary MR (Table 1.3). It is unclear where mild-to-moderate secondary MR at rest that significantly increases during exercise can be positioned along this spectrum, or whether alternative EROA thresholds for MR severity should apply for exercise-induced MR. Preoperative exercise echocardiography was performed only in the RIME trial. Based on the prognostic impact of exercise-induced secondary MR deterioration, European (ESC) guidelines suggest mitral valve intervention in such patients when there is an indication for other cardiac surgery²². However, the impact of the available surgical approaches on the dynamic MR and the respective exercise hemodynamics needs to be better understood.

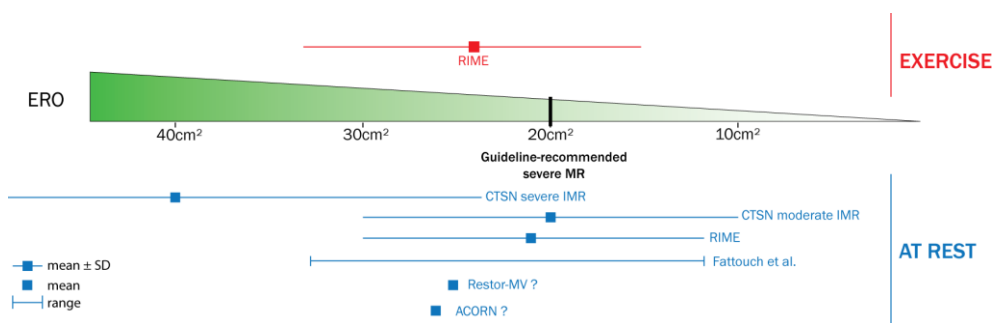


Figure 1.6 - Effective regurgitant orifice (ERO) in secondary mitral valve regurgitation (MR) patients of prospectively randomized studies.

Table 1.3 – Inclusion criteria and key results of the prospectively randomized trials studying mitral valve surgery for secondary MR.

	CTSN Severe MR		RIME		CTSN Moderate MR		Fattouch et al		RESTOR-MV		ACORN (RMA subgroup)	
ERO, mm² Pre-defined RMA population	≥40 40±17		20-39 21±9		20-39 20±10		MR=2/4 range 12-32mm ² *		MR: ≥2/4 ERO : NA Mean MR grade: 2.54±0.8		MR 3-4/4 in 58% ERO : NA Mean MR grade: 2.66	
Exercise MR	not evaluated		preop ExEcho: ERO exercise 24±9mm ²		not evaluated		post ExEcho only		not evaluated		not evaluated	
NYHA class III/IV	58%		33%		37%		2.3±1.1		48%		77%	
LV function												
EF, %	42±12		40±12		39±11		42±11		38±10		24±9	
LVESVI, mL/m ²	61±26		72±16 (CMR)		60±26		LVESD 45±8 mm		NA		NA	
LVEDVI, mL/m ²	NA		NA		NA		LVEDD 59±11 mm		LVEDD 59±7 mm		LVEDD 70 mm	
Demographics												
n	251		73		301		102		149		193‡	
age, yr	69yr		70yr		64yr		64yr		65yr		53yr	
male, %	62%		74%		71%		63%		77%		46%	
ischemic MR	100%		100%		100%		100%		100%		6%	
Study arms	RMA vs MVR		RMA+CABG vs CABG		RMA+CABG vs CABG		RMA+CABG vs CABG		RMA+CABG vs Coapsys+CABG		RMA vs RMA+CorCap	
Randomization	1:1		1:1		1:1		1:1		1:1		1:1	
+ CABG	74%		100%		100%		100%		100%		0%	
Primary endpoint	ΔLVESVI		peak VO ₂		ΔLVESVI		NYHA / LV remodelling		Mortality, adverse events, MR		all-cause mortality	
Key results												
ΔLVESV	RMA	MVR	RMA+CABG	CABG	RMA+CABG	CABG	RMA+CABG	CABG	RMA+CABG	Coapsy	RMA	+CorCap
1 yr	-6.6mL/m ²	-6.8mL/m ²	-22.2mL/m ²	-4.4mL/m ² †	-9.3mL/m ²	-9.4mL/m ²	ΔLVESD 8mm	2mm†	LVESD -3mm	-6mm†	ΔLVESV	-14.6mL†
MR ≥2/4, 1yr	32.6%	2.3%†	4%	50%†	11.2%	31.0%†	0%	60%†	0.52±0.66	1.4±1.00†	14.5%	2.6%
2yr	58.8%	3.8%†							0.35±0.63	1.2±0.97†		
NYHA III/IV	9%	14%	4%	15%†	7.9%	10.3%	≥II: 15.5%	≥II: 43.7%†	ΔNYHA≥1: 66%	71%	-	-
									ΔNYHA≥1: 72%	79%		
HF episode, 1yr	13.5%	11.2%	3%	8%	14.7%	13.2%	-	-	-	-	-	-
2yr	21.4%	17.6%										
Mortality, 1yr	14.3%	17.3%	9%	5%	6.7%	7.3%	4.2%	1.9%	-	-	14.8%	12.1%
2yr	19.0%	23.3%					(5-yr 6.3%)	(5-yr 11.2%)	23%	13%†§	15.9%	13.5%
Year	2014		2012		2014		2009		2010		2006	
Reference	Acker et al, ¹²⁸		Chan et al, ¹³⁴		Smith et al, ¹³¹		Fattouch et al, ¹³³		Grossi et al, ⁴³		Acker et al, ⁴⁴	

†significant (p<0.05) difference from RMA-group.

‡16% received MV replacement

§ in total population (n=165); not significant in RMA + CABG group (p=0.12), however significant (p=0.02) for complication-free survival (death, stroke, MI, reoperation).

*PISA radius 5-8mm; ERO calculated by simplified PISA (r²/2) for this summary.

ExEcho: exercise echocardiography; MVR, mitral valve replacement; RMA, restrictive mitral valve annuloplasty

Mitral valve annuloplasty

Mitral valve annuloplasty for secondary MR typically involves the insertion of an undersized prosthetic ring ('restrictive' annuloplasty), thereby reducing the anteroposterior dimensions of the mitral annulus, resulting in better apposition of the leaflets and increased coaptation (target coaptation length $\geq 8\text{mm}$)²⁶. The mechanism of action is two-fold: annular dimensions (typically dilated) are reduced, while the coaptation surface of the leaflets increases, thereby allowing more efficient use of closing forces during systole. At midterm follow-up, this procedure has shown to induce significant reverse left ventricular remodeling and improved systolic function, making it an effective strategy for patients with moderate to severe secondary MR^{26, 27, 134}.

Secondary MR did not recur during exercise in patients treated with restrictive mitral valve annuloplasty and CABG in the randomized study of Fattouch et al (Figure 1.7-A)¹³³. In another cohort study of 43 secondary MR patients, exercise echocardiography at 33 ± 17 months after restrictive annuloplasty showed absence of more than mild MR at rest and during exercise in all but 4 subjects¹³⁹. Hypothetically, inhibition of annular dilation during exercise, along with reverse left ventricular remodeling and optimization of the force balance, should be able to reduce the dynamic component of secondary MR, but not to abolish it, as tethering might still increase during exercise (**Central Illustration**).

In addition, there is some concern that increased transmitral gradients after restrictive annuloplasty are associated with exercise-induced pulmonary hypertension and worsening functional capacity³⁰. Although this was initially attributed to the small ring size, it was demonstrated recently that not the size of the prosthetic ring but rather the degree of subvalvular diastolic leaflet tethering is responsible for this functional stenosis after surgery^{33, 139}. The effective mitral valve area at peak exercise was the strongest predictor of

impaired exercise capacity and directly associated with all-cause mortality (Figure 1.7-B)^{139, 140}. This should certainly be taken into account in the decision-making of patients with dynamic secondary MR, and adjunctive approaches that relieve diastolic tethering after surgery should be further explored.

Finally, in patients with severe secondary MR at rest, recurrence of moderate MR in up to 30% in the course of the first year after surgery is well recognized^{34, 35}, with pathophysiological mechanisms mainly related to ongoing adverse remodeling and subvalvular tethering, usually in patients with already severely dilated left ventricles^{36, 37}. Importantly, preoperative presence of basal inferior wall aneurysm or dyskinesia was most predictive for MR recurrence in the annuloplasty group of the randomized severe MR CTSN trial³⁸. In such patients, either adjunctive subvalvular/ventricular procedures to relieve tethering or mitral valve replacement should be considered.

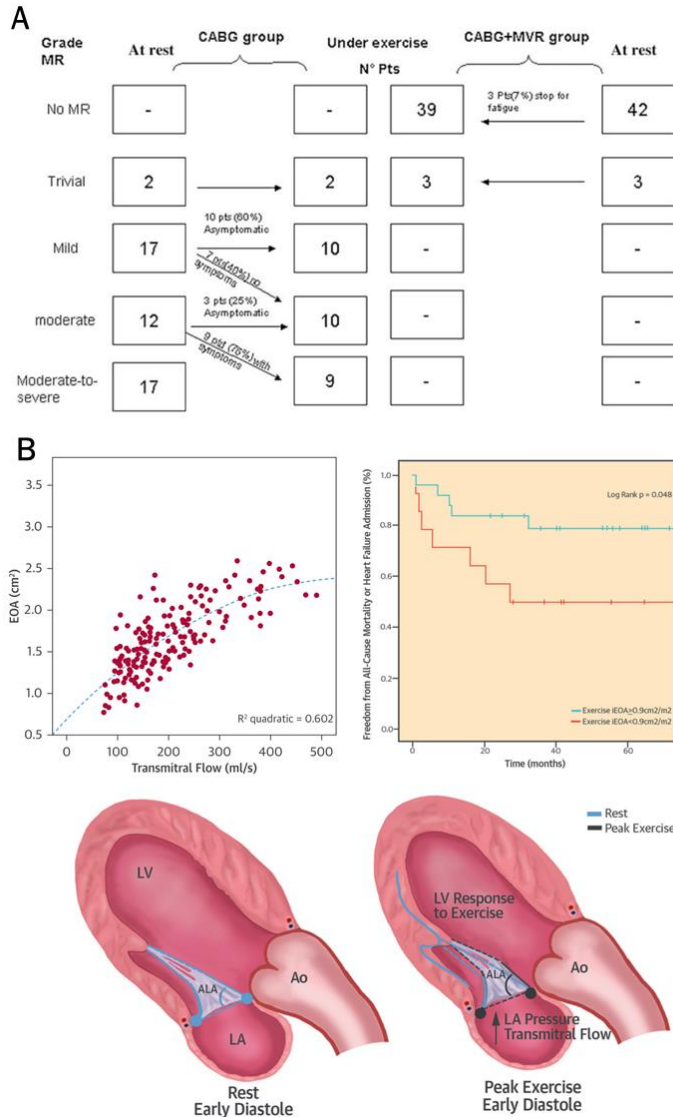


Figure 1.7 - Impact of restrictive mitral valve annuloplasty (RMA) on exercise hemodynamics in secondary mitral valve regurgitation (MR) patients. (A) Exercise echocardiography shows sustained MR reduction during exercise in patients undergoing additional RMA for secondary MR versus maintenance of dynamic exercise-induced MR deterioration in coronary artery bypass grafting only patients (adapted from Fattouch et al¹³³, with permission). (B) The mitral valve area after RMA increases during exercise because of an increasing anterior leaflet opening angle. This suggests that the functional stenosis after RMA relates to impaired diastolic anterior leaflet opening (i.e., ongoing tethering). Impaired effective orifice area at peak exercise is associated with worse outcomes. Adapted from Bertrand et al¹³⁹, with permission.

Mitral valve replacement

Exercise-induced MR is definitively abolished after successful mitral valve replacement. However, similar concerns of transmitral gradients and exercise-induced pulmonary hypertension apply, especially in patients with some degree of prosthesis-patient mismatch^{141, 142}. In patients with secondary MR treated with mitral valve replacement, effective orifice area was in fact an important independent predictor of exercise-induced pulmonary hypertension and functional capacity^{140, 143}. Therefore, when opting for mitral valve replacement for treating dynamic secondary MR, careful selection of prosthesis type and size is warranted to maximize postoperative effective orifice area and avoid abnormally high transprosthetic gradients during exercise.

Ventricular and/or subvalvular approaches

Since tethering is the primary mechanism causing secondary MR and its exercise-induced deterioration, targeted ventricular or subvalvular procedures reducing the degree of mitral leaflet traction is a particularly promising approach (**Central Illustration**). Furthermore, successful relief of tethering may also reduce the risk of functional mitral stenosis and thus improve exercise hemodynamics after restrictive annuloplasty¹³⁹. However, ventricular reshaping strategies have not been shown to be more effective in reducing MR than conventional mitral repair techniques (although they may be associated with independent survival benefits)^{43, 44, 144}, and data regarding impact on exercise dynamics are lacking. A number of subvalvular approaches have been developed in animal studies and applied in small observational clinical series, with mixed levels of success¹⁴⁵. Mitral leaflet augmentation¹⁴⁶, PM relocation³⁹ and/or approximation⁴², or secondary chordal cutting^{147, 148} have been proposed, but none have gained widespread clinical use or acceptance. Nevertheless, that should not be seen as a refutation of the concept; it rather reflects the fact that some of the techniques are novel or technically demanding. In fact, off-pump

papillary muscle repositioning under echocardiographic guidance using a transventricular suture, combined with less restrictive annuloplasty using a partial ring (RING plus STRING technique), has been shown to produce an effective and lasting relief of tethering in the most challenging group patients: those with a tethering distance of ≥ 10 mm¹⁴⁹.

Because the specific mechanisms of subvalvular tethering and secondary MR are heterogeneous and show large interindividual variations (Figure 1.3), the optimal subvalvular approach may require a personalized approach: targeting the individual patient's geometry, including individually observed exercise-induced aggravation in tethering and MR.

Transcatheter mitral valve interventions

Transcatheter edge-to-edge mitral valve repair using the MitraClip® device (Abbott Vascular, Menlo Park, California) involves a percutaneous transseptal left atrial approach emulating the Alfieri stitch by clipping the mitral valve leaflets together. Although randomized data from the Endovascular Valve Edge-to-Edge Repair Study (EVEREST II) mainly support MitraClip therapy in inoperable primary MR¹⁵⁰ (for which the Alfieri stitch was originally intended) real-world registries show that it is predominantly used for secondary MR in clinical practice¹⁵¹. The rationale for MitraClip in secondary MR arises from the uncertain risk-benefit ratio of mitral valve surgery in patients with left ventricular dysfunction, in particular if there is no other indication for cardiac surgery²⁴. The mechanism by which MitraClip may reduce secondary MR is (1) an acute increase in coaptation area improving closing force efficiency¹⁵²; and (2) a slight decrease in annular (antero-posterior) dimensions¹⁵³ relieving tethering. Tenting area is generally not reduced in the acute phase¹⁵², but may reduce over time in patients with significant reverse left ventricular remodeling post procedure¹⁵⁴. Furthermore, the therapy appears to be effective in promoting reverse remodeling in non-responders to CRT¹⁵⁵.

To investigate whether these beneficial effects on remodeling translate into reduction of dynamic secondary MR (**Central Illustration**) a prospective multicenter study was performed in three Belgian centers (substudy of the Belgian MitraClip Registry, NCT02506387) comparing exercise echocardiography before and 6 months after MitraClip in 31 secondary MR patients. Preliminary data (unpublished) show a significant reduction in secondary MR at peak exercise after 6 months, along with increased cardiac output and decreased pulmonary arterial pressures. However, a potential downside of the therapy is the reduction in mitral valve area caused by clipping the large mitral orifice into a double orifice of smaller size, causing increased transmitral pressure gradients at rest and during exercise^{156, 157}. The prospective Cardiovascular Outcomes Assessment of the MitraClip Percutaneous Therapy for Heart Failure Patients with Functional Mitral Regurgitation (COAPT) trial is currently recruiting secondary MR patients to compare MitraClip therapy with standard medical care. In a subset of patients, exercise testing will be performed. These data may provide important insight into the impact of MitraClip therapy on exercise hemodynamics and outcomes.

Numerous other percutaneous devices for mitral replacement and/or repair are currently under development in preclinical or phase I/II studies. Targets for repair include the mitral leaflets, chordae, annulus or left ventricle¹⁵⁸.

Future research

Due to the paucity of data on exercise MR the approach to exercise-induced MR must, for the time being, rely heavily on pathophysiological insights gained from resting studies. At this point, we cannot offer definitive answers, only more precise questions, the most important of which may be: Can reduction of the dynamic component of secondary MR independently improve outcome? Is there an EROA threshold for secondary MR at peak exercise beyond which intervention is warranted even if resting MR is relatively mild? Is

there a place for more aggressive 'unloading' of the heart using arterial and venous vasodilators on top of current guideline-recommended neurohormonal blockade in these patients?

Phenotyping secondary MR patients using exercise echocardiography should be incorporated in the protocol of prospective randomized studies assessing mitral interventions to help answer these questions. Finally, a patient-specific analysis of the three-dimensional geometry and dynamics causing mitral valve dysfunction is likely to improve our insights and therapeutic efficiency for secondary MR. Current advances in three-dimensional cardiac imaging and computational power already provide the ability to simulate mitral valve dynamics during physiological loading conditions, and virtually perform a therapy while evaluating its impact on patient-specific mitral valve function and dynamics (Figure 8)¹⁵⁹. Such innovative technology holds great potential to tailor treatments to the individual and unique patient.

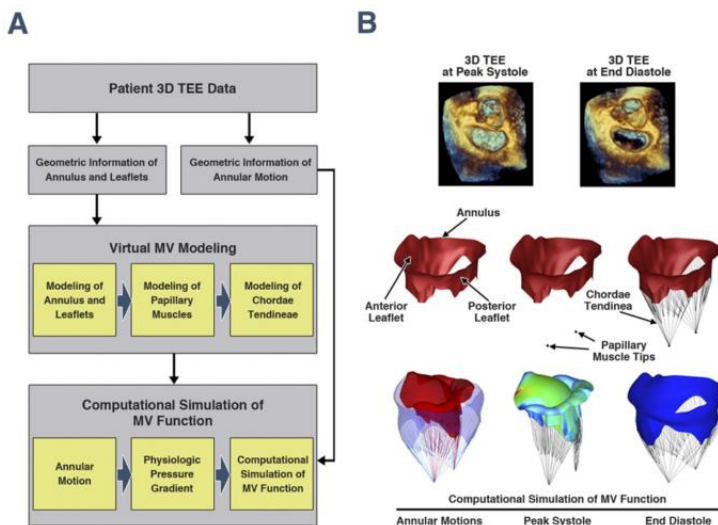


Figure 8 - Numerical mitral valve modeling and simulation as a tool to predict patient-specific (geometric) dynamics, and ultimately the response to targeted therapies. Adapted from Rim et al¹⁵⁹, with permission.

Summary

The dynamics of secondary MR are governed by the balance between mitral closing and tethering forces. Exercise-induced changes mainly result from the impact of hemodynamics on left ventricular geometry, specifically global and local deformation, dyssynchrony, and annular dilatation – all of which critically affect tethering. Exercise-induced worsening of secondary MR through the final common pathway of more tethering is associated with impaired exercise capacity and increased mortality. Therapies for secondary MR should focus not only on resting status, but also aim at reducing the dynamic component of the valvular lesion. Individualized targeting of underlying geometric culprits, aiming at inhibiting increases in tethering by improving left ventricular size, shape and function during exercise are key elements for success.

Chapter 2

Functional impact of transmitral gradients at rest and during exercise after restrictive annuloplasty for ischemic mitral regurgitation

Bertrand PB, Gutermann H, Smeets CJ, Van Kerrebroeck C,

Verhaert D, Vandervoort P, Dion R

Status of the manuscript:

Published

J Thorac Cardiovasc Surg. 2014 Jul;148(1):183-7. (IF 4.1)

Abstract

Objectives: Restrictive mitral valve annuloplasty (RMA) combined with coronary artery bypass grafting (CABG) is the treatment of choice for ischemic mitral regurgitation (IMR). Postoperative functional mitral stenosis and its potential impact on functional capacity remains the object of debate. The aim of this study was to assess functional and hemodynamic outcome at rest and during exercise in an IMR population following a standardized RMA.

Methods: 23 IMR-patients previously treated with CABG and RMA, underwent a semi-supine (bicycle) exercise test with Doppler echocardiography and ergospirometry. The surgical technique was identical in all patients, using a complete semi-rigid ring, downsized by two sizes after measuring the height of the anterior mitral leaflet, in order to achieve a coaptation length of at least 8mm.

Results: At a mean follow-up of 28 ± 15 months, mean transmitral gradients at rest and maximal exercise were 4.4 ± 1.8 mmHg and 8.2 ± 4.2 mmHg respectively ($p < 0.001$). Transmitral gradients did not correlate with exercise capacity (VO_2 max) or pulmonary artery pressures. Patients with resting mean gradient ≥ 5 mmHg ($n=9$) reached a significantly higher VO_2 max, however they had a better ejection fraction and cardiac output at rest and reached a higher cardiac output at peak exercise.

Conclusion: Transmitral gradients after RMA for IMR did not correlate with functional capacity as measured by VO_2 max during semi-supine bicycle testing. Functional capacity and transmitral gradients however are not only determined by the severity of mitral stenosis but also by hemodynamic factors such as ejection fraction and cardiac output. Transmitral gradients should be interpreted with respect to patient hemodynamics and not necessarily be considered as detrimental for functional capacity.

Introduction

Restrictive mitral valve annuloplasty (RMA) has become the preferred surgical approach in the management of ischemic mitral regurgitation (IMR), based on good short- and mid-term data from observational studies^{26, 27, 160}. RMA involves the insertion of an undersized prosthetic ring, thereby reducing antero-posterior dimensions of the mitral annulus, resulting in improved leaflet coaptation. At mid-term follow-up, this procedure has shown to induce significant reverse remodeling and improve systolic function, making it an effective strategy for patients with severe IMR¹⁶⁰. Recently, however, several studies have demonstrated the occurrence of moderate 'functional' mitral stenosis (MS) after RMA, i.e. a mean transmitral pressure gradient > 5mmHg, or a mitral valve area < 1.5cm², with incidences of MS ranging from 9%³¹ to 54%³² after RMA. The impact of a postoperative MS on functional and clinical outcome however remains controversial. Magne *et al*³⁰ demonstrated a significant negative correlation between mitral peak gradient at rest and six minute walking test distance, suggesting a deleterious effect on functional capacity. Other studies however failed to demonstrate an effect of transmitral gradients on survival^{32, 161, 162}, adverse cardiac events³¹, or New York Heart Association (NYHA) functional class¹⁶¹. In many of those patient groups however, operative techniques and surgical endpoints of RMA were heterogeneous and non-standardized.

The aim of this study therefore was to assess functional capacity and hemodynamic outcome in a homogeneous IMR-population following a standardized RMA, with a target postoperative coaptation length of at least 8mm.

Methods

Study Population. Between July 2007 and August 2012, 52 standardized RMA procedures in IMR patients have been performed in our center. These procedures comprised all urgent (within 72h of admission), semi-urgent (within 14 days during the same hospital stay) and elective procedures. At 39 ± 15 months postoperatively, all survivors ($n=34$) were contacted to undergo a resting echocardiography followed by an exercise stress echocardiography with ergospirometry, as approved by the local ethics committee. Written informed consent was obtained from all of the participating patients. Figure 2.1 displays the study flow chart, with 11 patients refusing participation for various reasons. The final study population therefore consisted of 23 IMR patients previously treated with CABG and standardized RMA that underwent a single study visit at our center with resting and exercise echocardiography.

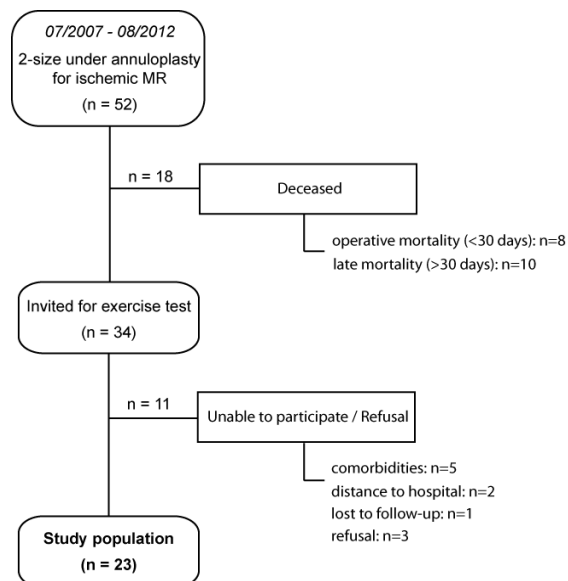


Figure 2.1 - Study flow chart

Surgical Procedure. All surgical procedures were performed through midline sternotomy under normothermic cardiopulmonary bypass with intermittent antegrade warmblood cardioplegia. After the revascularization procedure, the mitral valve was exposed through a vertical transeptal approach. Mitral annuloplasty ring size was determined after careful measurement of the height of the anterior leaflet, and downsized by two sizes with a complete semi-rigid annuloplasty ring (Carpentier-Edwards Physioring I®, Edwards Lifesciences, Irvine, CA). A saline test was performed to check symmetric and posteriorly located line of coaptation. After weaning cardiopulmonary bypass, intraoperative transesophageal echocardiography (TEE) was used to assess the result and to measure leaflet coaptation. A minimum coaptation length of 8mm in A2-P2 segment was pursued.

Transthoracic echocardiography. Preoperative two-dimensional (2D) echocardiography exams were retrospectively analyzed for comparison to the echocardiographic data at the follow-up visit. The postoperative mean transmitral gradient from all patients (also patients not participating in the exercise echocardiography) was retrospectively measured from 2D echocardiography, which was systematically performed immediately after Intensive Care Unit (ICU) discharge. All echocardiographic exams were performed with a commercially available system (Philips Healthcare, IE33®), and with standard 2D and Doppler echocardiographic images acquired in the left lateral decubitus position using a phased-array transducer in the parasternal and apical views by experienced cardiac sonographers. At the study visit, three consecutive cardiac cycles were recorded and stored for subsequent offline analysis. Left ventricular (LV) end-diastolic and end-systolic dimensions were measured from parasternal acquisitions. LV volumes and ejection fraction were calculated using the modified Simpson's biplane method. LV stroke volume was measured by pulsed-wave Doppler in the LV outflow tract. Color flow was applied in the apical 4-chamber view to assess severity of MR, which was graded by the vena contracta width. Peak and mean transmitral gradients were calculated using the modified Bernoulli equation on the

continuous wave signal. Systolic pulmonary artery pressure (PAP) was calculated using the modified Bernoulli equation on the transtricuspid continuous-wave Doppler signal, while adding right atrial pressure ¹⁶³.

Exercise protocol. All 23 patients underwent a symptom-limited graded bicycle test in semi-supine position on a tilting exercise table. Workload was initiated at 20 Watt, with increments of 20 Watt every 3 minutes. In patients with poor general condition, an adjusted protocol was applied with 10 Watt of initial workload and increments of 10 Watt every 3 minutes. Blood-pressure and a 12-lead electrocardiogram were recorded at each stage. Two-dimensional and Doppler echocardiographic recordings were made at each stage, i.e. for measuring LV geometry and function, LV stroke volume, MR vena contracta width, peak and mean transmitral gradient, and systolic PAP.

Cardiopulmonary exercise testing (CPET). Real-time ergospirometry data were assessed using a commercially available system (JAEGER®, Würzburg, Germany). Maximal oxygen uptake (VO₂max) during exercise was assessed in all patients.

Statistical Analysis. Results are expressed as mean ± standard deviation (SD) if normally distributed or otherwise by median and interquartile range (IQR). Normality was assessed by the Shapiro-Wilk statistic. The paired student's t-test and Wilcoxon signed-rank test were used when appropriate to compare between pre- and postoperative echocardiographic parameters and between resting and exercise data in the postoperative setting. Categorical values were compared using the Pearson Chi-Square test when appropriate. Cumulative survival curves were calculated according to the Kaplan–Meier method, and survival in high versus low gradient groups was compared with the log-rank test. Statistical significance was set at a two-tailed probability of $p < 0.05$. Statistical analyses were performed using the Statistical Package for Social Sciences release 20.0 (SPSS Inc., Chicago, Illinois, USA).

Results

Preoperative and operative clinical data. Preoperative patient characteristics are summarized in Table 2.1. The patient population consisted of 23 IMR patients, with a median (IQR) ring size of 26 (26-28) and with a median (IQR) postoperative coaptation length of 8.8mm (7.6-9.0mm). In 3/23 (12%) patients a concomitant aneurysmectomy was performed, another 3/23 (12%) patients received a cardiac resynchronization therapy (CRT) device prior to our study follow-up examination.

Comparison of preoperative versus postoperative (follow-up) echocardiography.

At mean follow-up of 28 ± 15 months, in the group of 17 patients without aneurysmectomy and CRT-implantation, there was a decrease in LV end-diastolic volume and end-systolic volume compared to the preoperative setting (preoperative 141 ± 52 mL and 86 ± 44 mL versus postoperative 113 ± 44 mL and 62 ± 37 mL, $p=0.035$ and $p=0.052$ respectively), and a non-significant increase in ejection fraction ($38 \pm 11\%$ versus $45 \pm 15\%$, $p=0.095$). In all 23 study patients MR jet vena contracta width significantly decreased (3.8 ± 1.8 mm versus 1.3 ± 1.0 mm, $p < 0.001$), with more than moderate recurrent MR (i.e. vena contracta width > 3 mm, but less than 5 mm) in 1 patient (4%). There was a non-significant decrease in systolic PAP (50 ± 8 versus 45 ± 14 , $p=0.093$) compared to preoperatively.

Exercise hemodynamics. Resting and exercise hemodynamics in the study group are displayed in Table 2.2. Resting mean and peak transmitral gradients were 4.4 ± 1.8 mmHg and 11.4 ± 3.6 mmHg respectively, with mean gradient ≥ 5 mmHg in 9 patients (39%). There was a significant increase in transmitral mean and peak gradient with exercise, along with a significant increase in systolic PAP and cardiac output. Exercise systolic PAP was not correlated with transmitral mean or peak gradients during exercise ($r=0.068, p=0.77$ and $r=0.258, p=0.26$ respectively).

Functional capacity. Full ergospirometry data were available in 22 patients, as one patient refused the ergospirometry mask. There was no correlation between VO_2 max and peak or mean transmitral gradients at rest, with $r=0.271, p=0.223$ and $r=0.181, p<0.421$ respectively. Patients with resting mean transmitral gradient ≥ 5 mmHg ($n=9$) had significantly higher exercise capacity, higher VO_2 max, and higher cardiac output both at rest and during maximal exercise compared to patients with <5 mmHg resting mean transmitral gradient ($n=14$) (Table 2.2).

Impact on survival. In 42 IMR patients with echocardiography data available at median (IQR) 7 (6-11) days after surgery (shortly after ICU discharge) the mean transmitral gradient was 4.7 ± 1.6 mmHg. When dichotomizing into patients with mean gradient ≥ 5 mmHg ($n=22$) versus <5 mmHg ($n=20$), there was no difference in the (late) survival rate (log-rank $p=0.92$, Figure 2.2).

Table 2.1 - Preoperative patient characteristics

Variables	IMR patients (n=23)
Age at surgery, years	65 ± 10
Male gender	18 (78%)
Body surface area, m ²	1.92 ± 0.16
NYHA class, I/II/III/IV	1/8/11/3
Cardiovascular risk factors	
Diabetes	9 (39%)
Hypertension	14 (61%)
Obesity	7 (30%)
Smoking habits	13 (57%)
Hyperlipidemia	16 (70%)
Familial history of ischemia	7 (30%)
Baseline medication	
ACE-I / ARB	17 (74%)
β-blockers	21 (91%)
Loop diuretics	15 (65%)
Statins	19 (83%)
Anticoagulation	4 (17%)
Antiplatelet therapy	22 (96%)
Comorbidity	
CKD	6 (26%)
COPD	6 (26%)
Prior PCI	7 (30%)
Operative data	
Cardiopulmonary bypass time, min	212 ± 51
Aortic cross-clamp time, min	158 ± 45
Coaptation length postoperatively, mm	8.8 (IQR 7.6-9.0)
+ concomitant TVP	10 (43%)
+ LV aneurysmectomy	3 (12%)
+ AVR (bioprosthesis)	1 (4%)

IMR, ischemic mitral regurgitation; NYHA, New York Heart Association; ACE-I, angiotensin-converting enzyme inhibitor; ARB, angiotensin receptor blocker; CKD, chronic kidney disease; COPD, chronic Obstructive Pulmonary Disease; PCI, Percutaneous coronary intervention; TVP, tricuspid valve annuloplasty; LV, left ventricular; AVR, aortic valve replacement

Table 2.2 - Comparison of postoperative parameters in resting condition and during exercise.

Variables	Total population			Mean gradient <5mmHg (n=14)			Mean gradient ≥5mmHg (n=9)			P-value†	
	Resting	Exercise	p	Resting	Exercise	p-value	Resting	Exercise	p-value	Resting	Exercise
LV ejection fraction, %	46 ± 14			42 ± 16			53 ± 7			p=0.036	
LV EDV, mL	125 ± 10			138 ± 55			105 ± 30			p=0.076	
LV ESV, mL	72 ± 9			86 ± 49			50 ± 15			p=0.020	
LV EDD, mm	54 ± 2			57 ± 8			50 ± 7			p=0.033	
LV ESD, mm	45 ± 2			48 ± 10			41 ± 7			p=0.064	
Decrease LV EDV [‡] , %	26 (46)			26 (43)			19 (49)			p=0.91	
NYHA class I/II/III/IV	10/11/2/0			5/7/2/0			5/4/0/0			p=0.40	
Physioring size	3/9/7/2/2 24/26/28/30/32			2/3/5/2/2			1/6/2/0/0			p=0.21	
Maximal workload, Watt	50 ± 23			38 ± 14			69 ± 23			p<0.001	
VO ₂ max, mL/kg/min	13.5 ± 3.4			12.3 ± 3.4			15.3 ± 2.6			p=0.035	
MV peak gradient, mmHg	11.4 ± 3.6	16.8 ± 6.1	p<0.001	9.5 ± 2.7	13.1 ± 4.3	p=0.004	14.5 ± 2.6	22.6 ± 3.4	p=0.001	p<0.001	p<0.001
MV mean gradient, mmHg	4.4 ± 1.8	8.2 ± 4.2	p<0.001	3.3 ± 1	5.7 ± 1.6	p<0.001	6.2 ± 1	12.0 ± 4.0	p=0.003	p<0.001	p<0.001
Systolic PAP, mmHg*	43 ± 13	53 ± 20	p<0.012	43 ± 15	46 ± 26	p=0.105	43 ± 11	50 ± 20	p=0.05§	p=0.94	p=0.71
Cardiac output	3.9 ± 0.8	5.8 ± 2.0	p<0.001	3.6 ± 0.8	4.7 ± 1.3	p=0.01	4.4 ± 0.8	7.3 ± 2.0	p=0.001	p=0.03	p=0.001
Cardiac Index	2.1 ± 0.4	3.0 ± 0.9	p<0.001	1.9 ± 0.4	2.5 ± 0.7	p=0.001	2.3 ± 0.4	3.7 ± 0.9	p=0.001	p=0.09	p=0.002
MR VC width, mm	1.3 ± 1.0	1.3 ± 1.2	NS	1.2 ± 1.2	1.2 ± 1.2	NS	1.4 ± 0.7	1.3 ± 1.3	NS	NS	NS

*paired samples only: (n=20) in total population, n=12 in low gradient group, n=8 in high gradient group.

†comparison between mean gradient <5mmHg and mean gradient >5mmHg.

‡measured as preoperative LV EDV minus postoperative LV EDV, divided by preoperative LV EDV; expressed as median (IQR)

§measured as preoperative LV EDV minus postoperative LV EDV, divided by preoperative LV EDV; expressed as median (IQR)
 LV, left ventricle; EDV, end-diastolic volume; ESV, end-systolic volume; EDD, end-diastolic diameter; ESD, end-systolic diameter; NYHA, New York Heart Association; MV, mitral valve; PAP, pulmonary artery pressure; MR VC, mitral regurgitation vena contracta.

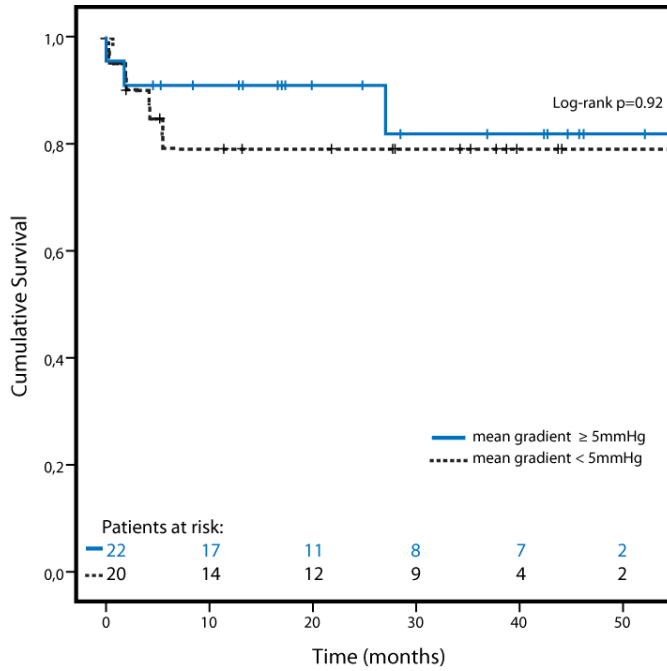


Figure 2.2 - Impact of postoperative gradient on late mortality. Kaplan-Meier survival curves according to the mean transmitral gradient at ICU discharge.

Discussion

RMA combined with CABG has been proposed as the procedure of choice for the management of IMR. Several recent observations however have demonstrated the risk of an iatrogenic mitral stenosis, with etiology of stenosis either due to a too stringent ring selection³⁰, or ongoing diastolic leaflet tethering³³. The functional impact of this mitral stenosis remains debated, with one study showing a deleterious effect of this stenosis on functional capacity³⁰, while other series could find no impact on NYHA class¹⁶¹ or clinical outcome^{31, 32, 162}. In many of those patient groups, operative techniques and surgical endpoints were heterogeneous and non-standardized.

In this study all patients underwent a standardized 2-size-under RMA for IMR using a complete semi-rigid (Physio I) annuloplasty ring. Our results confirm the positive effect of RMA on left ventricular remodeling and low recurrence of significant MR. Overall peak and mean transvalvular gradients at rest are mildly elevated and in line with previously published data. At a mean follow-up of 28±15 months a moderate functional mitral stenosis (mean transmitral gradient \geq 5mmHg) was present in 39% of patients, however we did not see an effect on functional capacity, measured by VO₂max. This is in contrast with previous findings³⁰ showing a strong negative correlation between resting transmitral gradients and exercise capacity as measured by a six-minute walking test. As the transmitral gradient is a flow-dependent variable, our findings possibly reflect the fact that in patients with a higher cardiac output a higher gradient will be observed over a comparable degree of stenosis. Indeed, ejection fraction and cardiac output at rest were significantly higher in our patients with gradients \geq 5mmHg, which could explain the higher gradients in this patient group without negative impact on functional capacity. These findings are in accordance with recent observations of Rubino *et al*¹⁶¹ and Williams *et al*³², both showing better postoperative remodeling in patients with a baseline gradient \geq 5mmHg. It is important to keep in mind

that the transmitral gradient depends on both intrinsic stenosis and transmitral flow, and therefore should always be interpreted with respect to cardiac output. As such, an increased transmitral gradient post-RMA in a patient with normal ejection fraction and cardiac output may be acceptable and have no impact on functional capacity, whereas a 'normal' transmitral gradient in a patient with poor LV function may mask significant mitral stenosis. In the future a more flow independent parameter such as mitral valve area should be validated to use in the assessment of functional mitral stenosis in RMA patients.

In functional MR surgery, the surgical end-point should be to achieve an optimal coaptation length. Previous studies have shown that a length of 8mm in A2-P2 can offer a durable result with only minor MR recurrence ¹⁶⁰. In the present study, in the homogeneous IMR population with structurally normal mitral leaflets, undersizing by 2 sizes using the Physio I ring was needed to obtain that particular end-point. It should be noted however that in patients with presence of leaflet calcifications and/or sclerotic alterations, i.e. in concomitant rheumatic valve disease, undersizing must be lessened (1 size) or even avoided, with or without leaflet augmentation to obtain the 8mm coaptation endpoint. When annuloplasty is impossible due to heavy annular calcifications, leaflet augmentation by means of autologous pericardium must be considered instead.

A limitation to this study is the retrospective study design, although postoperative echocardiography at rest and exercise was performed in a prospectively organized set-up. The small study sample might have led to type II statistical errors in our study results. The fact that not all IMR patients were able to participate in the study due to various reasons (Figure 2.1) might have induced some selection bias. However, when comparing the postoperative mean transmitral gradient after ICU discharge in the participating patients (n=23) versus the non-participating patients (n=11), no significant difference was observed (4.8±1.7mmHg versus 4.5±1.6mmHg respectively, p=0.85).

To conclude, this study demonstrated a standardized RMA combined with CABG induces left ventricular remodeling with concomitant improvement in functional status and very low incidence of recurrent IMR. Postoperative transmitral gradients did not correlate with functional capacity as measured by VO_2 max. Functional capacity however, as well as transmitral gradients, seem not only determined by the severity of mitral stenosis but also by other hemodynamic factors such as ejection fraction and cardiac output. For correct interpretation of transmitral gradients both at rest and during exercise, hemodynamics of the patient should be taken into account. In the future a more hemodynamically independent parameter, such as mitral valve area, may be better suited to assess the impact of functional mitral stenosis after RMA.

Chapter 3

Mitral Valve Area During Exercise After Restrictive Annuloplasty: Importance of Diastolic Anterior Leaflet Tethering.

Bertrand PB, Verbrugge FH, Verhaert D, Smeets CJ, Grieten L, Mullens W, Gutermann H,
Dion RA, Levine RA, Vandervoort PM.

Status of the manuscript:

Published

J Am Coll Cardiol. 2015 Feb 10;65(5):452-61. (IF 16.5)

Abstract

Background: Restrictive mitral valve annuloplasty (RMA) for secondary mitral regurgitation (MR) might cause functional mitral stenosis, yet its clinical impact and underlying pathophysiological mechanisms remain debated.

Objectives: To assess the hemodynamic and clinical impact of effective orifice area (EOA) after RMA, and its relationship with diastolic anterior leaflet (AL) tethering at rest and during exercise.

Methods: Consecutive RMA patients (n=39) underwent a symptom-limited supine bicycle exercise test with Doppler echocardiography and respiratory gas analysis. EOA, transmitral flow rate, mean transmitral gradient (TMG) and systolic pulmonary arterial pressure (sPAP) were assessed at different stages of exercise. AL opening angles were measured at rest and peak exercise. Mortality and heart failure readmission data were collected during at least 20 months post-surgery.

Results: EOA and AL opening angle were $1.5 \pm 0.4 \text{ cm}^2$ and $68 \pm 10^\circ$, respectively, at rest ($r=0.4$, $p=0.014$). EOA increased significantly to $2.0 \pm 0.5 \text{ cm}^2$ at peak exercise ($p < 0.001$), showing an improved correlation with AL opening angle ($r=0.6$, $p < 0.001$). Indexed EOA (EOAi) at peak exercise was an independent predictor of exercise capacity (VO_2max , $p=0.004$) and was independently associated with freedom from all-cause mortality or heart failure admission ($p=0.034$). Patients with exercise EOAI $< 0.9 \text{ cm}^2/\text{m}^2$ (n=14) compared to $\geq 0.9 \text{ cm}^2/\text{m}^2$ (n=25) had a significantly worse outcome ($p=0.048$). In multivariate analysis, AL opening angle at peak exercise ($p=0.037$) was the strongest predictor of exercise EOAI.

Conclusion: In RMA patients, EOA increases during exercise despite fixed annular size. Diastolic AL tethering plays a key role in this dynamic process, with increasing AL opening

during exercise being associated with higher exercise EOA. Indexed EOA at peak exercise is a strong and independent predictor of exercise capacity and is associated with clinical outcome. Our findings stress the importance of maximizing AL opening by targeting the subvalvular apparatus in future repair algorithms for secondary MR.

Introduction

Secondary mitral regurgitation (MR) in ischemic and/or dilated heart disease is associated with an unfavorable prognosis^{11, 18}. Restrictive mitral valve annuloplasty (RMA) has evolved as the gold standard treatment for severe secondary MR^{22, 26, 160, 164}. However, recurrence of MR after RMA has an incidence of approximately 30%³⁴, and mitral valve replacement (MVR) has been proposed as a potential alternative in selected patients^{35, 165-167}. In addition, several studies have demonstrated the occurrence of moderate mitral stenosis (defined as mean transmitral pressure gradient (TMG) >5mmHg or mitral valve area <1.5 cm²) following RMA^{30-32, 161, 168}. Functional mitral stenosis after RMA is generally attributed to undersizing of the annular ring, yet the subvalvular apparatus might play a role as well. Importantly, the impact of such functional mitral stenosis on exercise capacity and clinical outcome remains unclear, mainly because most studies have based stenosis grading on the mean TMG at rest^{31-33, 161, 162, 169}. However, this parameter is certainly flow-dependent, potentially masking severe stenosis in low-flow patients¹⁶⁸. There is currently little data on the use of less flow-dependent parameters such as the effective orifice area (EOA) to quantify stenosis in RMA patients.

The aim of this study was therefore to investigate the hemodynamic, functional and clinical impact of EOA after RMA, and its relationship with diastolic anterior leaflet (AL) tethering at rest and during exercise.

Methods

Study Design & Study Population. We included consecutive patients who underwent RMA with a complete semi-rigid Physioring® (Edwards Lifesciences, Irvine, CA), undersized by 1 or 2 sizes in order to obtain a minimal coaptation length of 8mm in the A2-P2 segment, for secondary MR (Carpentier Class IIIb, i.e. systolic leaflet restriction) between July, 2007, and September, 2012, at a single tertiary care center (Ziekenhuis Oost-Limburg, Genk, Belgium). Exclusion criteria were structural leaflet abnormalities at surgical inspection, inability to undergo a supine bicycle exercise test, more than mild aortic regurgitation (AR, vena contracta width >3mm) and/or more than mild MR recurrence (vena contracta width >3mm) at rest or during exercise. Eligible patients underwent a comprehensive resting transthoracic echocardiography (TTE) examination, followed by a semi-supine symptom-limited bicycle exercise test with concomitantly performed TTE. The study complied with the Declaration of Helsinki, the protocol was approved by the local ethics committee, and written informed consent was obtained from all participating patients.

Echocardiographic measurements. Resting and exercise echocardiography was performed with a commercially available system (Philips Medical Systems, IE33®, Andover, MA). Standard two-dimensional and Doppler images were acquired in the left lateral decubitus position, and stored digitally for offline analysis in the CardioView software (Tomtec Imaging Systems, Unterschleissheim, Germany). All measurements were averaged over 3 consecutive cardiac cycles for patients in sinus rhythm, and 5 consecutive cycles in atrial fibrillation patients according to the guidelines by the American Society of Echocardiography. The modified Simpson's biplane method was used to calculate ejection fraction at rest and peak exercise¹⁷⁰. Peak and mean TMG were calculated using the modified Bernoulli equation on the continuous-wave transmitral Doppler signal with EOA calculated by the continuity equation¹⁷¹. Systolic pulmonary artery pressure (sPAP) was

calculated using the modified Bernoulli equation on the transtricuspid continuous-wave signal, while adding an estimate of right atrial pressure¹⁶³. Since patients with more than mild MR and AR were excluded, mean transmitral flow rate was defined as the ratio of left ventricular (LV) stroke volume (measured from pulsed wave Doppler in the LV outflow tract) over diastolic filling time. During each stage of exercise, LV stroke volume, transmitral flow rate, peak and mean TMG, sPAP, and EOA were assessed. The mitral AL opening angle was measured on 2D TTE in an apical long axis view, both at rest and at peak exercise. Measures were taken at peak E-wave, and the angle of the maximal excursion of the AL was measured with respect to the plane of the prosthetic annular ring (Central Illustration).

Exercise test. All participating patients underwent a symptom-limited graded bicycle test in semi-supine position on a tilting exercise table. Workload was initiated at 20 Watt, with increments of 20 Watt every 3 minutes. In patients with poor general condition, an adjusted protocol was applied with 10 Watt of initial workload and increments of 10 Watt every 3 minutes. Blood-pressure, a 12-lead electrocardiogram, ergospirometry (JAEGER®, Würzburg, Germany) and echocardiography measurements were recorded at each stage.

Clinical endpoints. All-cause mortality and heart failure admissions (defined as hospitalization because of signs or symptoms of congestion warranting treatment with parenteral drugs) were registered in all study patients from the day of surgery until 31 July 2014, yielding a follow-up of at least 20 months post-surgery for every patient. This follow-up included retrospective clinical data collected during the postoperative period prior to the study visit, as well as prospective data from the study visit until 31 July 2014.

Statistical Analysis. Results of continuous variables were expressed as mean \pm standard deviation (SD) if normally distributed or otherwise by median and interquartile range (IQR). Normality was assessed by the Shapiro-Wilk statistic. The paired or unpaired student's t-test and Wilcoxon signed-rank test were used whenever appropriate. Categorical variables

were expressed as percentages and compared using Fisher's Exact test. Linear regression models were used to assess the correlation between TMG, EOA and the square of transmitral flow rate. Predictors of VO₂max and EOA with a p-value <0.1 at univariate analysis were entered in multiple linear regression models. Cox proportional-hazards regression was used to assess variables associated with freedom from all-cause mortality or heart failure readmission since surgery, and variables with p-value <0.1 were entered in a multivariate Cox regression model. Assumption was made that hemodynamic data at the time of study were representative for the entire follow-up period. Cumulative survival rates were calculated according to the Kaplan-Meier method, and groups were compared with the log-rank test. Receiver operating characteristic (ROC) curves were used to determine area under the curve, sensitivity and specificity of different parameters and cut-offs for the prediction of impaired exercise capacity (VO₂max <15mL/kg/min). Statistical significance was always set at a two-tailed probability of p<0.05. All statistical analyses were performed using the Statistical Package for Social Sciences release 20.0 (SPSS Inc., Chicago, Illinois, USA).

Results

Patient population. Of 103 screened patients, 27 patients had died. Nine were excluded because of structural leaflet abnormalities at surgical inspection, and 24 patients did not perform an exercise test due to various reasons, i.e. orthopedic or neurological limitations (n=9), distance to hospital (n=3), or refusal to participate (n=12). Four patients were excluded from the analyses because they had recurrent MR and/or AR at rest or during exercise at the time of the study visit. Accordingly, the final study population consisted of 39 patients. Table 3.1 summarizes their baseline characteristics. None of the study patients had angina pectoris at rest or during the exercise test, there were no new ischemic alterations on the 12-lead ECG monitoring during exercise, and no obvious new wall motion abnormalities were observed at peak exercise in standard apical views.

Transmitral pressure-flow relationship at rest and during exercise.

Echocardiographic measures at rest and at maximal exercise for all 39 patients after mean follow-up of 33±17 months are presented in Table 3.2. Mean and peak TMG, cardiac output and sPAP increased significantly during exercise. The evolution of the mean TMG with respect to cardiac output at each stage of exercise is displayed in Figure 3.1-A. There was a strong and significant correlation between the mean TMG and the square of the cardiac output ($r=0.81$, $p<0.001$), as as the square of the transmitral flow rate ($r=0.81$, $p<0.001$, Figure 3.1-B). This quadratic relationship is in agreement with fundamental hydraulic notions derived from the Bernoulli equation and the principle of continuity, in which the pressure gradient ΔP across a stenotic orifice EOA is known to be a function of the flow rate F squared ^{172, 173}, as displayed in equations (1)-(2).

$$EOA = \frac{F}{50.4 \sqrt{\Delta P}} \quad (1)$$

$$\Delta P = \left(\frac{F}{50.4 * EOA} \right)^2 \quad (2)$$

A display of this theoretical hydraulic relationship for various EOA-orifices ranging from 0.5cm² to 3.5cm² is superposed in Figure 3.1-B.

Relationship between transmitral flow rate and EOA. The average EOA at rest was $1.5 \pm 0.4\text{cm}^2$ (EOA indexed for body surface area or EOAI $0.8 \pm 0.2\text{cm}^2/\text{m}^2$) in RMA patients. Based on this resting value and assuming a constant EOA, the expected mean TMG at maximal flow rate, would be much higher than the observed mean gradient at maximal flow rate. During exercise however an increase in EOA was observed with increasing flow rate (quadratic correlation: $r=0.78$, $p<0.001$, Figure 3.2). EOA at maximal exercise was $2.0 \pm 0.5\text{cm}^2$ (EOAI $1.0 \pm 0.3\text{cm}^2/\text{m}^2$, $p<0.001$ for the change from rest).

Diastolic AL opening angle. The AL opening angle at rest ($68 \pm 10^\circ$) showed a moderate correlation with EOA at rest ($r=0.4$, $p=0.014$). However, exercise EOA was much better correlated to AL opening angle at peak exercise ($r=0.6$, $p<0.001$). Larger increases in AL opening angle during exercise were associated with higher relative increases in EOA ($r=0.42$, $p=0.001$). Univariate linear regression identified annuloplasty ring size ($r=0.4$, $p=0.007$), AL opening angle at peak exercise ($r=0.6$, $p<0.001$) and peak cardiac output ($r=0.5$, $p=0.002$) as determinants of EOAI at peak exercise. In the multivariate model, AL opening angle at peak exercise ($p=0.037$) remained the strongest determinant of EOAI, independently from ring size ($p=0.087$) and peak cardiac output ($p=0.137$).

Table 3.1 - Baseline characteristics

Variables	RMA patients (n=39)
Age at surgery, years	63±11
Male gender	30(77%)
Body surface area, m ²	1.88±0.17
Preoperative NYHA functional class, I/II/III/IV	1/12/21/5
Preoperative LV ejection fraction, %	40±12
Preoperative LV end diastolic volume, mL	153±57
Preoperative LV end systolic volume, mL	93±48
Preoperative sPAP, mmHg	50±12
Diabetes	12(31%)
Etiology of functional MR	
Ischemic	34(87%)
Non-ischemic dilated	5(13%)
Operative data	
Aortic clamp time, min	160±46
Physioring size, measured, 28/30/32/34/36/38	4/15/9/6/4/1
Physioring size, implanted, 24/26/28/30/32/34	3/10/12/7/5/2
Postoperative A2-P2 coaptation length, mm	8.6(7.7-9.0)
+ TVP	19(49%)
+ CABG	29(74%)
Study visit	
Time since surgery, months	33±17
Atrial fibrillation	4(10%)
NYHA functional class, I/II/III/IV	18/17/4/0

CABG, coronary artery bypass graft; LV, left ventricular; MR, mitral regurgitation; NYHA, New York Heart Association; sPAP, pulmonary artery pressure; TVP, tricuspid valve annuloplasty;

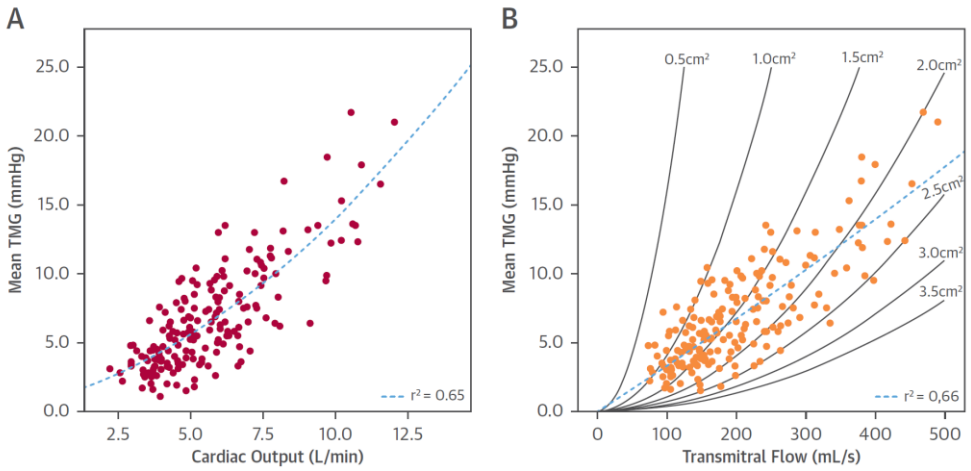


Figure 3.1 - Transmittal pressure-flow relationship during exercise. The mean TMG as a function of cardiac output (A) and transmittal flow (B) in RMA patients. Theoretical pressure-flow curves for fixed effective orifices ranging from 0.5 cm^2 to 3.5 cm^2 are superposed in B.

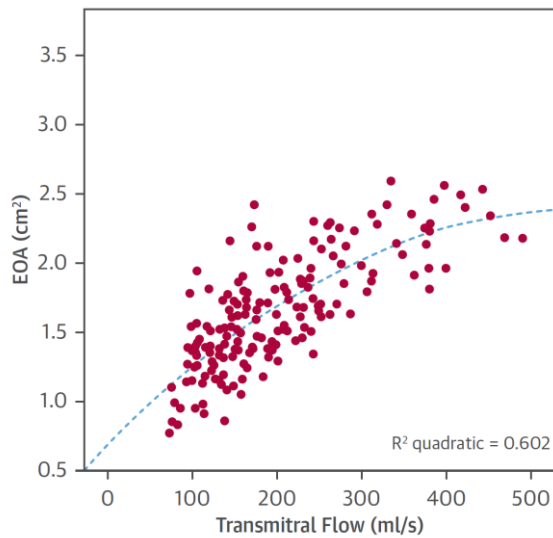


Figure 3.2 – EOA as a function of transmittal flow rate. Effective orifice area (EOA) as measured at each step of exercise with respect to the transmittal flow rate. A quadratic correlation curve is superposed as a dashed line.

Table 3.2 - Resting and exercise doppler echocardiography

Variables	Resting	Peak exercise	p-value
Heart rate, bpm	64±11	101±21	p<0.001
Stroke volume, mL/beat	64±12	72±18	p<0.001
Cardiac output, L/min	4.0±0.8	6.9±2.2	p<0.001
LV ejection fraction, %	50±13	56±14	P<0.001
LV end diastolic volume, mL	121±40	127±38	p=0.04
LV end systolic volume, mL	64±37	59±36	p=0.01
Mean transmitral flow rate, mL/s	132±41	263±99	p<0.001
Mean transmitral gradient, mmHg	4.1±1.9	9.4±4.6	p<0.001
Peak transmitral gradient, mmHg	10.8±3.8	18.4±6.4	p<0.001
EOA, cm ²	1.5±0.4	2.0±0.5	p<0.001
indexed EOA, cm ² /m ²	0.8±0.2	1.0±0.3	p<0.001
sPAP, mmHg †	40±15	54±16	p<0.001

LV, left ventricular; MR, mitral regurgitation; EAO, effective orifice area; sPAP, systolic pulmonary artery pressure;

† Echocardiographic assessment of sPAP during exercise only successful in n=33 due to absence of measurable tricuspid regurgitant signal in n=6.

Table 3.3 - Predictors of clinical endpoint on univariate and multivariate Cox regression analysis.

Parameter	Univariate analysis			Multivariate analysis		
	Hazard ratio	95% CI	P-value	Hazard ratio	95% CI	P-value
Age	1.09	1.02-1.17	0.013	1.09	1.02-1.17	0.008
Male gender	0.74	0.20-2.70	0.653			
Ring size	0.84	0.65-1.08	0.167			
Aortic clamp time	0.99	0.98-1.01	0.215			
Diabetes	2.05	0.65-6.50	0.222			
Atrial fibrillation	0.89	0.11-6.90	0.908			
LV end-diastolic volume	1.0	0.98-1.01	0.793			
LV end-systolic volume	1.0	0.99-1.02	0.944			
LV ejection fraction	0.99	0.95-1.04	0.770			
Cardiac output	0.52	0.23-1.14	0.103			
EOAi at rest	0.11	0.01-3.35	0.203			
EOAi at peak exercise	0.11	0.01-1.36	0.086	0.08	0.01-0.84	0.034
Mean TMG at rest	0.80	0.56-1.14	0.211			
Peak TMG at rest	0.95	0.82-1.10	0.492			

Impact of EOAI on exercise capacity and clinical outcome. VO₂max was 15.2±4.3mL/kg/min in the population overall. In multivariate analysis, patient age (p=0.004) and exercise EOAI (p=0.004) emerged as independent predictors of VO₂max. At a cut-off value of 0.9cm²/m², exercise EOAI (area under the curve 0.750) had 86% sensitivity and 62% specificity to predict an exercise capacity lower than 15mL/kg/min. During the entire follow-up period (55±16 months) 11 patients were admitted for decompensated heart failure, and 2 patients died. In a multivariate Cox regression model to assess freedom from all-cause mortality or heart failure admission (Table 3.3) exercise EOAI (p=0.034) and age (p=0.008) were independently associated with outcome. Patients

with exercise EOAi below the above-mentioned cut-off of $0.9\text{cm}^2/\text{m}^2$ ($n=14$) had significantly worse outcome than patients with higher exercise EOAi ($n=25$), as shown in Figure 3.3.

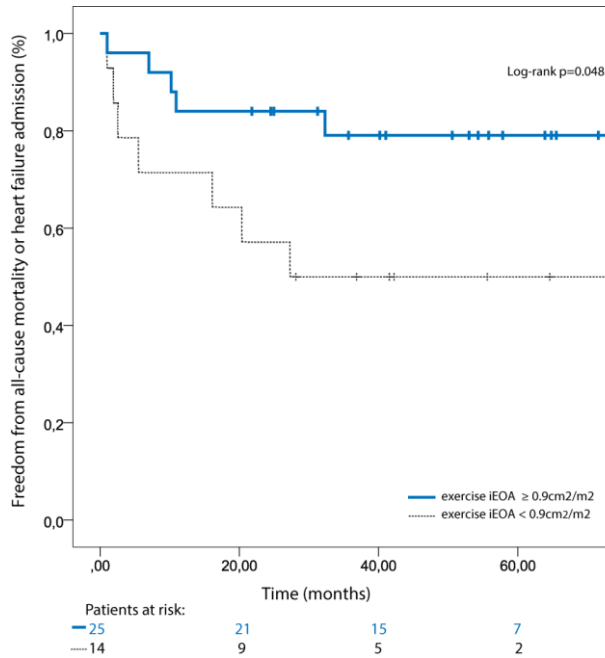


Figure 3.3 – Clinical outcome: freedom from all-cause mortality or heart failure admission in patients with respect to an exercise EOAi cut-off value of $0.9\text{cm}^2/\text{m}^2$. Kaplan Meier cumulative survival curve for freedom from all-cause mortality or heart failure admission in patients with exercise $\text{EOAi} \geq 0.9\text{cm}^2/\text{m}^2$ (blue line) versus patients with exercise $\text{EOAi} < 0.9\text{cm}^2/\text{m}^2$ (dashed line). Crosses indicate that patients' data were censored at that point.

Discussion

This study quantified the transmitral pressure-flow relationship in secondary MR patients treated with RMA, and demonstrated an increase in EOA during exercise. Exercise EOA_i was independently associated with outcome and was a stronger predictor of exercise capacity than was EOA_i at rest, stressing the importance of exercise echocardiography in this patient population. In addition, our findings challenge the concept that functional mitral stenosis from RMA for secondary MR solely results from a small annular size. If that were the case, the stenotic valve area would be fixed and less responsive to exercise. Instead, our findings suggest that the observed stenosis after RMA has an important subvalvular component as well (on top of ring size), dictated by the diastolic restriction of anterior leaflet opening, likely due to diastolic leaflet tethering.

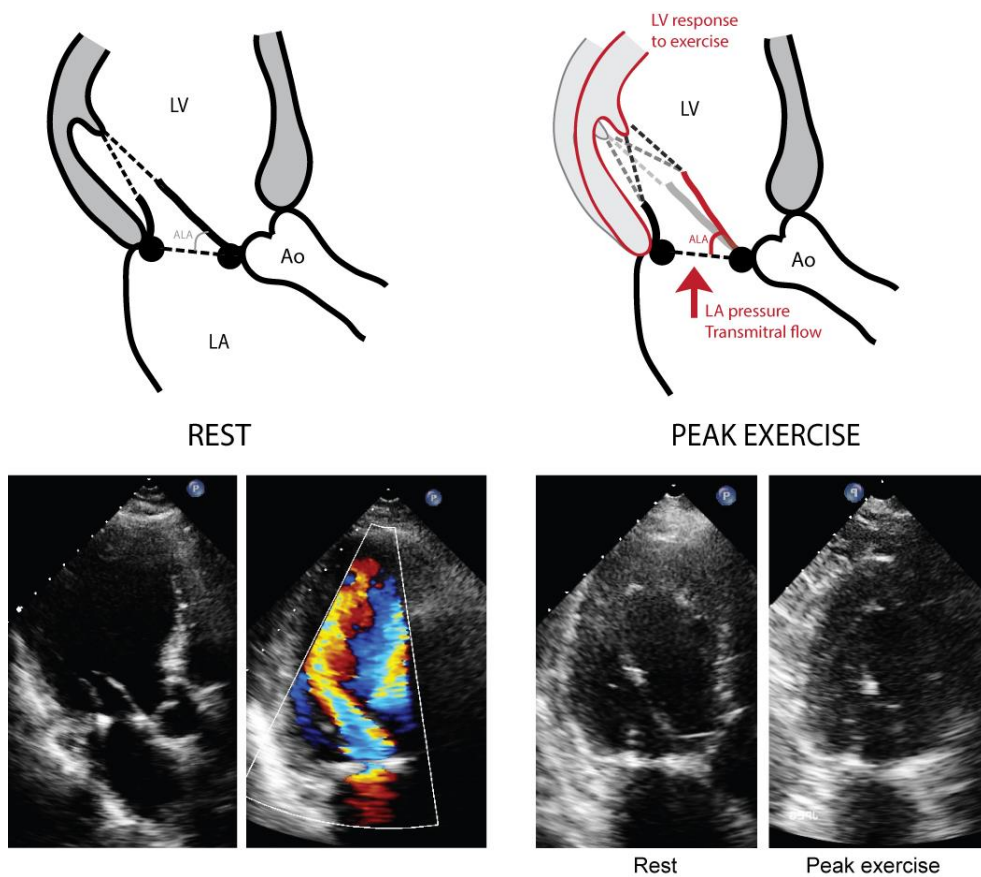
Diastolic leaflet tethering: pathophysiologic insights.

Secondary MR results from LV motion abnormalities and/or dilation, causing an imbalance between closing forces and papillary muscle tethering, thereby interfering with normal systolic coaptation²³. These 'culprit' LV abnormalities have diastolic implications as well, not only impairing LV relaxation but also inhibiting diastolic leaflet opening due to severe leaflet tethering. This phenomenon can be aggravated by insertion of a prosthetic ring, anteriorly displacing the posterior annulus and increasing the importance of the AL during diastole (which then acts like the lid of a pedal waste bin). AL tethering due to papillary muscle displacement decreases the opening angle of this lid and obstructs inflow (Figure 3.3). During exercise, increasing flow and left atrial pressure might (in part) overcome the tethering force and increase the opening angle to some extent. Importantly however, the AL 'opening reserve' might also be determined by the LV response to exercise³³. In patients with a positive LV response, i.e. a significant decrease in LV end-systolic volume, papillary muscle tethering decreases and AL opening and EOA increase (Central Illustration).

Importantly, increasing the AL opening angle will not only increase the geometric orifice area at the tip of the restricted leaflets, but has an impact on the coefficient of flow contraction as well. An alteration of the inflow angulation during exercise, due to a conformational change in the subvalvular apparatus, is known to increase the coefficient of contraction¹⁷⁴. Thus, any exercise-induced increase in leaflet angulation will both result in an increase in geometric orifice area, as well as an increase in the coefficient of contraction, compounding the effect on effective orifice area.

Comparison with previous work (Table 3.4).

In a similar RMA population Magne et al. also observed a significant increase in EOA during exercise with a concomitant rise in LV ejection fraction³⁰. Kubota et al. on the other hand observed a significant decrease in EOA during exercise after RMA³³. However, LV contractile reserve was severely impaired in this population with the ejection fraction decreasing during exercise. Moreover, the Kubota study suggested diastolic subvalvular tethering as an important contributor to functional mitral stenosis post-RMA. Finally, Fino et al. found no exercise-induced increase in EOA in RMA patients despite an increase in ejection fraction¹⁴³. Increasing ejection fraction during exercise however might be characterized by increased LV end-diastolic volume rather than a decrease in end-systolic volume. This might have caused a difference in exercise tethering in the Fino patient group as compared to the RMA population of Magne and the present study. Moreover, in the Fino patient group as well, exercise EOAI was an independent predictor of exercise sPAP (as a surrogate of exercise capacity).



Central Illustration. Mitral valve area during exercise after restrictive annuloplasty:

Mechanistic insights and clinical impact. At rest, diastolic AL tethering plays a role in the postoperative mitral stenosis due to restriction of leaflet opening and deviation of blood flow. During exercise, increases in LA pressure and flow as well as a positive LV response (i.e. a decrease in LV end-systolic volume) can augment the opening of the leaflet, thereby increasing EOA. Transthoracic echocardiographic images in apical long-axis view show the typical diastolic inflow restriction in a restrictive mitral valve annuloplasty patient with and without color Doppler flow. *Ao, aorta; ALA, anterior leaflet angle; LA, left atrium; LV, left ventricle.*

Table 3.4 - Comparison with previous exercise studies following RMA using Physioring I.

Author, Year, Ref.	n		Median ring size	Mean TMG (mmHg)	Peak TMG (mmHg)	CO (L/min)	EOA (cm ²)	sPAP (mmHg)	LVEF (%)
Present study	39	resting	28	4.1±1.9	10.8±3.8	4.0±0.8	1.5±0.4	40±15	50±13
	39	ESE		9.4±4.6	18.4±6.4	6.9±2.2	2.0±0.5	54±16	56±14
Magne et al., 2008, 30	24	resting	26	6±2	13±4	4.6±1.2	1.5±0.3	42±13	43±11
	24	DSE		8±3	19±6	7.8±1.6	1.8±0.3	58±12	56±13
	9	ESE		14.4±5	24±7	8.5±1.2	1.7±0.3	69±14	58±10
Kubota et al., 2010, 33	31	resting	28	3.5±2.7	10.6±6.2	-	1.6±0.2	-	42±13
	12	ESE		6.0±2.2	18.5±6.2	-	1.4±0.2		42±12
Fino et al, 2014 ¹⁴³	57	resting	28	4.5±1.3	8.6±2.6	4.6±1.0	1.8±0.5	38±7	40±4
	57	ESE		11±3.7	19.7±6.6	7.6±1.3	1.8±0.4	55±11	49±6

ESE, exercise stress echocardiography; DSE, dobutamine stress echocardiography; CO, cardiac output; EOA, effective orifice area; sPAP, systolic pulmonary artery pressure; TMG,transmitral gradient; LVEF, left ventricular ejection fraction.

In MVR patients, severe valve prosthesis-patient mismatch (defined as EOA_i <0.9cm²/m²) is known to be associated with postoperative pulmonary hypertension and worse outcomes ^{142, 175}. Our findings indicate that similar mismatch hemodynamics and physiology can also be observed in patients following RMA, with two important differences however: (1) not EOA_i at rest but at peak exercise was an independent predictor of outcome in RMA patients. We hypothesize that in MVR patients the EOA is fixed during exercise, and therefore is an identical predictor of outcome both at rest and peak exercise. (2) As the mechanism of inflow obstruction is related to diastolic leaflet restriction, patients with adverse remodeling and LV dilation will have the lowest EOA_i at peak exercise further aggravating exercise capacity and outcome in a vicious cycle. This might explain the independently strong association between exercise EOA_i, exercise capacity and outcome in this small sample population.

Clinical implications.

The demonstration of a dynamic mitral valve area in RMA patients due to diastolic leaflet restriction may add important insights with respect to functional capacity, exercise hemodynamics and treatment options in this patient population. First, the increase in TMG during exercise is more attenuated in RMA patients compared to patients with similar resting hemodynamics but with a more fixed orifice, as seen in organic mitral stenosis^{176, 177} and mechanical MVR¹⁷⁸. When describing and grading the degree of functional stenosis following RMA based on resting data alone, it is important to realize the possible dynamic behavior of the EOA, especially in patients with beneficial LV remodeling. In case of doubt, exercise echocardiography with assessment of EOA at peak exercise should be applied. Secondly, our findings strongly support further research of concomitant subvalvular procedures for secondary MR patients in order to relieve leaflet tethering. Prior studies have demonstrated that ongoing leaflet tethering is involved in the mechanism of MR recurrence^{36, 179}. Our study shows leaflet tethering probably plays a role in diastolic inflow restriction as well. Relieving tethering might therefore increase repair durability, reduce the degree of undersizing needed to obtain the target coaptation length and reduce the functional stenosis after surgery. Importantly, it should be noted that the increase in EOA tended to reach a plateau (2.0-2.5cm²) at higher flow rates. We hypothesize this plateau is influenced by the effective orifice of the ring in the absence of leaflet tethering. Indeed, in multivariate analysis, ring size remained associated with exercise EOA, independently from leaflet angle. Therefore, all efforts that could assure a durable repair while relieving tethering and increasing annuloplasty ring size should be subject to further research.

Study limitations

First, this was a single center study with limited sample size and small endpoint count (i.e. risk of over-fitting the Cox regression model). Therefore, our results should be considered hypothesis-generating. Second, clinical follow-up for outcome analysis started immediately

postoperative and thus preceded the exercise study visit. We assumed the hemodynamic and functional measures at the study visit are representative for the entire postoperative follow-up period. This assumption is based on prior RMA studies demonstrating stable hemodynamics (mean transmitral gradient at rest) from early postoperative till 18month follow-up²⁶, as well as evidence of early postoperative improvement in NYHA functional class that remains stable for up to seven years of follow-up in patients undergoing CABG with mitral valve annuloplasty for secondary MR ²⁹. Finally, it should be noted that patients with recurrent MR post-RMA at rest or during exercise were excluded from analysis to assure validity of the continuity equation. As the mechanism of MR recurrence is commonly related to ongoing leaflet tethering³⁶ and restricted leaflet motion¹⁷⁹, one could hypothesize the change in EOA and AL opening angle with increasing flow would be more limited or even negative in these excluded patients.

Conclusions

This study demonstrated that in secondary MR patients following RMA, the EOA increases with increasing transmitral flow rate despite fixed annular size. Diastolic AL tethering plays a key role in this dynamic process, with increasing AL opening during exercise being associated with higher exercise EOA. Indexed EOA at peak exercise is a strong and independent predictor of exercise capacity and is independently associated with outcome. Our findings stress the importance of maximizing AL mobility by targeting the subvalvular apparatus in future repair algorithms for secondary MR.

Chapter 4

Effective Orifice Area During Exercise After Mechanical Valve Replacement.

Bertrand PB, Pettinari M, De Cannière H, Smeets CJ, Gutermann H, Verhaert D, Dion RA,
Verdonck PR, Vandervoort PM

Status of the manuscript:

Submitted

J Am Soc Echocardiogr (IF 4.1)

Abstract

Objective: To investigate the evolution of the transprosthetic pressure gradient and effective orifice area (EOA) during dynamic bicycle exercise in bileaflet mechanical heart valves, and to explore the relationship with exercise capacity.

Methods: Patients with bileaflet aortic valve replacement (AVR, n=23) and mitral valve replacement (MVR, n=16) underwent a symptom-limited supine bicycle exercise test with Doppler echocardiography and respiratory gas analysis. Transprosthetic flow rate, peak and mean transprosthetic gradient, EOA, and systolic pulmonary artery pressure were assessed at different stages of exercise.

Results: EOA at rest, mid-exercise and peak exercise was $1.66 \pm 0.23 \text{cm}^2$, $1.56 \pm 0.30 \text{cm}^2$ and $1.61 \pm 0.28 \text{cm}^2$ respectively ($p=0.004$) in AVR patients, and $1.40 \pm 0.21 \text{cm}^2$, $1.46 \pm 0.27 \text{cm}^2$ and $1.48 \pm 0.25 \text{cm}^2$ respectively ($p=0.160$) in MVR patients. During exercise, the mean transprosthetic gradient and the square of transprosthetic flow rate were strongly correlated ($r=0.65$, $p<0.001$, and $r=0.84$, $p<0.001$ for AVR and MVR respectively), conform fundamental hydraulic principles for fixed orifices. Indexed EOA at rest was strongly correlated to exercise capacity (VO_2max) in MVR patients only (Spearman's $\rho=0.68$, $p=0.004$). In the latter group, systolic pulmonary artery pressures during exercise were strongly correlated to the peak transmitral gradient ($\rho=0.72$, $p<0.001$).

Conclusion: In bileaflet mechanical valve prostheses, there is no clinically relevant increase in EOA during dynamic exercise. Transprosthetic gradients during exercise closely adhere to the fundamental pressure-flow relationship and are therefore predictable from the evaluation at rest. Indexed EOA at rest is a strong predictor of exercise capacity in MVR patients. This should be taken into account in the therapeutic decision-making and prosthesis selection in young and dynamic patients.

Introduction

Mechanical valve prostheses are the prostheses of choice for aortic valve replacement (AVR) and mitral valve replacement (MVR) in young patients (<60 years and <65 years old for AVR and MVR respectively) if long-term anticoagulation is not contraindicated^{22, 180}. In this young and dynamic population optimal performance of the prosthesis is required not only at rest but during physical activities as well¹⁸¹. Knowledge of the hemodynamic behavior of these mechanical valve prostheses during dynamic exercise, with increasing heart rate and flow, therefore remains of timely importance. Although the geometric orifice area of a mechanical prosthesis is fixed, the orifice area that is effectively used by the flow (effective orifice area, EOA) exerts large interindividual variation for the same prosthesis size^{182, 183}, and is significantly lower than the geometric area for aortic and mitral valve prostheses^{184, 185}. It remains unclear whether EOA during dynamic exercise is fixed as well, or whether some degree of effective orifice 'opening reserve' is present, attenuating the rise in transprosthetic pressure gradients at increasing flow rate. Pulsatile *in vitro* assessment of mechanical valves in aortic position showed no change in EOA with increasing stroke volume¹⁸⁶. However, *in vivo* studies measuring EOA before and after dynamic exercise^{178, 187}, during dobutamine infusion^{188, 189}, or during rapid ventricular pacing¹⁹⁰ have rendered conflicting results in both mitral and aortic position.

The aim of this study was to investigate *in vivo* the step-wise evolution of the transprosthetic pressure gradient and EOA during dynamic bicycle exercise in bileaflet mechanical heart valves, in both mitral and aortic valve position. In addition, the impact of EOA at rest and during exercise on the respective exercise capacity was evaluated.

Methods

Study design & population. Consecutive patients that underwent mechanical bileaflet AVR at a single tertiary care center (Ziekenhuis Oost-Limburg, Genk, Belgium) between January 2008 and August 2014 (n=42) were screened for participation in the study protocol. In addition, all patients with St-Jude Medical (St. Paul, MN) bileaflet mitral prostheses that were in active out-patient follow-up at our center on 1 October 2012 (n=34) were screened for participation. Eligible patients were invited to undergo a single study visit comprising a resting transthoracic echocardiography (TTE) followed by a semi-supine bicycle exercise TTE with cardiopulmonary exercise testing. Exclusion criteria were (1) inability to undergo a bicycle exercise test at our center, (2) more than mild aortic regurgitation (vena contracta width >3mm), and (3) subaortic stenosis or left ventricular outflow tract (LVOT) obstruction impeding correct Doppler assessment of LV stroke volume. The study complied with the declaration of Helsinki, was approved by the local ethics committee, and written informed consent was obtained from all participating patients.

TTE. Resting and exercise echocardiography was performed with a commercially available system (Philips Medical Systems, IE33®, Andover, MA). Standard two dimensional and Doppler echocardiographic images were acquired in the left lateral decubitus position using a phased-array transducer in the parasternal and apical views, and stored digitally for offline analysis in the CardioView software (Tomtec Imaging Systems, Unterschleissheim, Germany). Each echocardiographic measurement was averaged from 3 consecutive cardiac cycles for patients in sinus rhythm, and from 5 consecutive cycles in atrial fibrillation patients. Left ventricular outflow tract (LVOT) dimension was measured from a zoomed parasternal long axis acquisition. LV volumes and ejection fraction were calculated using the modified Simpson's biplane method for apical windows¹⁷⁰. LV stroke volume was measured by pulsed-wave Doppler in the LVOT; cardiac output was calculated as the product of heart

rate and LV stroke volume. Color Doppler flow images were obtained in the parasternal and apical views to assess valve regurgitation. Peak and mean transprosthetic gradients were calculated using the modified Bernoulli equation on the continuous-wave transprosthetic Doppler signal. Importantly, care was taken to acquire the continuous-wave Doppler velocities through the side orifices of the bileaflet prosthesis whenever possible and not through the central orifice because of the higher pressure recovery phenomenon¹⁹¹. Prosthetic valve EOA was measured by the continuity equation¹⁷¹, i.e. dividing LV stroke volume by the velocity time integral of the transprosthetic flow. Since patients with more than mild AR were excluded, mean transmitral flow rate was estimated by dividing the LV stroke volume by the diastolic filling time measured on Doppler echocardiography. Mean transaortic flow rate was calculated by dividing LV stroke volume by the systolic ejection time. Systolic pulmonary artery pressure (PAP) was calculated using the modified Bernoulli equation on the transtricuspid continuous-wave Doppler signal, while adding an estimate of right atrial pressure¹⁶³.

Exercise test. All participating patients underwent a symptom-limited graded bicycle test in semi-supine position on a tilting exercise table. Workload was initiated at 20 Watt, with increments of 20 Watt every 3 minutes. At each stage of exercise, Doppler echocardiography assessing LV stroke volume, peak and mean transprosthetic gradient, EOA, transprosthetic flow rate and systolic PAP was performed. In addition, blood pressure, 12-lead electrocardiogram and ergospirometry (JAEGER®, Würzburg, Germany) was measured throughout the exercise test.

Statistical Analysis. Results of continuous variables were expressed as mean \pm standard deviation (SD) if normally distributed or otherwise by median and interquartile range (IQR). Normality was assessed by the Shapiro-Wilk statistic. Repeated measures analysis of variance (ANOVA) was used to compare Doppler hemodynamics at rest, mid-exercise and

peak-exercise. Linear regression models were used to assess the relationship between the mean transprosthetic gradient and the square of transprosthetic flow rate. Spearman's rho (ρ) was used to assess potential correlations between indexed EOA and exercise capacity in AVR and MVR patients. Statistical significance was set at a two-tailed probability of $p < 0.05$. All statistical analyses were performed using the Statistical Package for Social Sciences release 20.0 (SPSS Inc., Chicago, Illinois, USA).

Results

Study population. Of the 42 screened AVR patients, a total of 24 patients was able to participate. Reasons for exclusion in 18 patients was refusal to participate, lost to follow-up, or distance to the hospital. In addition, one participating patient was excluded because of LVOT obstruction with significant flow acceleration during the exercise test. Of the 34 screened MVR patients, 16 patients were eligible for study participation. Reasons for exclusion were aortic regurgitation (n=2), refusal to participate (n=9) and inability to exercise (n=7). Accordingly, the final study population consisted of 23 AVR patients and 16 MVR patients. Table 4.1 summarizes the patient characteristics of the two study groups. The studied valves were all St. Jude Medical bileaflet mechanical valve prostheses of different sizes.

Doppler echocardiography during exercise. Echocardiography measurements at rest, at mid-exercise (defined as half of the maximal workload achieved) and at maximal exercise are presented in Table 4.2 and 4.3 for AVR and MVR patients respectively. Heart rate, cardiac output, transprosthetic flow and transprosthetic gradients all increased significantly during exercise. The evolution of the mean transprosthetic gradient with respect to cardiac output at each stage of exercise is displayed in Figure 4.1. There was a significant relationship between the mean pressure gradient and the square of the cardiac output in AVR ($r=0.64$, $p<0.001$) and MVR ($r=0.82$, $p<0.001$) patients. Similarly, a significant relationship was observed between mean gradient and the square of the transprosthetic flow rate in both patient groups ($r=0.65$, $p<0.001$, and $r=0.84$, $p<0.001$ respectively), as shown in Figure 4.2.

Table 4.1 – Patient characteristics

Variables	AVR group	MVR group
n	23	16
Age at study visit, years	51±10	63±8
Male gender	16 (70%)	6 (36%)
Body surface area, m ²	1.95±0.20	1.88±0.20
Mitral valve disease		
Carpentier class, II/IIIa/IIIb	NA	2/12/2
Aortic valve disease		
stenosis/regurgitation/mixed	7/6/10	NA
bicuspid aortic valve disease	16 (70%)	NA
Operative data		
Aortic clamp time, min	122±35	152±51
SJM bileaflet MVR size, 25/27/29/31mm	NA	1/4/7/4
SJM bileaflet AVR size, 19/21/23/25/27mm	1/3/9/8/2	NA
+ aortic root replacement (Bentall)	7 (29%)	NA
+ CABG	5 (21%)	5 (31%)
Study visit		
Time since surgery, months	31±19	51(31-77)
Atrial fibrillation	2 (9%)	10 (63%)
NYHA functional class I/II/III	16/6/1	9/6/1
LV ejection fraction, %	62±9	58±8
LV end-diastolic volume, mL	107±29	91±32
LV end-systolic volume, mL	42±18	40±22
Maximal oxygen uptake (VO ₂ max), mL/kg/min	21.4±5.4	14.4±2.7

NA, not applicable; SJM, St Jude Medical; MVR, mitral valve replacement; AVR, aortic valve replacement; NYHA, New York Heart Association; LV, left ventricular; TVP, tricuspid valve annuloplasty; CABG, coronary artery bypass graft;

Table 4.2 – Exercise doppler echocardiography in AVR patients

Variables	Resting	Mid-Exercise	Peak exercise	ANOVA
Workload (W)	-	54±20	104±40	
Heart rate, bpm	72±13	106±11	141±22	p<0.001
Mean transaortic gradient, mmHg	11.0±3.2	16.1±5.6	19.3±8.1	p<0.001
Peak transaortic gradient, mmHg	21.3±6.0	30.6±11.0	37.4±14.8	p<0.001
Peak transaortic velocity, m/s	2.3±0.4	2.7±0.5	3.0±0.6	p<0.001
Stroke Volume, mL	67±10	73±14	67±14	p=0.041
Cardiac output, L/min	4.8±1.0	7.6±1.5	9.4±2.3	p<0.001
Mean transaortic flow rate, mL/s	238±41	285±62	322±83	p<0.001
Effective orifice area, cm ²	1.66±0.27	1.56±0.30	1.61±0.28	p=0.004
Indexed effective orifice area, cm ² /m ²	0.86±0.16	0.80±0.15	0.83±0.16	p=0.003

Table 4.3 – Exercise doppler echocardiography in MVR patients

Variables	Resting	Mid-Exercise	Peak exercise	ANOVA
Workload (W)	-	34±12	64±21	
Heart rate, bpm	71±14	93±18	116±33	p<0.001
Mean transmitral gradient, mmHg	5.8±1.6	10.9±4.2	15.1±6.5	p<0.001
Peak transmitral gradient, mmHg	15.0±3.4	23.0±4.8	27.2±6.7	p<0.001
Systolic PAP, mmHg*	41±9	55±8	64±11	p<0.001
Stroke Volume, mL	58±10	59±10	56±10	p=0.37
Cardiac output, L/min	4.0±0.5	5.5±1.5	6.4±1.9	p<0.001
Mean transmitral flow, mL/s	150±37	225±76	272±89	p<0.001
Effective orifice area, cm ²	1.40±0.21	1.46±0.27	1.48±0.25	p=0.16
Indexed effective orifice area, cm ² /m ²	0.75±0.13	0.78±0.15	0.78±0.11	p=0.21

PAP, pulmonary artery pressure; ANOVA, analysis of variance;

*unable to measure reliable systolic PAP at rest and/or during exercise in n=2 patients.

Transprosthetic pressure-flow relationship. The observed relationship between gradient and flow in Figure 4.1 and 4.2 is in agreement with fundamental hydraulic notions derived from the Bernoulli equation and the principle of continuity, as described earlier^{139, 173}. Briefly, the pressure gradient ΔP across an effective stenotic orifice EOA is a function of the flow rate F squared^{172, 173}, as displayed in Equation (1). The numeric constant 50.4 in this equation results from the conversion of pressure metric units from dyne/cm² to mmHg and includes blood density¹⁷³.

$$\Delta P = \left(\frac{F}{50.4 * EOA} \right)^2 \quad (1)$$

A display of this theoretical relationship for various EOA ranging from 0.5cm² to 3.5cm² is superposed in Figure 4.2. Subdivision of the data according to the size of prosthetic valve in Figure 4.2 demonstrates a close adherence to the theoretical flow-pressure relationship during dynamic exercise in both AVR and MVR patients.

Effect of dynamic exercise on the prosthetic EOA. EOA at rest was 1.66±0.23cm² in AVR patients, and 1.40±0.23cm² in MVR patients. During exercise, a small - yet significant - decrease in EOA was observed in AVR patients at mid-exercise and peak exercise (p=0.004), whereas in MVR patients no difference in EOA could be demonstrated at mid and peak exercise (p=0.17) (Figure 4.3, Table 4.2).

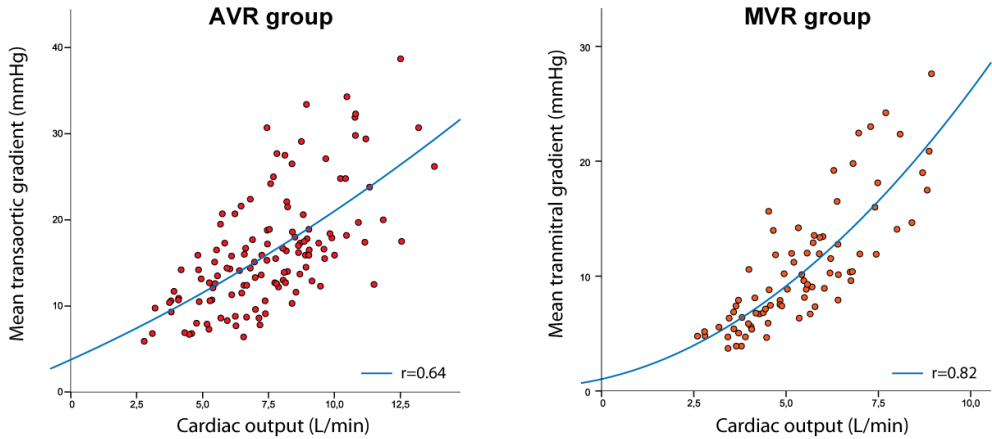


Figure 4.1 – Evolution of the mean transprosthetic gradient with increasing cardiac output in aortic valve (*left*) and mitral valve replacement (*right*) patients at each point of exercise. A quadratic correlation curve for both groups of patients ($r=0.64$, $p<0.001$ and $r=0.82$, $p<0.001$ respectively) is displayed.

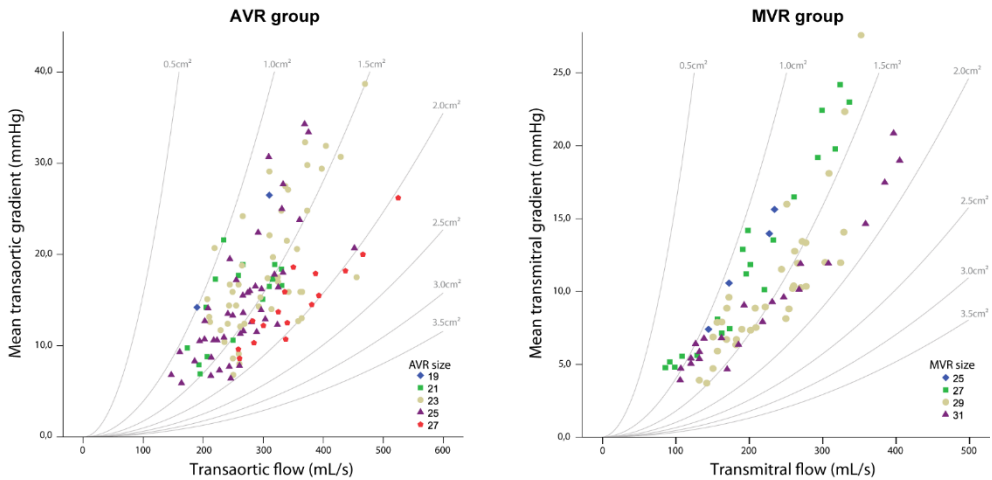


Figure 4.2 – Evolution of the mean transprosthetic gradient with increasing transprosthetic flow rate in aortic valve (*left*) and mitral valve replacement (*right*) patients at each point of exercise. Theoretical pressure-flow curves for fixed effective orifices ranging from 0.5cm² to 3.5cm² are displayed. Different valve sizes are discriminated by color codes.

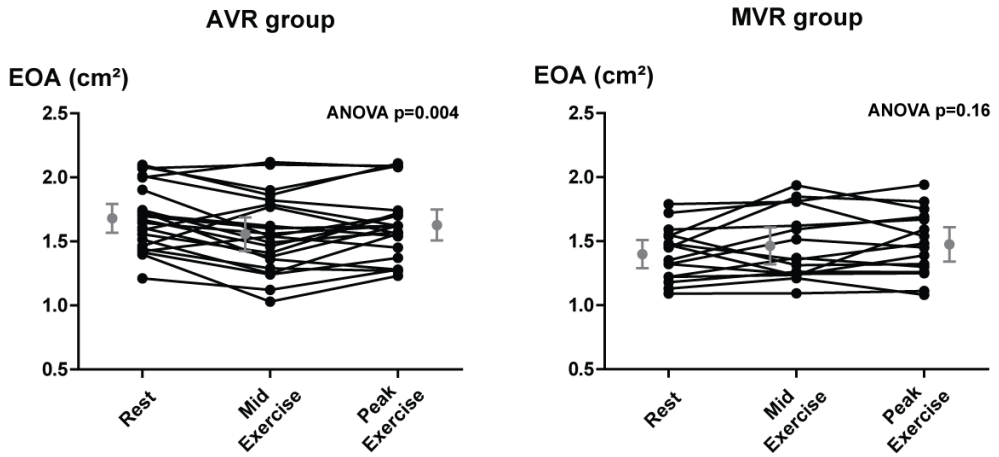


Figure 4.3 – Effective orifice area (EOA) at rest, mid-exercise and peak exercise in aortic valve (*left*) and mitral valve replacement (*right*) patients. Error bars indicate 95% confidence interval.

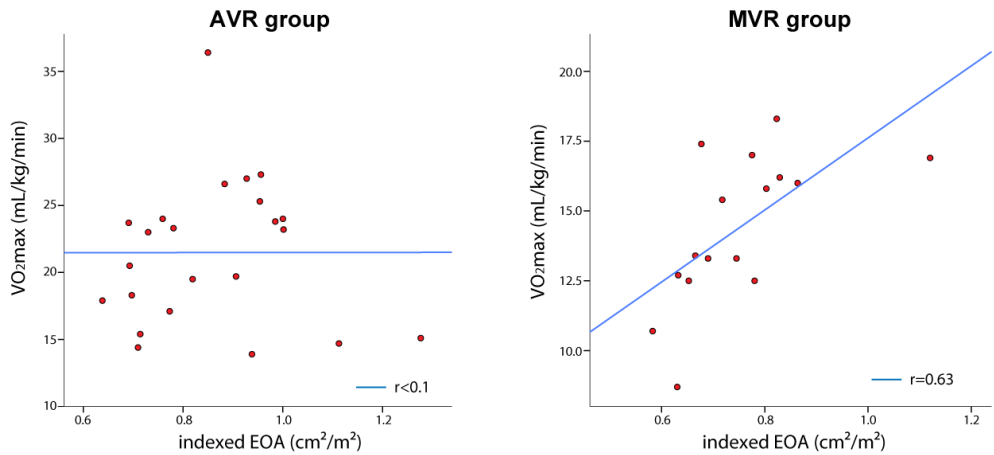


Figure 4.4 – Maximal oxygen uptake (VO₂max) versus indexed effective orifice area (EOA) at rest, showing a significant correlation in mitral valve replacement (MVR) patients. In aortic valve replacement (AVR) patients this immediate impact of indexed EOA on exercise capacity was not observed.

Impact on exercise capacity. In AVR patients, maximal oxygen uptake (VO_{2max}) was 21.4 ± 5.4 mL/kg/min. There was no correlation between the indexed EOA at rest and VO_{2max} , nor between indexed EOA at peak exercise and VO_{2max} in these patients ($\rho=0.16$, $p=0.48$ and $\rho=-0.19$, $p=0.38$ respectively). In contrast, in MVR patients ($VO_{2max} = 14.4 \pm 5.4$ mL/kg/min) a strong and significant correlation was observed between indexed EOA at rest and VO_{2max} ($\rho=0.68$, $p=0.004$)(Figure 4.4), and between indexed EOA at peak exercise and VO_{2max} ($\rho=0.59$, $p=0.016$). In addition, in MVR patients, systolic PAP increased significantly during exercise (Table 4.3), and was most strongly correlated to the peak transmitral gradient at each stage of exercise ($\rho=0.72$, $p<0.001$), independently from flow rate.

Discussion

This study quantified the *in vivo* pressure-flow relationship during dynamic exercise in bileaflet mechanical valve prostheses in aortic and mitral position, and showed no increase in EOA during exercise in these prostheses. Exercise hemodynamics are therefore predictable from the prosthetic evaluation at rest, and closely adhere to the fundamental hydraulic relationship between pressure gradient and flow rate for a *fixed* EOA (Figure 4.2, Equation 1). Moreover, the indexed EOA at rest was strongly correlated to exercise capacity in MVR patients. In contrast, in AVR patients prosthetic performance at rest or peak exercise was not directly related to exercise capacity at 31±19 months after surgery.

Effective versus true orifice area.

Flow passing through a narrow orifice experiences a flow contraction phenomenon leading to a vena contracta distal to the orifice that constitutes the “effective” area of the orifice¹⁷³. The factor relating the true geometric orifice area (GOA) and the effective area is called the discharge coefficient, or coefficient of contraction C_c :

$$EOA = C_c * GOA \quad (2)$$

It has been shown that the geometry of the narrowing has significant impact on the flow contraction pattern and thus C_c , with more gradually tapered orifices exerting more “effective” area for the same geometric area^{174, 192, 193}. Flow rate by itself has no significant impact on C_c ¹⁷³.

EOA following mechanical valve replacement.

In prosthetic valves, similar flow contraction occurs and EOA is always smaller than the true geometric orifice reported by the manufacturer (Figure 4.5). The coefficient of contraction, also called the “performance index” in prosthetic valves, shows large interindividual variation and values are in the range of 0.50-0.60 in aortic position¹⁸⁴, and in the range of 0.30-0.50

in the mitral position^{185, 194}. The latter explains why EOA is often smaller in MVR compared to AVR even for larger prosthetic valve sizes¹⁹⁴, a finding potentially related to a less efficient flow “guidance” by the larger left atrium compared to the “funneling” LVOT (Figure 4.5). More importantly however, these performance values indicate that EOA could potentially increase by more than 100% in case a more favorable flow contraction within the geometric orifice would be obtained.

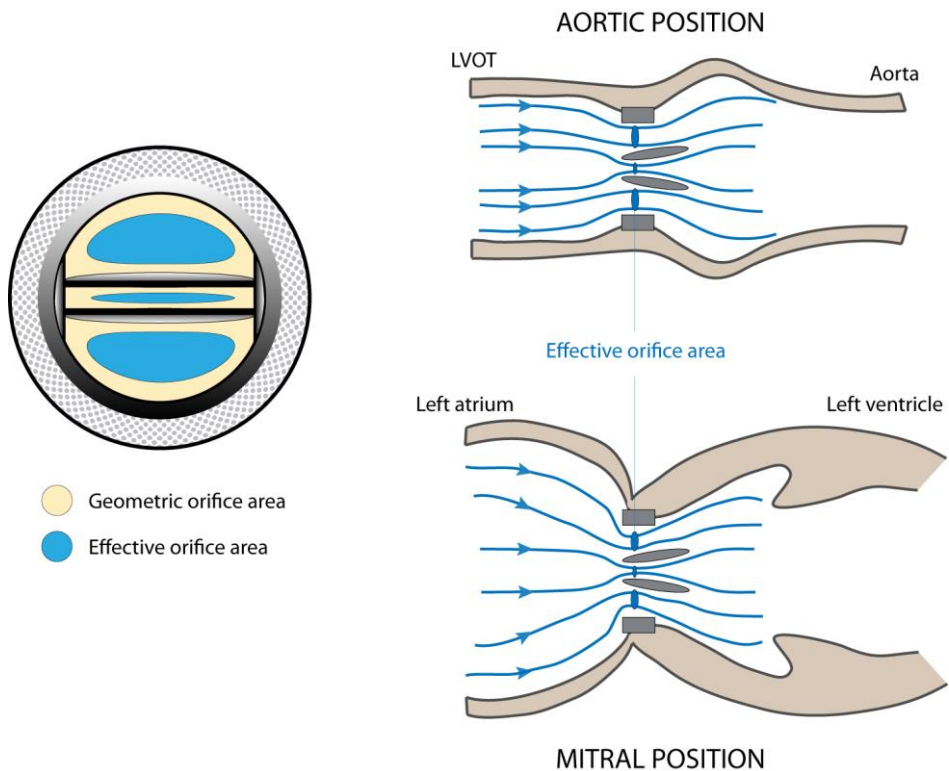


Figure 4.5 – Difference between geometric orifice area and effective orifice area in bileaflet mechanical valves. The convergence of flow lines in both aortic and mitral position determine the effectiveness (i.e. performance) of the prosthesis. More pronounced flow contraction in the prosthesis results in less effective use of the geometric orifice area.

Flow- and heart-rate independency of prosthetic EOA.

In this study, however, we could not demonstrate an increase in EOA during dynamic exercise in AVR or MVR patients, despite significantly increased heart rate and flow rate. On the contrary, in AVR patients a small yet significant decrease in EOA was observed, most pronounced at mid-exercise. Whether this reflects a genuine transient decrease in EOA during exercise, or relates to limitations in the Doppler measurement technique remains unclear. Nevertheless, the relative decrease (6%) in EOA is likely too small to be of clinical significance in AVR patients. These findings in AVR patients are in line with prior results, showing no increase in EOA during dynamic exercise^{187, 195} or dobutamine stress^{188, 196} after mechanical bileaflet AVR.

In MVR patients prior results are more conflicting. Table 4.4 summarizes the available data from clinical exercise studies in St Jude Medical bileaflet mitral valve prostheses. EOA was measured by use of the pressure half-time method in the majority of studies. However, the use of this method is not valid for bileaflet orifice quantification^{197, 198}. Careful interpretation is therefore warranted with respect to the data in Table 4.4. In the only other exercise study employing the continuity equation for EOA measurement in St Jude Medical mitral valves, Fino et al found a small (+10%) significant increase in EOA during exercise, although 50% of the studied patients were bioprosthetic valves¹⁴³. Our current findings are in line with the exercise echocardiography study of Shigenobu et al. in 100 mechanical MVR patients (size 25, 27 and 29 mm) showing similarly increased gradients during exercise, and small insignificant increases in EOA¹⁹⁹. Furthermore, the strong and significant correlation between exercise capacity and the indexed EOA at rest in MVR patients supports the fact that no divergent changes in EOA occur during exercise. In contrast, in a similar study protocol in patients following restrictive mitral valve annuloplasty for secondary mitral regurgitation a significant increase in EOA during exercise (average increase 35%) was observed; in those

patients indexed EOA at rest was not correlated to exercise capacity, whereas the indexed EOA at peak exercise was an independent predictor of exercise capacity and outcome¹³⁹.

Clinical implications.

The finding of a fixed EOA during exercise in mechanical valve prostheses has implications for the approach and evaluation of the typically young and dynamic mechanical prosthesis patient. In both the mitral and aortic position exercise hemodynamics can be predicted based on the evaluation of EOA at rest and the fundamental pressure flow relationship (Equation 1). It has previously been shown that a postoperative EOA that is too low for the patient's hemodynamic profile (i.e. patient-prosthesis mismatch) causes increased pressure gradients and is associated with less regression in left ventricular mass in AVR patients, as well as increased early and late mortality¹⁴¹. However, in line with previous studies in bioprosthetic valves²⁰⁰, there is no "immediate" impact of decreased EOA on the exercise capacity in these AVR patients, likely because the impact of low EOA in aortic position is a more gradual process of left ventricular mass and diastolic dysfunction. In contrast, in the MVR group, exercise capacity was strongly correlated to indexed EOA, and systolic pulmonary pressures correlated with the peak transmitral gradient during exercise. Indeed, in the mitral position, the impact of EOA on pulmonary pressures and exercise capacity is directly linked, as was also shown previously¹⁴². The present study therefore (re-)emphasizes that all efforts should be made to maximize postoperative EOA in every single patient (i.e. by maximizing geometric orifice, or by selecting the most favorable valve design that maximizes the effective use of geometry in the individual patient) because of the impact on the respective exercise hemodynamics as well. Finally, the difference in exercise hemodynamics with alternative surgical approaches (valve repair, stentless bioprosthetic replacement, etc.) should be taken into consideration in the clinical decision-making when young patients with severe aortic and/or mitral valve disease are referred for valve surgery.

Limitations

This was a single center study with limited sample size, potentially leading to type II statistical errors. In addition, we only studied the St Jude Medical bileaflet mechanical valve prosthesis in both AVR and MVR patients. Our findings therefore cannot be extrapolated to other bileaflet valve prostheses.

Conclusions

This study could not demonstrate an increase in EOA during exercise in patients with bileaflet mechanical AVR or MVR. Transprosthetic gradients during exercise are therefore predictable based on the hemodynamic evaluation at rest, and closely adhere to the fundamental pressure-flow relationship. Indexed EOA at rest was strongly correlated with exercise capacity in MVR patients, but not in AVR patients. The finding of a fixed EOA during exercise should be taken into account in the therapeutic decision-making and prosthesis selection in young and dynamic patients.

Chapter 5

Mechanism of symptomatic improvement after MitraClip therapy for secondary mitral regurgitation: the role of improved resting and exercise hemodynamics

Van De Heyning CM*, Bertrand PB*, Debonnaire P, De Maeyer C , Vandervoort PM,
Coussement P, Paelinck B, De Bock D, Vrints C, Claeys MJ

*shared first authorship

Status of the manuscript:

Accepted as "Research Letter"

(shortened version of the manuscript)

J Am Coll Cardiol (IF 16.5)

Abstract

Background: Percutaneous mitral valve repair using MitraClip offers symptomatic benefit in patients with severe secondary mitral regurgitation (MR), yet data regarding altered resting and exercise hemodynamics post-MitraClip and their relation to symptomatic status are lacking.

Objectives: To assess the effect of MitraClip therapy on resting and exercise hemodynamics in secondary MR patients, and determine the relationship with symptomatic improvement.

Methods: Consecutive patients (n=31, 72±10years) with symptomatic severe secondary MR were prospectively evaluated by Doppler echocardiography at rest and during symptom-limited exercise on a semi-supine bicycle pre- and 6 months post-MitraClip procedure. MR severity, cardiac output (CO), transmitral gradient, systolic pulmonary artery pressure (SPAP) and a flow-corrected SPAP/CO ratio were assessed at rest and peak exercise. NYHA class and 6-minute walk test (6MWT) were evaluated pre- and 6 months post-MitraClip.

Results: At rest 6 months pre- versus post-MitraClip, reduced MR severity (MR jet/left atrial area 34±12 vs 18±13%, p<0.001), increased CO (3.4±1.0 vs 3.9±1.3L/min, p=0.033) and lower SPAP (42±11 vs 38±10mmHg, p=0.041) were found. During exercise, MR severity was equally reduced post-MitraClip (32±12 vs 21±14%, p<0.001), with higher peak CO (5.1±1.3 vs 7.2±2.8L/min, p=0.008) and similar peak SPAP (64±13 vs 56±16mmHg, p=0.213) at these higher flow rates. Symptomatic benefit (NYHA class improvement ≥1 grade) occurred in 21/31 patients (68%, responders) while 10/31 did not improve (32%, non-responders). Responders versus non-responders had more improvement in 6MWT (+74±83 vs -42±79m, p=0.006), more SPAP reduction at rest (p=0.015) and exercise (p=0.020), higher exercise CO (p=0.008) and lower exercise SPAP/CO (p=0.043). MR severity tended to be lower in responders versus non-responders

at rest ($p=0.089$) and exercise ($p=0.095$), while the transmitral gradient had increased more in non-responders ($p=0.023$).

Conclusions: MitraClip therapy for secondary MR reduces MR at rest and during exercise, and improves the patients' hemodynamic profile. Symptomatic improvement 6 months post-MitraClip relates to more favorable resting and exercise hemodynamics.

Introduction

Percutaneous mitral valve repair using MitraClip (Abbott Vascular, Santa Clara, California) may be considered to treat symptomatic severe mitral regurgitation (MR) in patients at high or prohibitive surgical risk ^{22, 47, 150}. Large observational registries of patients treated with MitraClip for predominantly secondary MR show a significant reduction in resting MR coinciding with functional improvement in the majority of patients ^{151, 201}. Furthermore, the hemodynamic impact of successful MitraClip therapy has been documented at rest, comprising increased cardiac output (CO) due to enhanced forward stroke volume ²⁰², mild to moderately increased transmitral pressure gradient due to a reduction in mitral valve area ²⁰³ and reduced systolic pulmonary artery pressures (SPAP) at midterm follow up ²⁰⁴. However, secondary MR is characteristically dynamic and sensitive to changes in ventricular geometry and loading conditions ¹⁰, a phenomenon with important prognostic and symptomatic implications ⁹⁶. It remains unclear whether, besides reduction in resting MR, MitraClip therapy is effective in reducing secondary MR during exercise. Comparative data on exercise hemodynamics before versus after MitraClip therapy for all MR etiologies are currently lacking, although such data are most relevant in secondary MR. Moreover, the relation of resting and exercise hemodynamics to the symptomatic status in secondary MR patients treated with MitraClip remains to be explored.

The aim of this study in a cohort of secondary MR patients was 1) to evaluate the effect of MitraClip therapy on resting and exercise hemodynamics and 2) to determine the relationship between symptomatic status and hemodynamic alterations before and after MitraClip therapy.

Methods

Study design

We prospectively included consecutive patients with symptomatic moderate-to-severe or severe secondary MR referred for percutaneous mitral valve repair using MitraClip at 3 Belgian centers. Secondary MR was defined as valvular dysfunction due to local or global left ventricular dysfunction in the absence of primary mitral valve disease ²⁰⁵. All patients were judged to be at high or prohibitive surgical risk by the Heart Team.

Eligible patients were scheduled for a comprehensive transthoracic echocardiography at rest and during symptom limited exercise test on a semi-supine bicycle before and 6 months after MitraClip procedure. Symptomatic status and functional capacity were evaluated by New York Heart Association (NYHA) class and 6-minute walk test (6MWT) respectively, at baseline and 6 months after MitraClip therapy. Clinical characteristics of the patients were extracted from the Belgian MitraClip database which gathers clinical information on all MitraClip procedures in Belgium ²⁰⁶. The ethical committee of the Antwerp University Hospital approved the study protocol and all patients gave written informed consent. The database is registered with clinicaltrials.gov (NCT02506387).

A total of 39 patients were screened, of which 4 patients were excluded due to inability to perform a bicycle exercise test. In addition, post-MitraClip 3 included patients died and 1 patient required cardiac surgery (all prior to the 6 month visit); these patients were excluded from further analysis. Accordingly, the final study population comprised 31 patients.

MitraClip procedure

All patients underwent transesophageal echocardiography guided percutaneous mitral valve repair using MitraClip under general anesthesia via transfemoral venous approach. Procedural success was defined as non-complicated placement of ≥ 1 clip coinciding with per-procedural estimated MR reduction to \leq grade 2+.

Transthoracic echocardiography

A comprehensive two-dimensional transthoracic echocardiography was performed at rest and during symptom limited exercise test on a semi-supine bicycle in all patients using a cardiovascular ultrasound system (Vivid 7 or Vivid E9, GE Healthcare or iE33, Philips Healthcare) equipped with a M5S or S5-1 transducer. Conventional B-mode, color Doppler, pulsed and continuous wave Doppler images were acquired in still or cine-format using ECG-gating. A protocol of 20 Watt with 10 Watt increments per minute was chosen for exercise testing and acquisitions were made through every 20 Watt increments starting from 30 Watt. Peak exercise was defined as the highest workload (Watt) achieved. Echocardiographic data were analyzed off-line and blinded for symptomatic status of the patients (EchoPAC, version 112, GE Medical Systems, Horten, Norway). All measurements were averaged over 3 cardiac cycles for patients in sinus rhythm and 5 cycles for patients with atrial fibrillation. Left ventricular ejection fraction (LVEF) was quantified by the modified Simpson's method in the apical four- and two-chamber view ²⁰⁷. MR severity was graded qualitatively using a multi-integrative approach, as recommended ²⁰⁸ (grade 0: no MR ; grade 1+: mild ; grade 2+: moderate ; grade 3+: moderate-to-severe ; grade 4+: severe) and quantitatively as percentage jet area over left atrial area in the apical four-chamber view ²⁰⁹. The mean transmitral gradient was obtained by continuous wave Doppler of the transmitral flow during diastole in the apical four-chamber view ²¹⁰ ; care was taken to measure the mean transmitral gradient at the residual orifices post-MitraClip. Forward stroke volume was calculated from the pulsed wave Doppler signal in the left ventricular

outflow tract (apical five-chamber view) and the baseline left ventricular outflow tract diameter in mid-systole (parasternal long-axis view). CO was calculated as the product of the heart rate and the forward stroke volume. The transtricuspid pressure gradient was measured by continuous wave Doppler of the regurgitant tricuspid jet in the apical four-chamber view. SPAP was calculated as the sum of the maximal transtricuspid pressure gradient and an estimate of the right atrial pressure based on inferior caval vein dimension and collapsibility, as recommended²¹¹. To correct for the typical flow-dependency of SPAP, "SPAP/CO" was calculated as SPAP divided by CO and expressed in mmHg per liter per minute.

Statistical analysis

Results are expressed as mean \pm SD or percentages unless otherwise specified. Differences between functional and hemodynamic data at baseline and 6 months after MitraClip procedure were evaluated with the paired Student t test or the Wilcoxon Signed Rank test as appropriate. Furthermore, patients were studied in 2 groups according to the presence of symptomatic benefit, defined as NYHA class improvement ≥ 1 grade. Differences between groups were analyzed using the independent Student t test, the Mann-Whitney U test or the Fisher's exact test as appropriate. Pearson correlation analysis was performed to detect possible correlations between changes of MR severity, mean valve gradient and SPAP. Statistical significance was set at a 2-tailed probability of $p < 0.05$. All statistical analyses were performed with IBM SPSS Statistics for Windows version 20.0 (IBM Corp., Armonk, NY).

Results

Study population

Baseline clinical and hemodynamic characteristics of the study population are summarized in Table 5.1 and 5.2, respectively. All patients underwent MitraClip therapy with a 94%

acute procedural success rate and a mean of 1.4 ± 0.5 clips implanted per patient. At 6 months post MitraClip, NYHA functional class was improved ($p < 0.001$) and there was a trend towards increased functional capacity as assessed by 6MWT ($p = 0.108$).

Resting and exercise hemodynamics after MitraClip therapy

Hemodynamic data at rest and during maximal exercise, pre- and 6 months post-MitraClip procedure, are summarized in Table 5.2. At rest, 6 months post-MitraClip therapy, MR severity was reduced compared to baseline ($p < 0.001$) (Figure 5.1). In addition, CO increased ($p = 0.033$), essentially by increase of forward stroke volume. Furthermore, SPAP was reduced ($p = 0.041$) despite a significant increase in mean transmitral gradient after MitraClip procedure ($p < 0.001$).

At maximal exercise MR severity was reduced when compared to pre-MitraClip exercise echocardiography ($p = 0.001$) (Figure 5.1). Furthermore, a higher peak CO was observed at maximal exercise ($p = 0.039$), while a similar exercise SPAP ($p = 0.170$) was obtained at these higher flow rates (Figure 5.2); therefore SPAP/CO at maximal exercise was reduced compared to pre-MitraClip ($p = 0.036$).

At 6 months after MitraClip intervention there was no significant difference between MR at rest and during exercise (MR jet area/left atrial area 18 ± 13 vs. $21 \pm 13\%$, $p = 0.265$) and Pearson correlation analysis showed a good correlation between both parameters ($r = 0.597$, $p = 0.002$).

Table 5.1 - Baseline clinical characteristics of the study population

	Study population (n=31)
Age	72±10
Male, n (%)	19 (61)
Risk factors, n (%)	
Hypertension	22 (71)
Diabetes	8 (26)
Hypercholesterolemia	27 (87)
Ex/current smoker	14 (45)
Medication use, n (%)	
Diuretic	26 (84)
Beta-blocker	24 (77)
ACE-I/AIIRB	21 (68)
Statin	24 (77)
Sinus rhythm at baseline, n (%)	23 (74)
History, n (%)	
Coronary artery disease	27 (87)
Cardiac surgery	17 (55)
HF hospitalization last 2 years	21 (68)
Atrial fibrillation	12 (39)
CRT device	5 (16)
EuroSCORE II (%)	8.3±5.7

ACE-I = angiotensin-converting enzyme inhibitor ; AIIRB = angiotensin II receptor blocker; CRT = cardiac resynchronization therapy ; HF = heart failure

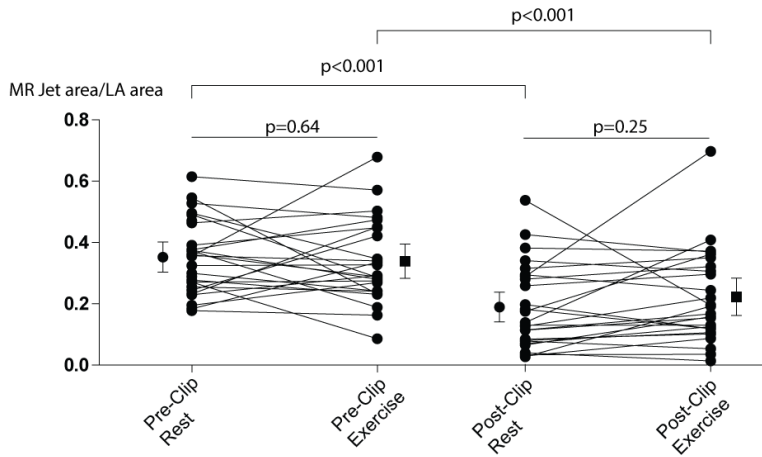


Figure 5.1 - Mitral regurgitation severity at rest and during peak exercise before and 6 months after MitraClip therapy. Improved mitral regurgitation severity is noted 6 months after MitraClip therapy both at rest and during peak exercise. MR = mitral regurgitation ; LA = left atrial.

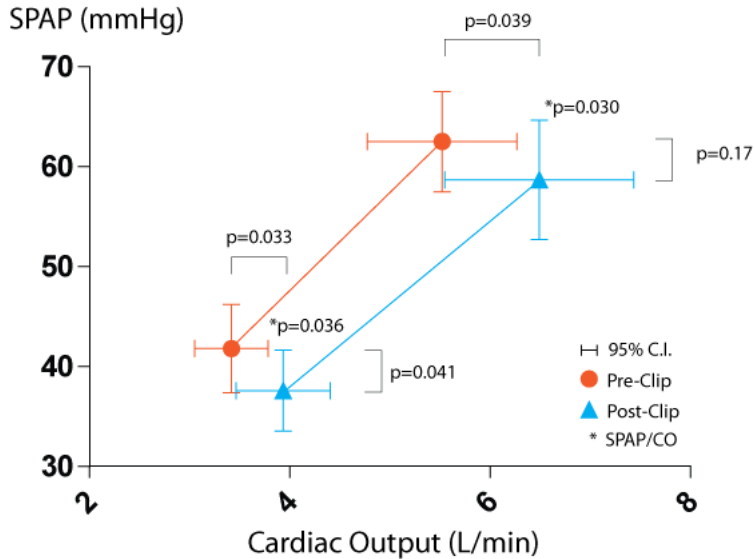


Figure 5.2 - Effect of MitraClip therapy on resting and peak exercise hemodynamics. MitraClip therapy allows obtaining of a higher cardiac output both at rest and during peak exercise at lower peak systolic pulmonary arterial pressures.

Table 5.2 - Symptomatic status and hemodynamic data pre and 6 months post MitraClip procedure

	Pre MitraClip	Post MitraClip	P-value
NYHA			p<0.001
Class I	0 (0%)	6 (19%)	
Class II	12 (39%)	21 (68%)	
Class III	18 (58%)	4 (13%)	
Class IV	1 (3%)	0 (0%)	
6-minute walk test (m)	304±110	340±111	p=0.108
LVEF (%)	37±8	39±11	p=0.305
Grade MR			p<0.001
0-1+	0 (0%)	15 (48%)	
2+	8 (25%)	11 (36%)	
3+	16 (52%)	4 (13%)	
4+	7 (23%)	1 (3%)	
MR jet area/ LA area (%)			
at rest	34±12	18±13	p<0.001
during exercise	32±12	21±14	p=0.001
Mean transmitral gradient (mmHg)	2.7±1.5	4.3±2.2	p<0.001
Heart rate (bpm)			
at rest	72±15	75±17	p=0.486
during exercise	105±23	112±25	p=0.038
Forward stroke volume (mL)			
at rest	48±14	54±17	p=0.071
during exercise	53±15	58±18	p=0.091
Cardiac output (L/min)			
at rest	3.4±1.0	3.9±1.3	p=0.033
during exercise	5.5±2.0	6.5±2.6	p=0.039
SPAP (mmHg)			
at rest	42±11	38±10	p=0.041
during exercise	63±13	59±16	p=0.170
SPAP/CO (mmHg/L.min-1)			
at rest	13.8±5.4	11.2±4.7	p=0.030
during exercise	13.1±5.6	10.6±4.8	p=0.036

NYHA = New York Heart Association functional class ; LVEF = left ventricular ejection fraction; MR = mitral regurgitation ; LA = left atrial ; SPAP = systolic pulmonary artery pressure ; CO = cardiac output.

Symptomatic responders versus non-responders

Symptomatic response, defined as NYHA class improvement ≥ 1 grade 6 months after MitraClip, was observed in 21/31 patients (68%, responders), while 10/31 did not improve (32%, non-responders). Symptomatic response was concordant with an increase of functional capacity during 6MWT in responders versus a decrease in walking distance in non-responders ($p=0.006$). Differences between responders and non-responders are summarized in Table 5.3. Similar age and gender distribution was noted in both groups.

Pre-MitraClip, resting and exercise hemodynamics were comparable in responders versus non-responders, except for more severe exercise MR in non-responders ($p=0.034$).

At 6 months post-MitraClip, MR severity and SPAP both at rest and during maximal exercise tended to be lower in responders. Interestingly, responders had more reduction of SPAP both at rest ($p=0.015$) and during exercise ($p=0.020$) versus non-responders, and a higher exercise CO ($p=0.008$). As a result, SPAP/CO at maximal exercise was reduced in responders versus non-responders after MitraClip therapy (Central Illustration). In addition, the increase in mean transmitral gradient following MitraClip procedure was higher in non-responders versus responders ($p=0.023$). Pearson correlation analysis showed an inverse correlation between the increase of the mean transmitral gradient and the reduction of resting SPAP ($r = 0.546$, $p=0.004$).

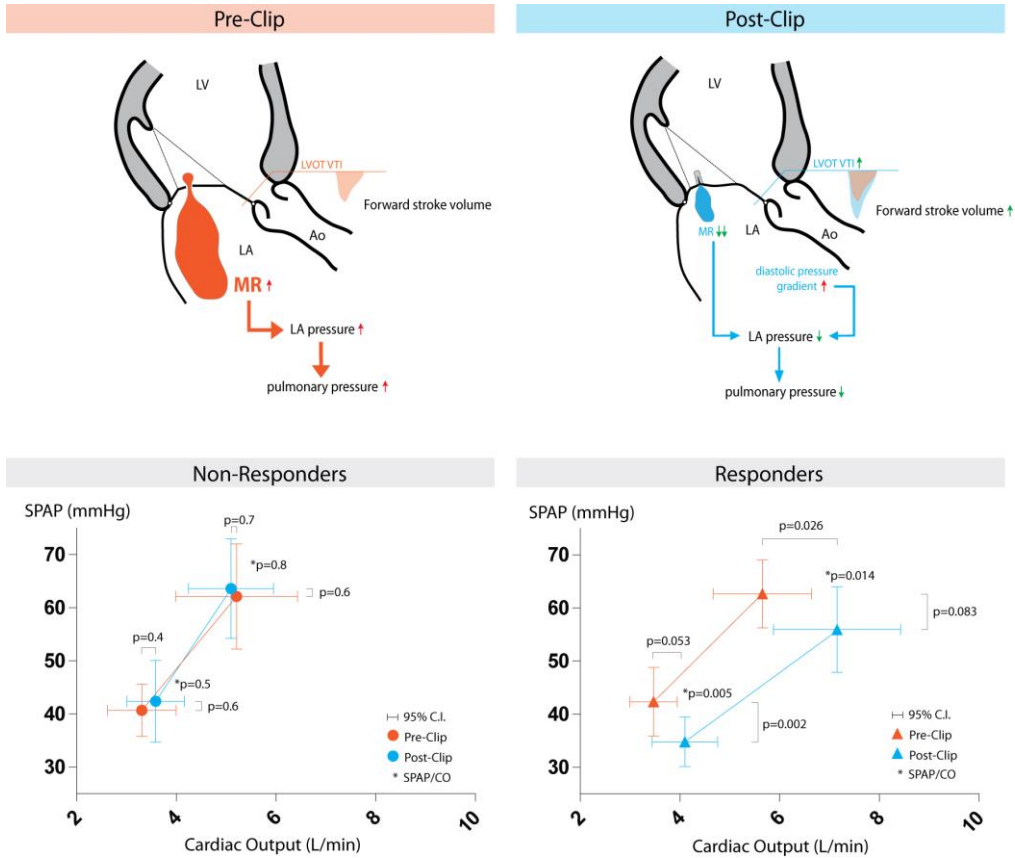
Of note, there was no difference between responders and non-responders regarding exercise related increase of MR (3 ± 7 vs 3 ± 18 %, $p=1$).

Table 5.3 - Comparison of functional capacity and rest and exercise hemodynamics between patients with and without symptomatic benefit after MitraClip procedure

	Responders n=21	Non-responders n=10	p-value
Age (years)	74±9	68±13	p=0.192
Gender (male/female)	13/8	6/4	p=1.000
6-minute walk test (m)			
pre MitraClip	270±92	346±110	p=0.078
post MitraClip	351±111	316±91	p=0.448
Δ 6-minute walk test	74±83	-42±79	p=0.006
LVEF (%)			
pre MitraClip	40±7	33±9	p=0.044
post MitraClip	40±12	37±11	p=0.557
Δ LVEF	0±9	4±7	p=0.239
MR jet area/ LA area (%)			
at rest			
pre MitraClip	33±13	35±10	p=0.616
post MitraClip	15±12	24±13	p=0.089
Δ MR jet area/ LA area	-18±17	-11±15	p=0.325
during exercise			
pre MitraClip	28±10	38±12	p=0.034
post MitraClip	18±11	27±15	p=0.095
Δ MR jet area/ LA area	-12±16	-11±13	p=0.886
Mean transmitral gradient (mmHg)			
pre MitraClip	2.6±1.1	2.7±2.2	p=0.874
post MitraClip	3.7±1.2	5.5±3.3	p=0.135
Δ mitral valve mean gradient	1.1±1.2	2.8±2.7	p=0.023
Heart rate (beats per minute)			
at rest			
pre MitraClip	73±17	72±9	p=0.839
post MitraClip	75±21	75±15	p=0.957
Δ heart rate	2±20	3±18	p=0.833
during exercise			
pre MitraClip	105±22	105±26	p=0.979
post MitraClip	115±23	104±27	p=0.240
Δ heart rate	11±19	0±16	p=0.168
Forward stroke volume (mL)			

at rest			
pre MitraClip	49±14	47±14	p=0.701
post MitraClip	55±17	51±15	p=0.456
Δ forward stroke volume	9±18	4±17	p=0.684
during exercise			
pre MitraClip	53±15	51±16	p=0.762
post MitraClip	61±18	51±15	p=0.146
Δ forward stroke volume	8±17	-1±18	p=0.213
Cardiac output (L/min)			
at rest			
pre MitraClip	3.5±1.0	3.3±1.0	p=0.684
post MitraClip	4.1±1.4	3.6±0.8	p=0.312
Δ cardiac output	0.6±1.4	0.3±1.0	p=0.490
during exercise			
pre MitraClip	5.7±2.2	5.2±1.6	p=0.587
post MitraClip	7.2±2.8	5.1±1.3	p=0.008
Δ cardiac output	1.5±2.9	-0.1±1.1	p=0.110
SPAP (mmHg)			
at rest			
pre MitraClip	42±14	41±7	p=0.666
post MitraClip	35±9	42±11	p=0.062
Δ SPAP	-8±9	2±10	p=0.015
during exercise			
pre MitraClip	63±13	62±13	p=0.915
post MitraClip	56±16	64±13	p=0.213
Δ SPAP	-7±16	2±11	p=0.020
SPAP/CO (mmHg/L.min ⁻¹)			
at rest			
pre MitraClip	14.1±7.6	13.1±4.1	p=0.716
post MitraClip	10.1±4.2	12.5±5.3	p=0.194
Δ SPAP/CO	-4.0±4.9	-0.6±7.1	p=0.165
during exercise			
pre MitraClip	13.5±6.4	12.1±2.8	p=0.444
post MitraClip	9.6±5.3	12.7±2.5	p=0.043
Δ SPAP/CO	-4.0±6.3	0.8±2.9	p=0.014

BMI = body mass index ; Δ = difference post and pre MitraClip procedure ; LVEF = left ventricular ejection fraction ; MR = mitral regurgitation ; LA = left atrial ; SPAP = systolic pulmonary artery pressure ; CO = cardiac output.



Central Illustration - Difference in resting and peak exercise hemodynamics before and after MitraClip therapy between symptomatic responders and non-responders. Patients with symptomatic improvement after MitraClip intervention (= responders) reach a higher cardiac output both at rest and during peak exercise at lower peak systolic pulmonary arterial pressures in comparison with patients without symptomatic relief (= non-responders).

Discussion

The present prospective analysis pioneers the evaluation of the impact of MitraClip therapy on echocardiographic resting and exercise hemodynamics in patients with secondary (functional) MR. The main study findings are that MitraClip therapy both at rest and during dynamic exercise 1) successfully reduces secondary MR; 2) increases CO but not SPAP at these higher flow rates 6 months after intervention despite a higher transmitral gradient; and finally 3) beneficially alters the patients' hemodynamic profile favoring symptomatic improvement.

MitraClip therapy for secondary MR

Although prospectively randomized data mainly support MitraClip therapy in inoperable primary (organic) MR ^{47, 150}, real-world registries ^{151, 201, 212} indicate that patients referred for MitraClip therapy are typically elderly (70-80 years old), male (60-65%) patients with predominantly secondary MR. The rationale to perform MitraClip therapy in secondary MR arises from the uncertain risk-benefit ratio of classic mitral valve surgery in these higher risk patients with left ventricular dysfunction, especially in patients without indication for revascularization ²⁴. In the 27% secondary MR patients included in the EVEREST II trial, the composite endpoint of death, mitral valve surgery or MR grade 3+/4+ at both 1 and 4 years was non-inferior in the MitraClip group compared to the mitral valve surgery group (2). Furthermore, above-described registries report a significant reduction in secondary MR at rest to grade $\leq 2+$ in approximately 80% of patients at 6 months after MitraClip therapy, with concomitant improvement in NYHA functional class and 6MWT (4). Our findings are in line with these real-world data, including patients with similar demographics and demonstrating resting MR reduction at 6 month after MitraClip therapy to grade $\leq 2+$ in 84% of patients.

Importantly, our study additionally showed that secondary MR at maximal exercise was equally reduced compared to baseline exercise data. It has been shown in patients with ischemic and non-ischemic cardiomyopathy that increases in secondary MR during exercise are prevalent and associated with worse exercise capacity¹⁹ and outcome⁹⁶. Our results indicate that MitraClip therapy has an impact on the typical dynamic component of secondary MR as well. Indeed, in our cohort 6 months post-MitraClip there was no significant difference between MR at rest and during exercise and a good correlation between both parameters was observed.

Resting and exercise hemodynamics after MitraClip therapy

Siegel et al²⁰² reported an acute increase in CO at rest as a result of enhanced forward stroke volume after MitraClip therapy. More recently, Giannini and colleagues²¹³ found that this effect is maintained at 6 months follow-up, similar to our findings. Moreover, present study indicates that CO at maximal exercise is increased 6 months after MitraClip therapy compared to baseline exercise data, presumably by combination of a higher stroke volume and higher achieved maximal heart rate.

Furthermore, a significant reduction in SPAP at rest and a trend towards lower SPAP at maximal exercise (at higher flow rates than pre-MitraClip) was noted at 6 months follow up. These results at rest are compounded by several prior studies demonstrating a decrease in resting SPAP after MitraClip therapy at midterm follow up^{204, 213}. Since the pulmonary artery pressure is flow-dependent²¹⁴, we introduced the variable SPAP/CO as a more pragmatic parameter to evaluate exercise hemodynamics. In this respect, our data demonstrated significant improvement in both resting and exercise hemodynamics after MitraClip therapy. Interestingly, increase in transmitral gradient after MitraClip seemed to oppose reduction of SPAP at rest. This finding is in line with 2 recent studies^{157, 215} demonstrating that SPAP at rest was higher in patients with a mean transmitral gradient ≥ 5 mmHg after MitraClip.

Symptomatic responders versus non-responders

At 6 months after MitraClip procedure, 65% of patients in the present study reported class NYHA improvement ≥ 1 , while only 13% were in NYHA class III and no patients remained in NYHA class IV. Such symptomatic response is comparable to the mid-term outcomes reported in a recent meta-analysis comprising 875 secondary MR patients compiled from 9 studies (19% of patients in NYHA class III/IV after MitraClip)²⁰⁴. Classification of patients according to self-reported symptoms is inherently prone to subjectiveness, however improvement of NYHA class coincided with improvement of functional capacity as assessed by 6MWT. Intriguingly, despite the amount of data in real-world registries, determinants of symptomatic improvement after MitraClip procedure in secondary MR patients have not been clearly defined. Exercise echocardiography provides a powerful tool in this respect allowing assessment of the dynamic character of secondary MR and its hemodynamic consequences (CO, SPAP) during exercise in relation to symptoms and outcome⁴⁸. Our data suggest that symptomatic response after MitraClip therapy hemodynamically relates to the ability of achieving higher CO states at lower SPAP both at rest and during peak exercise, in concert with MR severity reduction. In contrast, patients without improvement in terms of NYHA class lacked such favorable hemodynamic changes (Central Illustration).

There was no difference in exercise-related increase in MR between symptomatic responders and non-responders. In symptomatic responders favorable hemodynamics were noted despite limited though significant increase in transmitral gradient. In these patients the extent of MR reduction probably outweighs the 'stenotic' impact of the clip both at rest and during exercise. However, MR severity and transmitral gradients tended to be higher in the symptomatic non-responders, likely explaining the higher SPAP and lower cardiac output in these patients preventing any symptomatic benefit. We hypothesize that in a subset of secondary MR patients the reduction in mitral valve area after MitraClip, whether or not combined with a higher degree of residual MR or pre-existing diastolic

dysfunction, negatively impacts on hemodynamics at rest and during exercise as has also been shown after mitral valve annuloplasty for secondary MR¹³⁹.

Clinical implications

Our findings lend further support to promote MitraClip therapy to alleviate symptoms in patients with secondary MR, at least partly explained by improved resting and exercise hemodynamics coinciding with dynamic MR reduction, despite transmitral gradient increase. Therefore maximization of MR reduction seems key to perform successful percutaneous mitral valve repair using ≥ 1 MitraClip(s), a contention sustained by recent reports indicating that the extent of secondary MR reduction strongly relates to outcome after MitraClip therapy ^{212, 216}. As secondary MR is a complex multifactorial phenomenon, accurate prediction and selection of those patients that might ultimately benefit from MitraClip therapy should be the scope of future research.

Study limitations

Firstly, due to the limited sample size, multiple regression analysis of determinants of NYHA class improvement or outcome analysis was not feasible. Nevertheless, current analysis is the only study available to date prospectively reporting on exercise hemodynamic data before and after MitraClip therapy.

Secondly, quantification of MR severity after MitraClip therapy using the jet area percentage method yields inherent drawbacks, but correlates well with angiographic MR severity assessment (15), is reliable to apply during exercise (20) and provides a useful alternative in the absence of any alternative validated 2D echocardiographic method. Vena contracta width and PISA method are technically not suitable after MitraClip therapy due to the creation of a double orifice ²¹⁷ and due to acoustic shadowing caused by the device ²¹⁸. The volumetric Doppler method has inherent pitfalls as well, especially during exercise, and suboptimal inter-observer agreement after MitraClip therapy has been reported ²¹⁸.

Conclusion

MitraClip therapy for secondary MR reduces MR both at rest and during exercise, and ameliorates the patients' hemodynamic profile, allowing to obtain higher CO at lower SPAP both at rest and during exercise. These favorable hemodynamics coincide with symptomatic improvement and increased functional capacity after MitraClip. Eventual iatrogenic stenosis post-MitraClip procedure might attenuate these beneficial effects.

Epilogue
'Surgical treatment of moderate ischemic MR'

Letter-to-the-Editor

Bertrand PB, Vandervoort PM, Dion RA

Status of the manuscript:

Published

N Engl J Med (IF 55.9)

Smith et al reported no clinically meaningful advantage of adding mitral valve repair to CABG in moderate ischemic mitral regurgitation at 1 year. However, only measures of clinical advantage at rest were evaluated. Ischemic mitral regurgitation is characteristically dynamic, and sensitive to exercise-induced changes in loading and regional wall motion¹⁰. Marked exercise-induced worsening of mitral regurgitation is associated with poor exercise capacity and long-term outcome⁴⁸. It remains unclear whether CABG alone is as effective as ring annuloplasty in tackling the dynamic component of the disease. Alternatively, undersized annuloplasty might cause functional stenosis due to increased diastolic leaflet tethering also impairing exercise capacity¹³⁹. In contrast to the Randomized Ischemic Mitral Evaluation (RIME) trial¹³⁴, with maximal oxygen uptake (VO₂max) as a clinical end point, the current study does not account for exercise-related changes in this dynamic pathology. The clinical end point of New York Heart Association functional status is only poorly correlated to actual exercise capacity measured by cardiopulmonary testing²¹⁹. Therefore, until longer follow-up data are presented, the current 1-year results should be interpreted carefully.

The authors respond: *"...We agree with Bertrand et al. regarding the dynamic nature of ischemic mitral regurgitation and the role of exercise testing in the assessment of outcomes. Longer patient follow-up should also identify important clinical differences if they exist..."*

PART II:
PATIENT-SPECIFIC FINITE ELEMENT MODELING
OF THE MITRAL VALVE APPARATUS

Chapter 6

Clinical validity of numerical mitral valve modeling: towards a patient-tailored approach in secondary mitral regurgitation

Bertrand PB, Debusschere N, Dezutter T, Mortier P, De Santis G, Vrolix M, Heyde B, Claus P, Verdonck PR, Vandervoort PM, De Beule M

Status of the manuscript:

Under review

Circulation (IF 14.4)

Background. An individualized analysis of the culprit dynamics in secondary mitral regurgitation (MR) is expected to improve therapeutic efficacy. The aim of this study was to develop a patient-specific numerical model of the mitral valve apparatus based on three-dimensional transesophageal echocardiography (3D-TEE) and to evaluate its clinical potential in secondary MR patients.

Methods & Results. Full volume 3D-TEE datasets with invasive left atrial and ventricular pressures were collected in 5 healthy individuals, and 5 secondary MR patients. A patient-specific finite element model was developed and used to predict mitral valve dynamics. Different material properties were evaluated based on literature data on explanted porcine, human and cardiomyopathy valves. The model predicted a realistic closure and opening of the leaflets in all datasets. In normal valves, the human material properties provided the best overall fit, with a mid-systolic prediction error of 1.32 ± 0.30 mm. In secondary MR, the stiff cardiomyopathy material properties fitted best, with prediction error of 1.53 ± 0.49 mm. Mid-systolic tenting volume was accurately predicted by the model ($r=0.92$, $p<0.001$), and this prediction correlated strongly with the measured effective regurgitant orifice area ($r=0.87$, $p=0.001$).

Conclusions. Patient-specific mitral valve modeling allows a realistic prediction of valvular dynamics in normal mitral valves as well as in secondary MR. In vivo leaflet stiffness is higher in secondary MR, possibly contributing to pathophysiology. Predicted geometric determinants of secondary MR correlate with MR severity. Patient-specific numerical modeling of the mitral valve therefore shows great potential for improving mechanistic insights and enhancing therapeutic efficacy by enabling pre-procedural planning and simulation.

Introduction

The mitral valve (MV) is a complex yet finely tuned apparatus composed of multiple components: mitral annulus, anterior and posterior mitral valve leaflet, chordae tendineae, anterolateral and posteromedial papillary muscles (PM) and adjacent left ventricular (LV) wall. All components are ingeniously designed to work together in 'sealing' the passage from the LV to the left atrium (LA) during systolic contraction. Disturbances in any of the components, organic or functional, can disrupt their harmonious interplay and cause mitral regurgitation (MR)⁸. Especially in left heart disease, geometric disturbances of papillary muscle position and/or dynamics, along with altered annular dimensions and/or dynamics, and changes in loading conditions are prone to disrupt normal valve function and lead to 'secondary' MR²³. Treatment of such patients remains highly debated and results are suboptimal^{24, 25}. A patient-specific analysis of the three-dimensional geometry and dynamics causing the dysfunction is likely to improve mechanistic insight and therapeutic efficiency in secondary MR²²⁰. Furthermore, the ability to (1) simulate MV dynamics during physiological loading conditions, and (2) virtually perform a therapeutic intervention while evaluating its impact on the individualized MV function and dynamics, holds a great potential to tailor our treatment to the patient's needs.

Patient-specific finite element modeling of the MV apparatus might fulfill these requirements, and could be a major progress in current health care²²¹. Several efforts have already been made to characterize the mechanical properties of mitral leaflet tissue and chordae tendineae for finite element modeling purposes²²²⁻²²⁵, and a number of models have been established based on ex vivo porcine MV data^{226, 227}. However, the validity of patient-specific numerical MV models in clinical practice – and for secondary MR in particular – has yet to be proven.

The purpose of this study was to (1) develop a patient-specific finite element model of the MV apparatus, based on three-dimensional transesophageal echocardiography (3D-TEE), and (2) to validate its clinical potential in predicting human MV dynamics in healthy and secondary MR patients.

Materials & Methods

Study population

We prospectively included 5 patients with a structurally and functionally normal MV ('Control' group) and 5 patients with severe secondary MR ('Secondary MR' group). Control patients were consecutive patients who were scheduled to undergo a patent foramen ovale (PFO) closure at a tertiary referral center (Ziekenhuis Oost-Limburg, Genk). Secondary MR patients were consecutive patients scheduled for a MitraClip procedure. Exclusion criteria in the control group were (1) structural or functional mitral leaflet abnormalities, (2) atrial fibrillation and (3) poor TEE windows. Exclusion criteria in the secondary MR group were (1) concomitant structural leaflet abnormalities and (2) atrial fibrillation. The study was approved by the local ethics committee and all patients gave written informed consent.

Data acquisition and processing

The PFO closure procedures and the MitraClip procedures were performed under general anesthesia, with endotracheal intubation and mechanical ventilation in all patients. 3D-TEE images were acquired using an X7-t probe on a commercially available workstation (iE33, Philips Medical Systems, Andover, MA). LA access was obtained via femoral vein catheterization and cannulation through the PFO using a 10F Mullins sheath, or via transseptal puncture with placement of the steerable guide catheter during MitraClip procedure. Left heart catheterization was performed via the ipsilateral femoral artery, and a pig-tail catheter (6F) was placed in the LV for pressure recording purpose. Simultaneous LA and LV pressure recordings were obtained along with a 12-lead ECG registration (Mac-

Lab, GE Healthcare). Simultaneously, ECG-gated full volume TEE datasets (4 beat interpolation, target frame rate > 20Hz) were acquired during ventilator breath-hold to avoid stitching artifacts. The start of the full volume image acquisition was marked in the ECG signal of the pressure recordings. DICOM images were exported in Cartesian DICOM format using Philips QLab software, and imported into a custom non-commercial MatLab®-based package for 3D echocardiograms (Speqle3D, developed at the University of Leuven)²²⁸. Pressure recordings and ECG data were exported as text-files from the Mac-Lab software and imported in custom MatLab® routine for further processing. Figure 6.1 summarizes the processing of the collected data. Real-time pressure data for each of the 4 consecutive beats of the full volume acquisition were averaged to obtain the overall LA-LV pressure gradient for the dataset. Manual point-by-point segmentation of the anterior and posterior mitral leaflet in one frame (end-diastolic frame) was performed by an echocardiographer (P.B.B.) using the Speqle3D package. The mitral annulus was manually segmented in all frames with the use of 9 orthogonal long axis planes (rotated in steps of 20°, two annular points per plane). The positions of the anterolateral and the posteromedial papillary muscles were segmented in each frame as well. The centroid position was used in case of multiple papillary muscle heads. In addition, for validation purposes, manual segmentation of the mid-systolic frame was performed for all datasets. The segmented point clouds were labeled and exported as MatLab-files for generation of the finite element mesh.

Patient-specific MV modeling

Numerical MV simulations were performed using the commercial finite element solver ABAQUS/Explicit 16.4 (Dassault Systèmes, Providence, USA) after generation of the mesh geometry and definition of boundary conditions in pyFormex (an open-source Python-based framework for processing complex 3D geometries). The mitral leaflet geometry in “unloaded” condition was determined by the end-diastolic frame. An algorithm was

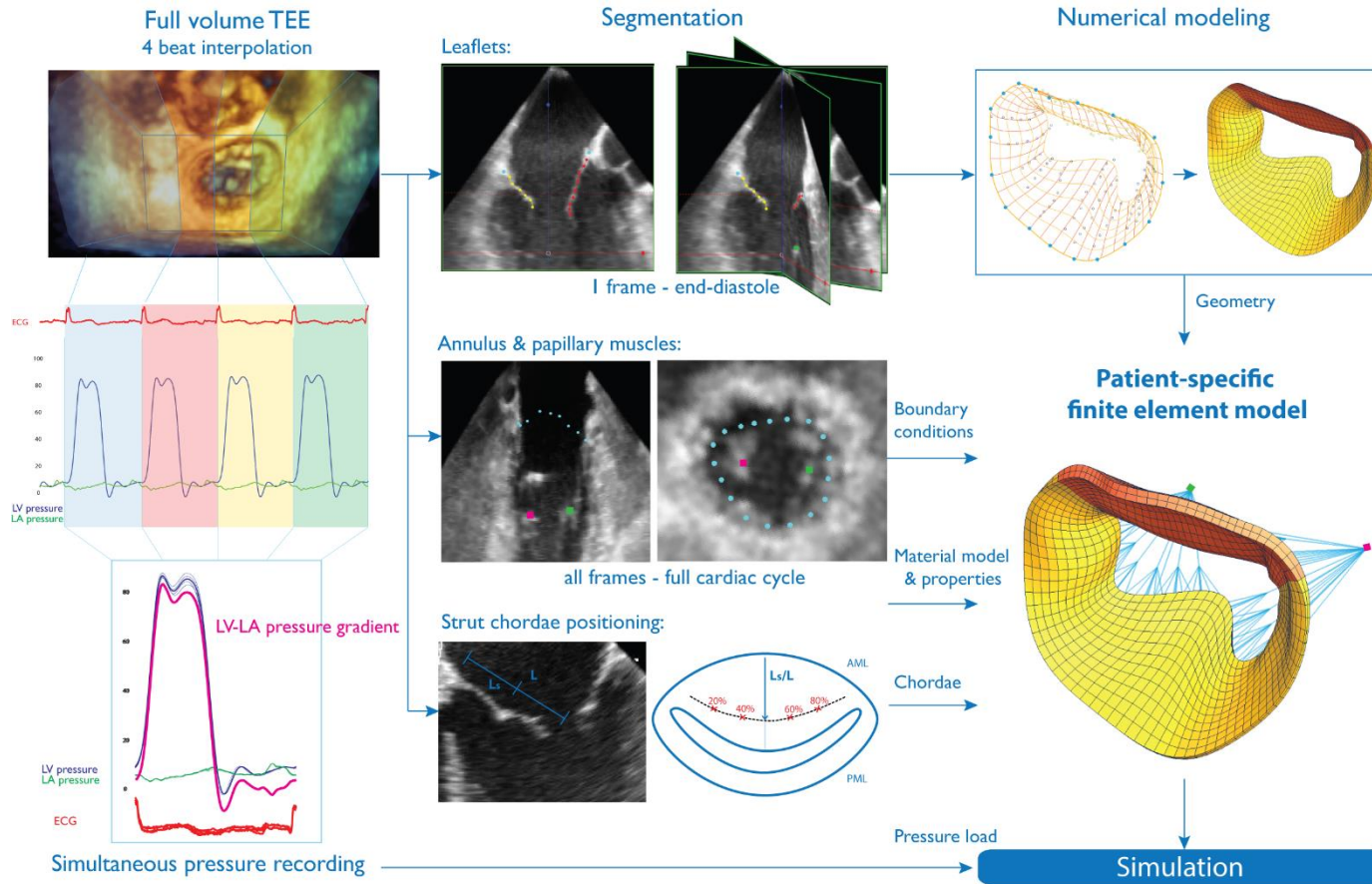
developed to automatically generate a finite element mesh from the segmented end-diastolic point cloud. Briefly, the algorithm fits a set of Bezier splines through the data points in longitudinal and circumferential direction. These splines are used as guidelines to define a new set of evenly distributed splines in both directions, the number of these splines in each direction being equal to the desired mesh density. The resulting surface mesh of quadrilaterals is subsequently extruded over a distributed leaflet thickness to obtain a mesh of hexahedral elements (C3D8R-elements with hourglass control in ABAQUS/Explicit). The thickness of the anterior leaflet was determined 1.5mm in the trigone area (defined as 40% of leaflet height), with tapering to 0.5mm in the free edge area^{224, 226}. Thickness of the posterior leaflet was set at a uniform thickness of 0.5mm²²².

Chordae tendineae were modeled as truss elements (T3D2) connecting the tip of the papillary muscles with the leaflets. At the insertion into the leaflets each chord splits into multiple smaller parts to divide the load applied by that respective chord. Three types of chordae were modeled: marginal chords that connect to the free edge of the leaflets, strut chords inserting at the body of the anterior leaflet, and basal chords inserting at the body of the posterior leaflet. The insertion height of the strut chords was measured patient-specifically in the echocardiography images. A total of 30 evenly distributed marginal chords (15 each papillary muscle) connecting to the free edge, 4 strut chords (anterior leaflet) and 4 basal chords (posterior leaflet) were modeled based on prior anatomic studies^{3, 4, 65}. Figure 6.1 shows the relative positioning of the strut chords that was applied based on the patient-specific insertion height and the human data of Song et al⁶⁵. Cross-sectional area of the marginal chords was set at 0.4mm² ; cross-sectional area of the basal chords was set at 0.8mm², and strut chords were set at 2.05mm² ^{229, 230}. Material properties for the three types of chordae tendineae were based on the human chordal mechanical testing in the work of Zuo et al²³⁰ and implemented in ABAQUS by means of a hyperelastic Ogden model.

Mitral leaflet material models

Mitral leaflet tissue was modeled as a hyperelastic transversely isotropic biological tissue. Three material models were calibrated based on the respective mechanical behavior of porcine, human healthy and human cardiomyopathy valve tissue in prior studies. The porcine material properties previously described by Prot and Holzapfel²²⁵ were based on the ex-vivo porcine biaxial MV leaflet testing in the work of May-Newman and Yin²²². The human valve leaflet mechanical characteristics were based on the data reported by Grande-Allen²³¹ et al of 21 normal MV (after autopsy) and 23 MV from transplant recipient hearts. Figure 6.2 displays the respective stress-strain curves for the porcine, healthy and cardiomyopathy leaflet tissue behavior. These three leaflet material models were evaluated in the computer simulations for the 10 clinical datasets.

Figure 6.1 - Overview of the modeling strategy. L, anterior leaflet length; Ls, leaflet length to strut chord insertion.



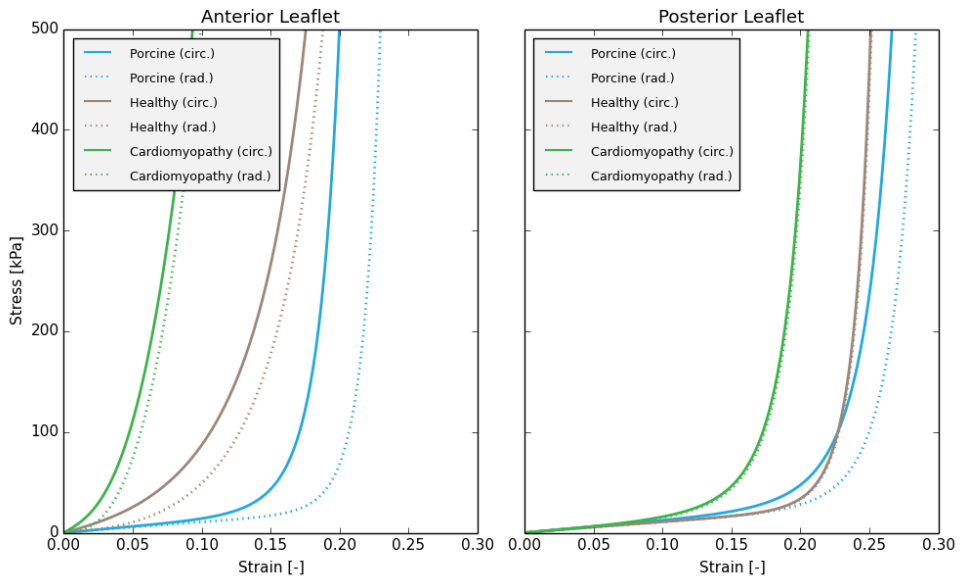


Figure 6.2 – Stress-strain curves for the here used anisotropic hyperelastic materials. The curves were generated under equi-biaxial tensile loading conditions and show the stress response in the circumferential (full line) and the radial (dashed line) conditions.

Patient-specific boundary (and loading) conditions

For each step in the cardiac cycle the patient-specific time-dependent annular motion and dynamics of the papillary muscle tips were extracted from the manually segmented full volume dataset, as described above, and imposed as boundary conditions. The invasively and simultaneously measured LA-LV pressure gradient was imposed as a loading condition on the ventricular side of each leaflet element (Figure 6.1).

Clinical validation strategy

Predicted MV closure and opening was first evaluated qualitatively for overall abnormalities. Quantitative comparison with the true situation (manual segmentation of mid-systolic 3D-TEE frame) was reported as the mean distance error (MDE) between the predicted leaflet mesh and the manually segmented leaflet mesh, and as the maximal mesh-to-mesh distance error. Mid-systolic tenting volume and closed leaflet area was extracted from the

numerical predictions, and compared to the actual tenting volume and closed leaflet area as reported for this dataset in a clinically available software package (4D MV-Assessment, TomTec Imaging, Germany). The difference between open-to-closed leaflet area was calculated to obtain the coaptation zone and 'coaptation index' as previously described²³². Briefly, the coaptation zone is the difference between (total) open leaflet area in end-diastole minus the closed leaflet area at mid-systole. The coaptation index is the coaptation zone divided by the open leaflet area. Finally, geometric predictions made by the computer model were correlated to the effective regurgitant orifice area measured immediately after the full volume acquisition by use of the proximal isovelocity surface area method.

Statistical analysis

Clinical data are presented as mean \pm SD for continuous variables and percentages for categorical variables. Comparison between healthy and secondary MR patients was performed using the unpaired Student's t-test. Repeated measures analysis of variance (ANOVA) was used to compare simulation results between porcine, normal and cardiomyopathy parameter sets. Linear regression was used to evaluate correlation between geometric valve parameters and effective orifice area. Statistical significance was set at a two-tailed probability of $p < 0.05$. All statistical analyses were performed using the GraphPad Prism version 5.00 for Windows, (GraphPad Software, San Diego, CA).

Results

Study population

Table 6.1 summarizes the clinical characteristics of the 10 studied patients. Secondary MR patients were older, had lower left ventricular ejection fraction, and larger left ventricular and atrial dimensions. At mid-systole, secondary MR patients compared to controls had a larger MV annular area and circumference, larger closed leaflet area, and more severe tenting volume and area (Table 6.2).

Predicted closure of normal mitral valves

In the normal datasets, all computational simulations with the porcine, healthy and cardiomyopathy leaflet material models provided realistic dynamic opening and closure of the valves during a full cardiac cycle. Figure 6.3 displays a typical example of predicted closure in a patient with a normal MV (animated cardiac cycle in Movie Clip 1). In the mid-systolic frame, simulation errors were the highest for the porcine material model (Table 6.3, Figure 6.4). MDE and peak error were comparable for the healthy and cardiomyopathy material model. However, leaflet coaptation became visually insufficient in a majority of control patients with the latter material model. Combining prediction error, predicted tenting volume and coaptation index, the human healthy material model provided the best fit for control patients (Figure 6.4).

Predicted closure of secondary MR valves

Mitral valve simulation in the secondary MR dataset accurately demonstrated dysfunctional closure due to subvalvular tethering and annular dilation (Figure 6.5, Movie Clip 2). Mid-systolic valve geometry, coaptation index and tenting volume were best predicted by the stiff cardiomyopathy material model (Table 6.4, Figure 6.4).

Geometric determinants of secondary MR

In secondary MR patients versus healthy controls, coaptation index was smaller ($p=0.058$) and tenting volume significantly larger ($p<0.001$) (Table 6.2). In the numerical simulations, irrespective of the material properties used, coaptation index and tenting volume remained significantly different in secondary MR versus controls (Table 6.3-6.4, Figure 6.4). The predicted tenting volume using the stiff material properties correlated strongly to the clinically measured tenting volume ($r=0.92$, $p<0.001$) of the total population, and importantly, to the clinically measured effective regurgitant orifice area ($r=0.87$, $p=0.001$, $y=12.5x-25.9$, Figure 6.6). This correlation is even stronger when controls are modeled with the healthy material properties, and secondary MR valves with the stiff material model ($r=0.90$, $p<0.001$).

Table 6.1 – Study population

Characteristics	Control group	Secondary MR group	p-value
No of patients	5	5	-
Age, yrs	60±10	75±9	0.044
Male, n	4 (80%)	4 (80%)	NS
BSA, m ²	1.9±0.2	2.0±0.2	NS
Image acquisition			
Frame rate, Hz	24±2	20±3	0.036
Imaging depth, cm	12±1	15±3	0.045
Echocardiography			
LV ejection fraction, %	63±6	39±13	0.01
LV EDV, mL	83±36	190±53	0.006
LV ESV, mL	31±14	120±55	0.02
LA area, cm ²	17±4	32±7	0.003
LA volume, mL	42±13	128±50	0.006
ERO, mm ²	NA	37±20	-
Rvol, mL	NA	56±22	-

BSA, body surface area; LV, left ventricle; EDV, end diastolic volume; ESV, end systolic volume; LA, left atrium; ERO, effective regurgitant orifice; Rvol, regurgitant volume.

Table 6.2 – Mitral valve geometry at mid-systole in healthy versus secondary MR patients

Characteristics	Control group (n=5)	Secondary MR group (n=5)	p-value
Annulus			
A-P diameter, cm	3.2±0.2	3.6±0.2	0.008
AL-PM diameter, cm	3.6±0.3	4.2±0.2	0.014
Circumference (3D), cm	11.4±0.8	13±0.8	0.012
Area (projected 2D), cm ²	9.3±1.6	12.3±1.3	0.012
Area (3D), cm	9.6±1.5	12.6±1.3	0.012
Height, cm	0.8±0.2	0.8±0.2	NS
Leaflets			
Tenting volume, mL	1.6±1.0	5.2±0.8	<0.001
Tenting area, cm ²	1.1±0.5	2.5±0.5	0.002
Total leaflet area, cm ²	12.4±1.5	15.3±2.8	0.068
Closed leaflet area, cm ²	10.4±1.8	14.3±2.7	0.025
Coaptation zone, cm ²	2.0±0.8	1.0±1.1	0.15
Coaptation index, %	16.5±7.5	6.5±6.8	0.058

Table 6.3 – Predicted mid-systolic geometry for the control valves for the three material models

	Porcine	Healthy	Cardiomyopathy	Real situation
Mean distance error, mm	1.58±0.42	1.32±0.30	1.23±0.25	-
Peak distance error, mm	4.73±0.94	4.41±5.60	4.42±1.06	-
Tenting volume, mL	0.8±0.3	1.7±0.3	2.2±0.5	1.6±1.0
Closed leaflet area, cm ²	11.0±2.0	10.7±2.1	10.8±2.0	10.4±1.8
Coaptation index, %	11.3±8.6	13.8±10.3	13.2±9.2	16.5±7.5
Average strain, %	35.0±0.4	26.1±0.9	20.8±0.1	-

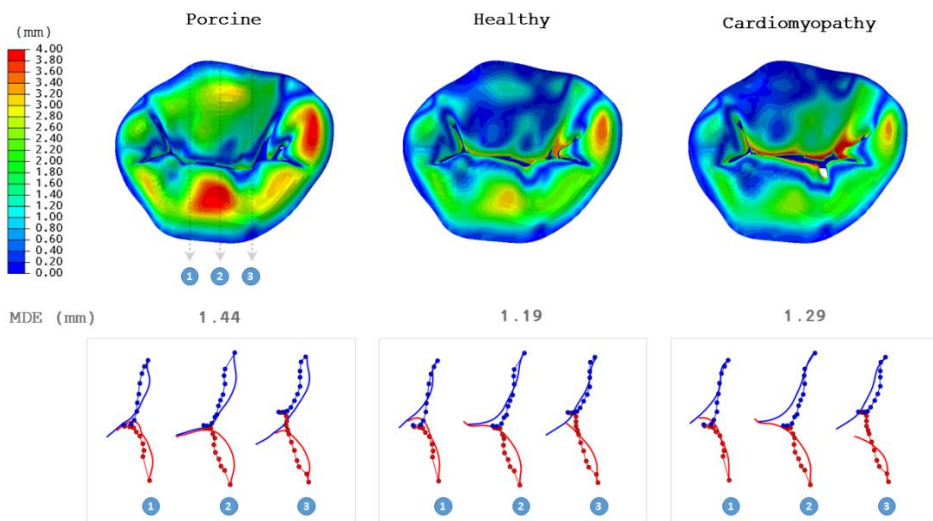


Figure 6.3 – En face view of the simulated mitral valve at mid-systole for the three material models in one healthy dataset ('Control' group). Colors indicate the distance error with respect to the true situation. Cross-sectional comparisons between simulation (complete line) and the manually segmented leaflet position (dots) are shown for both the anterior leaflet (blue) and the posterior leaflet (red). In this example the 'Healthy' material properties provide the best fit with respect to mean distance error (MDE) and tenting volume. The stiffer 'Cardiomyopathy' material properties provide a good leaflet fit, but valve closure is already impaired.

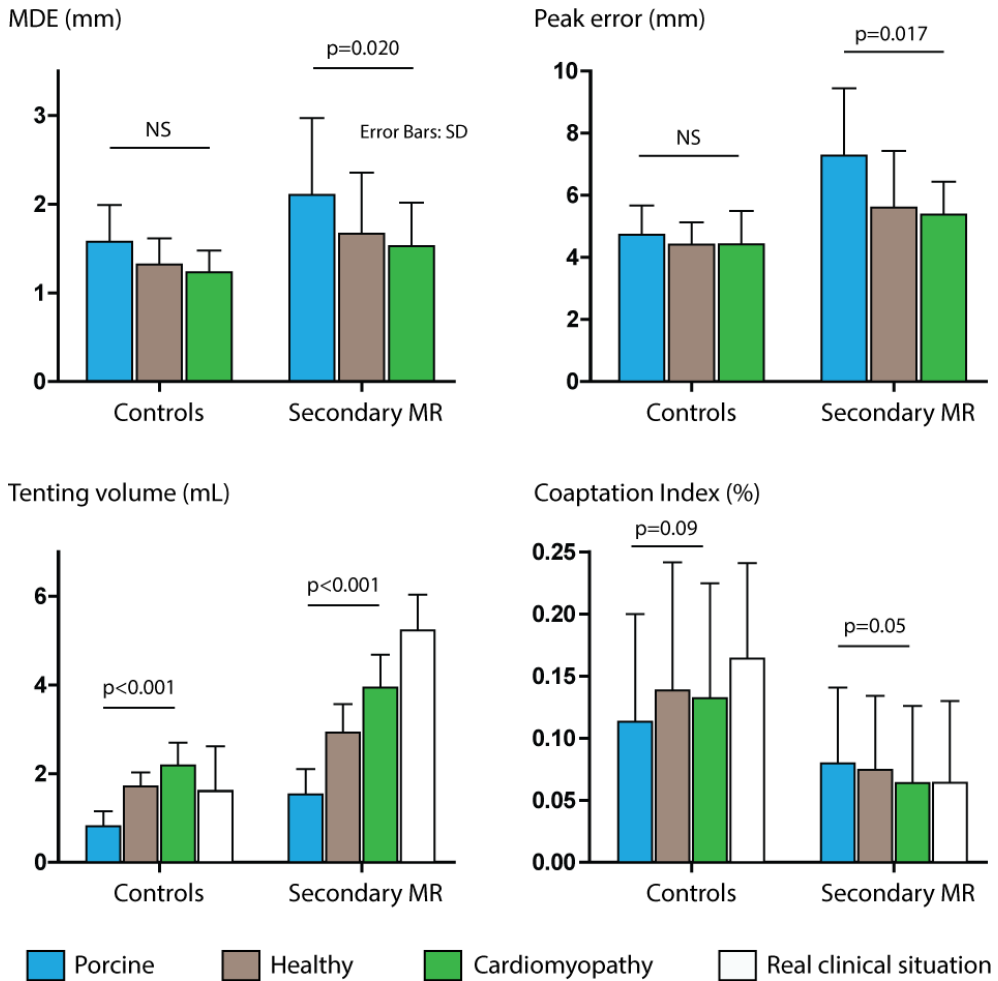


Figure 6.4 – Simulation results in control and secondary MR group for the different material properties. Mean distance error (MDE), peak distance error, predicted tenting volume and predicted coaptation index are reported for the three material models.

Table 6.4 - Predicted mid-systolic geometry for the secondary MR valves for the three material models and the real clinical situation

	Porcine	Healthy	Cardiomyopathy	Real situation
Mean distance error, mm	2.10±0.87	1.67±0.69	1.53±0.49	-
Peak distance error, mm	7.28±2.17	5.60±1.83	5.38±1.06	-
Tenting volume, mL	1.53±0.57	2.93±0.64	3.94±0.74	5.2±0.8
Closed leaflet area, cm ²	14.1±2.4	14.1±2.4	14.3±2.3	14.3±2.7
Coaptation index, %	8.0±6.1	7.4±6.0	6.4±6.2	6.5±6.8
Overall strain, %	36.6±1.8	27.3±1.5	21.9±1.2	-

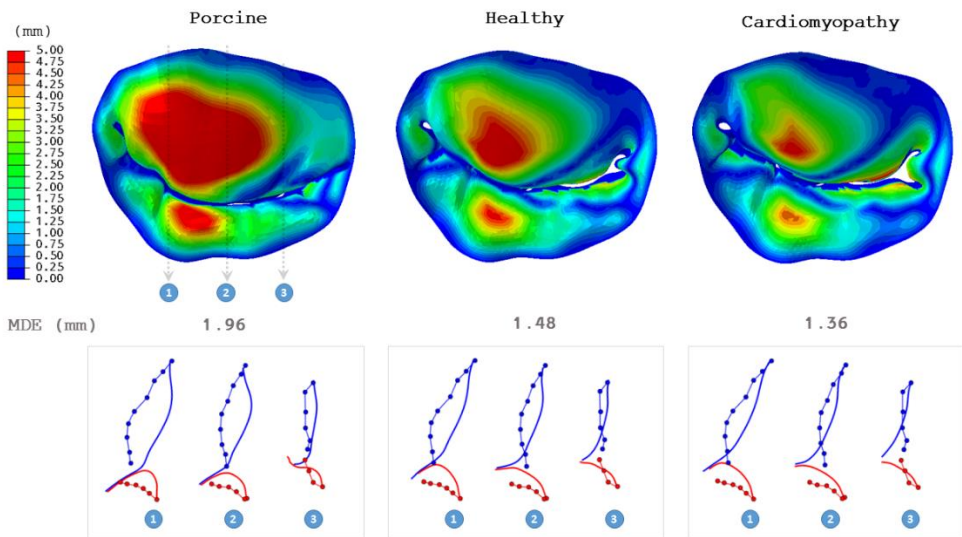


Figure 6.5 – En face view of the simulated mitral valve at mid-systole for the three material models in one secondary MR dataset. Colors indicate the distance error with respect to the true situation. Cross-sectional comparisons between simulation (complete line) and the manually segmented leaflet position (dots) are shown for both the anterior leaflet (blue) and the posterior leaflet (red). In this example the ‘Cardiomyopathy’ material properties provide the best fit with respect to mean distance error (MDE) and tenting volume.

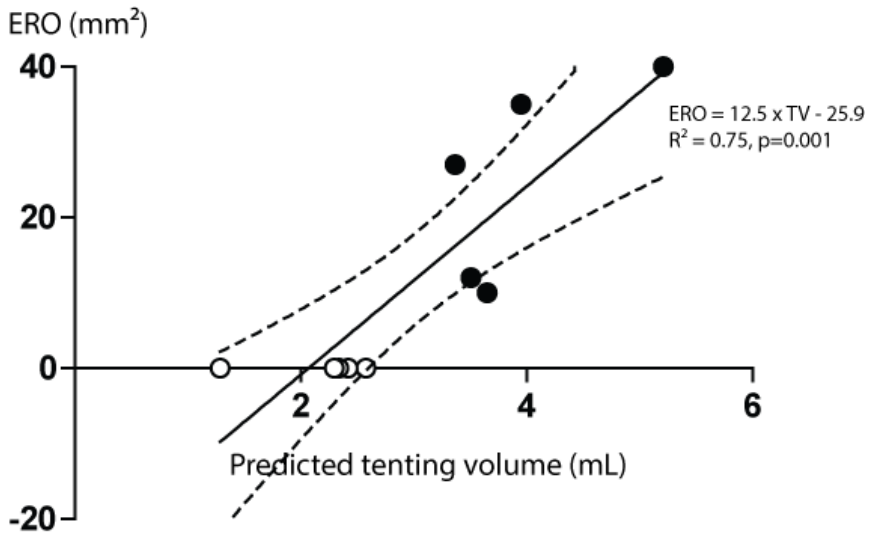


Figure 6.6 – Effective regurgitant orifice area (ERO) in function of the predicted tenting volume (TV) for the stiff ‘cardiomyopathy’ material model in the studied population. Secondary MR patients are displayed in full circles, while control patients are displayed in empty circles. The mid-systolic tenting volume as predicted by the computer model was strongly correlated to the clinically measured ERO.

Discussion

This study demonstrates the clinical validity of patient-specific MV modeling in normally functioning valves and in secondary MR in particular. Full volume 3D-TEE datasets with invasively measured loading conditions and a maximum available amount of patient-specific boundary conditions were used to assess the accuracy of currently adopted material models and properties in the prediction of human MV behavior. Three important observations can be made: (1) finite element modeling of the MV apparatus allows a realistic prediction of human valve dynamics in physiological loading conditions; (2) *in vivo* human leaflet behavior is different from the commonly applied porcine leaflet behavior, exerting relatively more stiffness in the radial direction; (3) simulations in secondary MR valves reliably predict geometric disturbances in the MV apparatus underlying the MR, and confirm an increased *in vivo* stiffness compared to human controls (possibly contributing to the pathophysiology).

Human versus porcine mitral leaflet behavior: comparison with previous work.

In the last decades, several efforts have been made to characterize the mechanical properties of mitral leaflet tissue and chordae tendineae²²²⁻²²⁵. Mitral leaflets typically exert an anisotropic (or transversely isotropic) hyperelastic behavior²²², i.e. leaflet stiffness increases with increasing stretch and stiffness is higher in the circumferential (direction of the collagen fibers) than in the radial direction. Chordae tendineae exert hyperelastic behavior as well²²³. However, most of this knowledge comes from *ex vivo* porcine MV, and *in vivo* validation has mainly been documented in animal studies^{226, 227}. Studies in human valves have either used more simplified material models and automation^{233, 234}, or were limited to well-established case reports of single patients²³⁵⁻²³⁷. Material properties of human MV leaflets and chordae tendineae are different from animals^{230, 236}, and prominent differences in leaflet behavior have been observed in healthy versus secondary MR valves²³¹.

In the present study, we have adopted the available knowledge from prior studies, using a hyperelastic transversely isotropic mitral leaflet material model described by Prot and Holzapfel²²⁵, and evaluated the commonly used porcine valve behavior as described by May-Newman and Yin²²² versus the human data provided in the study of Grande-Allen et al²³¹ in the prediction of human valve behavior. Our results demonstrate that the human valve behavior indeed is relatively stiffer than the porcine valves, especially in the radial (annulus-to-free edge) direction. This might in part explain the leaflet 'bulging' that has been observed in prior simulation studies^{234, 238}, which seems dictated by radial flexibility and extensibility. Furthermore, in healthy controls, the average simulation error in the leaflet belly tended to further improve with the stiff cardiomyopathy parameters, although correct closure of the valve then became compromised. This observation could indicate presence of localized *in vivo* stiffening within the leaflet belly, as was previously described²³⁹. This should certainly be subject to further exploration in future model refinements.

In contrast, in secondary MR patients, the stiff parameter set resulted in the closest leaflet concordance, while also demonstrating the best fit with respect to tenting volume and coaptation zone. These findings suggest that the *in vivo* behavior of chronically tethered secondary MR valves indeed is stiffer than healthy valves (as demonstrated *ex-vivo* by Grande-Allen et al²⁴⁰). Intriguingly, while this is likely an adaptive mechanism of the body to protect the leaflet from the high stresses imposed, this increased leaflet stiffening likely plays a role in the impaired valve closure (see the impaired closure occurring when the normal valves are stiffened) and thus likely contributes to the pathophysiology of secondary MR.

Patient-specific modeling in secondary MR.

To the best of our knowledge, this study is the first to evaluate, and demonstrate, the clinical validity of numerical modeling in secondary MR. The overall simulation accuracy and,

importantly, the close concordance between predicted and true mid-systolic tenting volume as well as the correlation with the clinically measured effective regurgitant orifice area, foretells a great clinical potential for individualized modeling as a tool in secondary MR patients. Indeed, secondary MR remains a challenging problem in current clinical practice, with a high prevalence and impaired prognosis in both ischemic and non-ischemic cardiomyopathy^{11, 15, 17}. Although the underlying mechanisms are gradually being elucidated, with secondary MR resulting from an imbalance between valve closing forces and tethering forces on the leaflets⁵⁶ (i.e. traction from dilated LV and/or displaced papillary muscles), the optimal approach to tackle secondary MR remains debated. Moreover, this debate is highly actual in the light of recent outcome results in the randomized CardioThoracic Surgical Trials Network (CTSN) trial showing moderate or more MR recurrence in 32.6% at 1 year, and in 58.8% at 2 years following restrictive mitral annuloplasty for severe secondary MR^{138, 241}. As ongoing leaflet tethering (i.e. tenting) is the primary cause of MR recurrence³⁶ and impaired leaflet opening¹³⁹ after surgery, additional approaches addressing the subvalvular apparatus (papillary muscle relocation³⁹, strut chordal cutting⁴¹, external constraint devices⁴³) are being proposed. However, none of the subvalvular approaches has gained clinical acceptance yet^{45, 46}; the reason being that the underlying mechanisms causing the tenting are highly individual, and a “one-size-fits-all” approach is destined to fail. A patient-specific 3D evaluation of the individual valve dynamics and leaflet tenting could therefore provide a major clinical benefit, and might even allow pre-intervention simulation of different approaches (e.g. papillary muscle relocation: in what direction? to what extent?) while evaluating the respective impact on the individualized leaflet geometry, tenting volume and coaptation zone. The proposed modeling strategy in this study provides validated clinical evidence to start moving in such direction^{242, 243}.

Limitations

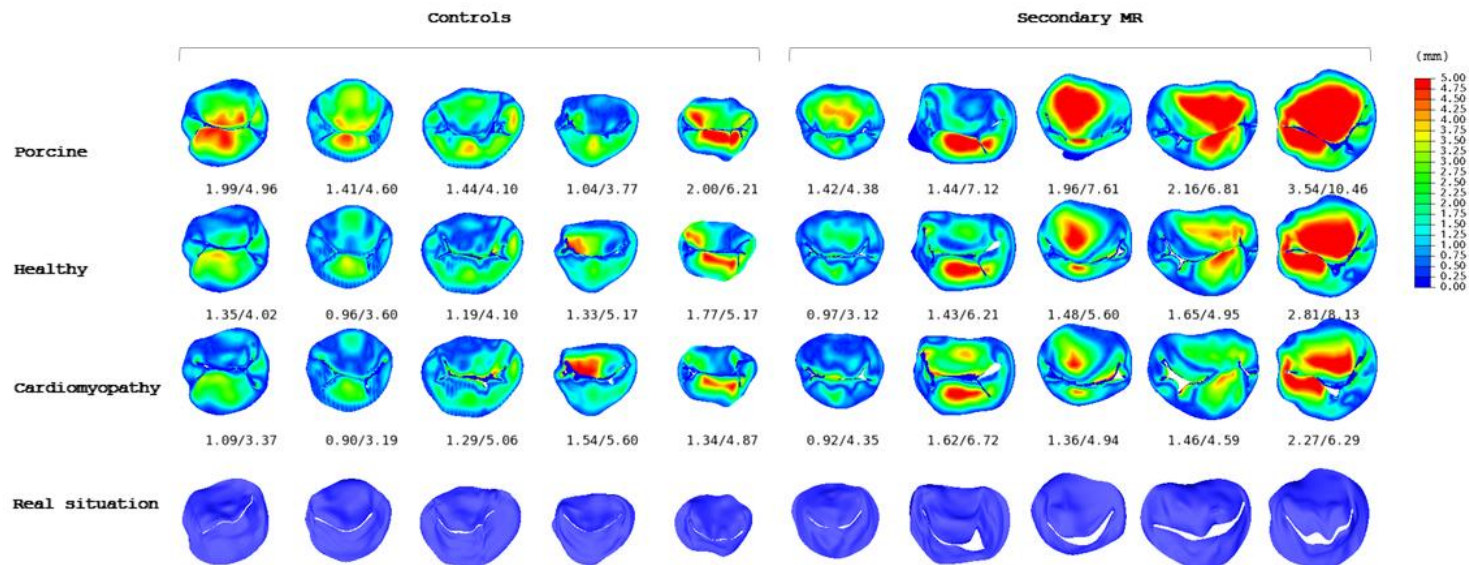
This was a single center study with small sample size. Extreme care was taken to obtain high quality datasets avoiding stitching artifacts, and with simultaneous LV and LA pressure recordings. Further increase in processing power will allow to obtain true beat-to-beat 3D full-volumes at acceptable frame rates. In addition, we deliberately avoided the use of automation in the segmentation of the datasets (annulus, papillary muscles, leaflet geometry) to obtain a 'ground truth' dataset for validation that was not affected by errors introduced by an automated segmentation or tracking algorithm. Finally, echocardiography does not allow to determine the exact number and location of the chords. Therefore, assumptions were made based on prior autopsy studies^{3, 4, 65} and all chords started from the centroid papillary muscle position. However, we did incorporate the patient-specific relative insertion of the strut chords (Figure 6.1), which was recently shown to be of importance in the pathophysiology of secondary MR⁶⁵. In the future, with further increases in ultrasound image quality and processing power, or by use of fusion imaging with computed tomography (in which the chords could be delineated²³⁵), further improvements in the model can be expected.

Conclusions

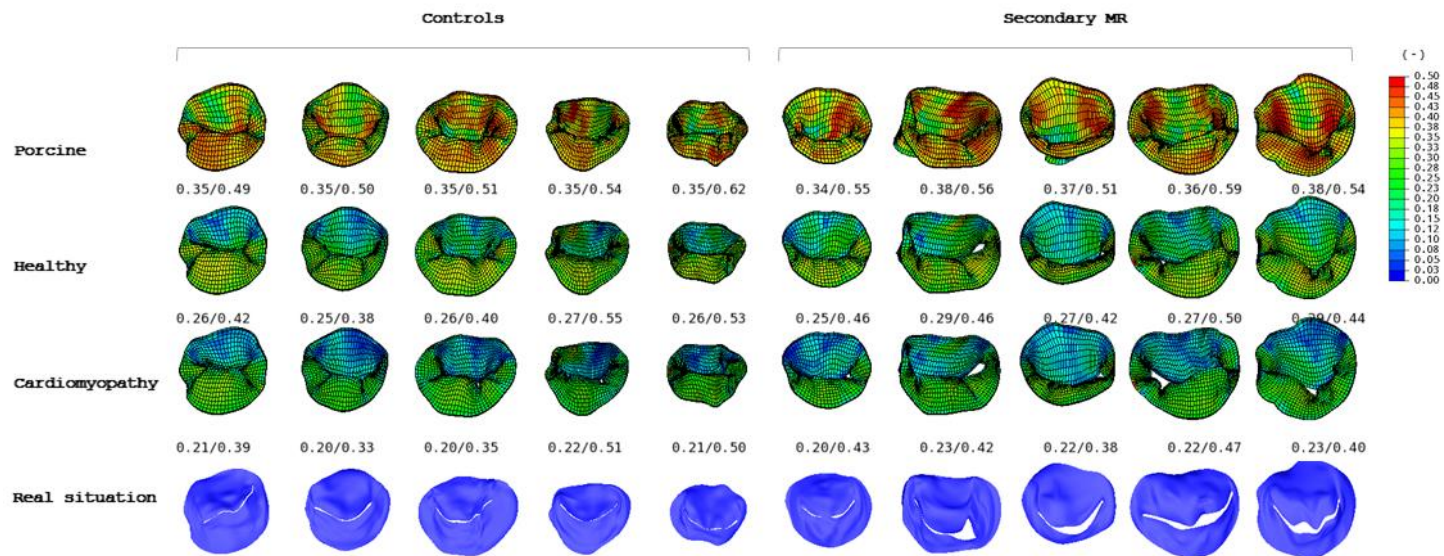
Echocardiography-based patient-specific MV modeling allows a realistic prediction of valve dynamics in physiological loading conditions in healthy and secondary MR patients. Secondary MR valves exert more in vivo stiffness than healthy valves, a finding of particular importance in our understanding of the pathogenesis of secondary MR. The strategy developed in this study shows great potential for improving insights in MV pathology, and for enhancing therapeutic efficacy by enabling pre-procedural planning and simulation. The latter could be particularly interesting in secondary MR patients.

APPENDIX : ALL PATIENT DATA

Supplemental Figure 1 – Distance error plots for all datasets. Mean and peak error (mm) are displayed for each case.



Supplemental Figure 2 – Strain distribution plots for all datasets. Mean and peak strain (-) are displayed for each case.



PART III:
IN VITRO SET-UP AND HEMODYNAMIC
STUDIES

Chapter 7

Influence of left ventricular outflow tract size on discrepancies in aortic stenosis grading: in vitro study and clinical relevance.

Bertrand PB, Verboven M, Nijst P, Grieten L, Ameloot M, Verdonck PR, Vandervoort PM.

Status of the manuscript:

Under review

JACC Cardiovascular Imaging (IF 7.2)

Abstract

Objectives: To investigate whether the size of the left ventricular outflow tract (LVOT) plays a role in discrepancies of aortic stenosis (AS) grading.

Background: Accurate assessment of AS severity is crucial for timing of intervention but discrepancies in AS grading are frequent, in part related to issues of flow contraction and pressure recovery.

Methods: Straight and tapered LVOT profiles with diameter of 25mm, 20mm and 15mm were mounted before an identical 1cm² stenosis in an in vitro steady-state flow model. Maximal and net pressure drop, flow velocities and coefficient of flow contraction (Cc) were measured by pressure catheter pullback and Doppler echocardiography. In 42 consecutive severe AS patients referred for transcatheter valve replacement, planimetry was compared with Doppler hemodynamics in small (<20mm) versus large (≥20mm) LVOT diameter.

Results: In vitro, Cc was 0.63±0.04, 0.71±0.03 and 0.80±0.02 for the straight 25mm, 20mm and 15mm diameter LVOT profiles respectively (p<0.001, n=48 measurements per profile). Mean pressure drop at 250mL/s steady-state flow over the same 1cm² stenosis was therefore 65±7mmHg, 50±6mmHg and 38±2mmHg for the respective straight LVOT profiles (p<0.001). This discrepancy was not observed in case of tapering in the LVOT profiles. In the severe AS patients, flow was more efficient in small versus large LVOT diameter (Cc=0.88±0.10 vs 0.80±0.13, p=0.03). Anatomic valve area was therefore smaller in the former group (0.63±0.13cm² vs 0.78±0.13cm², p=0.002) for the same Doppler hemodynamics (mean gradient 47±15mmHg vs 49.5±0.65mmHg respectively, p=0.65).

Conclusions: LVOT size plays a role in the contraction of flow through a stenotic orifice, with smaller LVOT sizes exerting a lower pressure gradient and higher effective orifice area

for the same stenotic aortic valve area. Hypothetically, patients with small LVOT are at a more advanced stage of disease when symptoms develop and/or hemodynamic thresholds for intervention are reached.

Introduction

Aortic valve stenosis (AS) is the most common valvular heart disease in the developed countries and is associated with significant mortality if left untreated^{244, 245}. The prevalence of severe AS is increasing with age, and by 2025 is expected to be 1.3 million patients in European countries and 0.8 million patients in North America²⁴⁶. Outcome depends on accurate assessment of the severity of AS, and timely referral for aortic valve replacement according to the latest guidelines⁴⁷. However in the assessment of AS severity using echocardiography and/or left heart catheterization, discrepancies in AS grading are frequent²⁴⁷⁻²⁴⁹. A source of discrepancy is the interchangeable use of the term 'aortic valve area' (AVA) that can be the 'true' geometric orifice area (GOA) traced by planimetry, an estimate of GOA calculated by use of the Gorlin equation in the cathlab or the effective orifice area (EOA) calculated on Doppler echocardiography using the continuity equation²¹⁰. For the same anatomic orifice significant differences between these AVA calculations can be observed, in part due to differences in flow contraction and/or the pressure recovery phenomenon^{250, 251}. Flow contraction depends on factors such as orifice geometry¹⁷³ and valve shape^{193, 252}, whereas pressure recovery is known to depend on the size and geometry of the outlet trajectory, i.e. ascending aorta¹⁹².

This study sought to investigate whether the size of the left ventricular outflow tract (LVOT) plays a role in the discrepancies between planimetry, invasive catheterization and Doppler echocardiography when evaluating patients with AS.

Theoretical background

Flow passing through a narrow orifice typically 'contracts' distal to the orifice, converging into a vena contracta being the smallest cross-sectional area encountered by the flow. This is the EOA, and is related to the 'true' GOA by a dimensionless coefficient of contraction (C_c):

$$EOA = C_c \cdot GOA \quad (1)$$

The flow rate F and flow velocity v through this narrow orifice are simply related by the continuity equation,

$$F = EOA \cdot v \quad (2)$$

and the instantaneous pressure gradient ΔP across the orifice can be approximated by the simplified Bernoulli equation:

$$\Delta P = \frac{\rho v^2}{2} \quad (3)$$

In this equation inertial and viscous losses are neglected. As previously described this simplification is possible because (1) boundary layer formation is suppressed except in the immediate vicinity of the walls; (2) the mass of blood being accelerated across the valve at any instant is small; and (3) proximal to the orifice, most energy is present as potential energy and the proximal velocity can be omitted¹⁹¹. Combining equations (2) and (3), while converting pressure units to mmHg and applying a blood fluid density ρ of 1.05 g/cm^3 results in the fundamental hydraulic relationship between EOA [cm^2], F [mL/s] and ΔP [mmHg].

$$EOA = \frac{F}{50.4 \sqrt{\Delta P}} \quad (4)$$

This relationship is similar to the Gorlin formula (equation 5), although that formula calculates 'true' GOA by implicitly incorporating a coefficient of contraction in the formulation:

$$GOA = \frac{F}{C_c \cdot 50.4 \sqrt{\Delta P}} \quad (5)$$

The Gorlin constant for aortic valves is typically 44.3, hence a C_c of 0.879 is applied for all situations^{172, 173}. Furthermore, ΔP used in the Gorlin equation is often the 'net' pressure

difference measured in the cathlab after occurrence of some pressure recovery, whereas ΔP in equation 4 is the 'maximal' pressure difference in the vena contracta.

The purpose of the current study was to investigate the influence of the LVOT on the flow contraction and pressure recovery in severe AS, and hence on the discrepancies between planimetry, Gorlin area and EOA.

Materials & Methods

In vitro set-up

The in vitro model consisted of two perspex chambers: a proximal chamber (10x30x50 cm) that could be sealed and a distal larger outflow chamber (40x30x50 cm) at atmospheric pressure (Figure 7.1). A modular orifice was provided in the perspex septum separating both chambers, in which a stenotic circular orifice of 1cm² was mounted. Circular, axisymmetric LVOT profiles with a straight, tapered or semi-tapered profile and varying diameter of 15mm, 20mm and 25mm were mounted in front of the stenotic orifice (Figure 7.2). Behind the stenotic orifice of 1cm² either no profile, a 37.5mm diameter tube of 10cm length, or a 25mm diameter tube of 10cm length was mounted to simulate a severely dilated, a large-to-normal and a small ascending aorta respectively. A frequency-controlled centrifugal pump (EBARA, Rock Hill, SC) was used, driven by a 1-phase inverter (FI-E11, Indumex, The Netherlands) and controlled by a feedback loop implemented in LabVIEW (National Instruments, Austin, TX) via a data acquisition module (DAQ X Series, National Instruments). A vortex-based flow sensor (Huba Control 230, Würenlos, Switzerland) was mounted between the pump and the entrance of the sealed chamber and connected to the data acquisition module. Polyvinylchloride tubings of 40mm diameter were used to connect the pump with the perspex chambers. The fluid (1% aqueous solution of cornstarch) was

pumped into the proximal chamber at predefined flow rates between 10L/min (or 167mL/s) and 25L/min (or 417mL/s), and left the distal chamber via an overflow outlet.

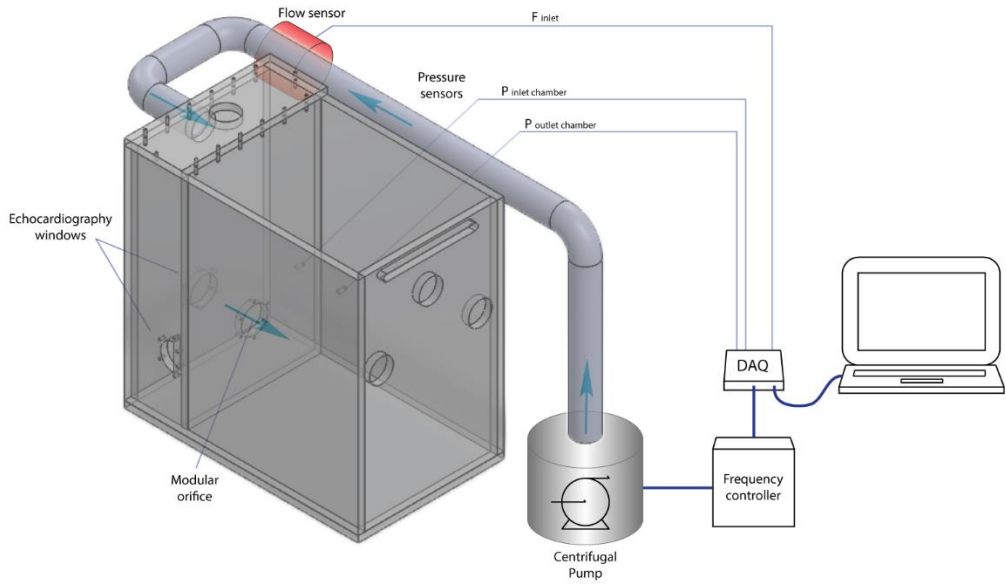
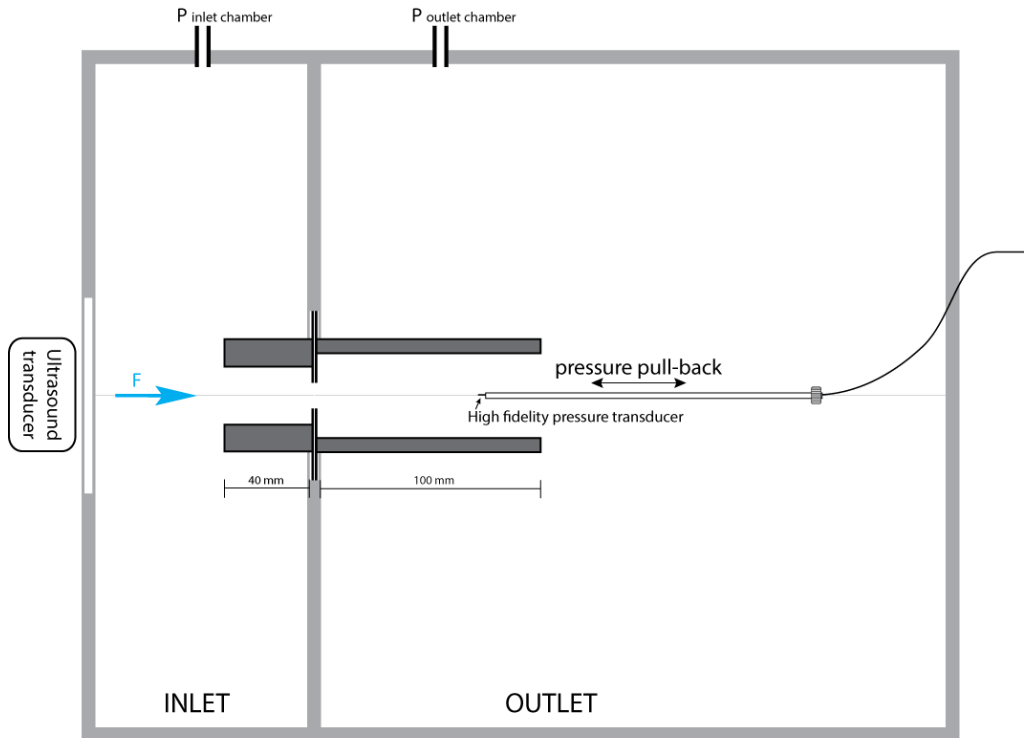


Figure 7.1 – In vitro set-up.



25mm		GOA 1.0 cm ²		no outlet profile
20mm				37.5 mm
15mm				25 mm
25mm		GOA 1.0 cm ²		no outlet profile
20mm				37.5 mm
15mm				25 mm

Figure 7.2 – Cross-sectional view of the in vitro set-up at the level of the orifice.

Data acquisition

Pressure pullback measurements through the center of the orifice were obtained using an SPR-320 MikroTip high-fidelity pressure transducer (Millar Inc, Houston, TX), connected to a commercially available pullback device R-100 (Volcano, Zaventem Belgium). The pressure catheter (2F) was stabilized with a 3F introducer sheath to ensure stable and straight pullbacks (1mm/s) through the center of the orifice. A quad-bridge amplifier and PowerLab 26T module (AD Instruments, Oxford, United Kingdom) was used to transfer the pressure transducer data to LabChart v7.3.7 software. (AD Instruments). The pressure waveforms were digitized at 1000 Hz and exported as text-files to process data in custom-written MATLAB routines (The Mathworks Inc, Natick, MA). Pressure measurements started 5cm proximal to the valve and were acquired continuously until 5cm downstream from the valve. In addition, the pressure at the end of the outflow profile (10cm downstream) was registered, at which point the recovery of pressure has typically occurred²⁵³.

Flow rate was set at 10L/min, 15L/min, 20L/min and 25L/min, i.e. 167mL/s, 250mL/s, 333mL/s and 417mL/s steady-state flow respectively. All pressure pull-back measurements were repeated at least 4 times and at 2 different days for each inflow-outflow geometry and each flow rate to ensure repeatability. Simultaneous continuous wave Doppler velocity measurements were obtained using an iE33 workstation (Philips Medical Systems, Andover, MA) and an S-3 ultrasound transducer positioned proximal to the orifice along the centerline (Figure 7.2).

Data analysis

The proximal pressure (P_{prox} , measured 5 cm proximal to the orifice), the minimal pressure (P_{min} , at the vena contracta), and the distal pressure (P_{dist} , measured at 10 cm distal to the orifice) were read out from the pressure recordings for each profile and at each flow rate (Figure 7.3).

The maximum pressure gradient ($\Delta P_{\max} = P_{\text{prox}} - P_{\text{min}}$) was used for EOA calculation using equation 4, with F being the imposed flow rate in mL/s. The net pressure drop ($\Delta P_{\text{net}} = P_{\text{prox}} - P_{\text{dist}}$) was used to calculate the estimated GOA using the Gorlin equation (equation 5). The recovery of pressure between P_{min} and P_{dist} was calculated as the pressure recovery coefficient $C_p = \frac{P_{\text{dist}} - P_{\text{min}}}{P_{\text{prox}} - P_{\text{min}}}$. Using echocardiography, the maximal velocity V_{\max} of the continuous wave Doppler signal was used to calculate $\text{EOA}_{\text{doppler}} = F/V_{\max}$. Invasively, V_{\max} was obtained by inverting the simplified Bernoulli equation ($\Delta V = \sqrt{\Delta P_{\max}/2}$) and neglecting the proximal velocities along the centerline. Moreover, the invasive calculation of EOA by use of equation 4 implies that proximal velocities are omitted as well.

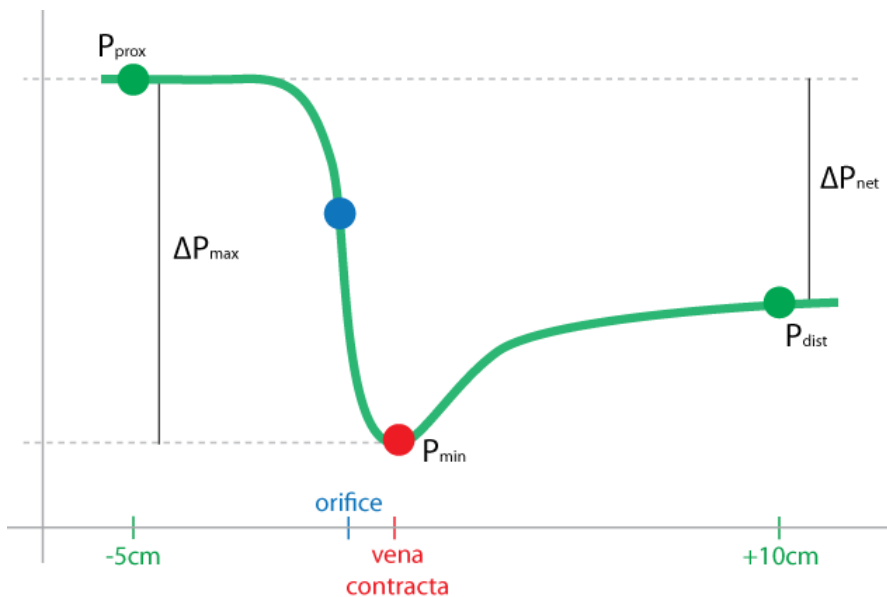


Figure 7.3 – Pressure registration during catheter pullback.

Clinical data

All 54 consecutive patients that underwent a transcatheter aortic valve replacement (TAVR) in a single tertiary referral center (Ziekenhuis Oost-Limburg, Genk, Belgium) from January 2009 until January 2016 were retrospectively screened. These comprised typically elderly, high-risk patients with severely calcified aortic valves, in whom dedicated preoperative transesophageal short-axis images for GOA planimetry were acquired in addition to the standard transthoracic Doppler assessment of transvalvular velocities, pressure gradients and EOA. To exclude confounding geometric factors that might influence flow contraction, only tricuspid aortic valves without 'doming' of the leaflets were included. A total of 12 patients were excluded because of incomplete image data or inability to reliably delineate the GOA in zoomed short axis window (n=6), bicuspid aortic valve disease (n=2), doming of the valve leaflets, defined by leaflet-to-annular plane angle $>20^\circ$ (n=3) and a valve-in-valve procedure (n=1). In the 42 eligible patients, LVOT diameter was measured in a zoomed transesophageal long-axis view, and GOA was traced by planimetry in a zoomed short axis transesophageal image. The pulsed wave LVOT velocity time integral (VTI) and the continuous wave aortic valve VTI were acquired in apical transthoracic images and used to calculate EOA using the continuity equation. Cc was calculated for each patient as EOA/GOA. The study was approved by the locally appointed ethics committee, who waived the need for individual consent due to the retrospective and observational nature of the study.

Statistical analysis

In vitro hemodynamic data (ΔP , ΔV) are averaged over at least 4 separate measurements and presented as mean \pm standard deviation. Repeatability of the pressure measurements within the in vitro set-up was excellent with coefficient of variation (i.e. SD relative to the mean) of $3.2 \pm 2.1\%$ for all individual profile and flow situations. In vitro Cc and Cp are therefore presented as mean value only for individual profiles, and as mean \pm SD when

averaged for a group of profiles. Repeated measures analysis of variance (ANOVA) was used to compare results among different sizes of the same LVOT profile, whereas the student's T-test was used to compare among different LVOT geometries. Pearson's correlation coefficient was used to assess linear correlation between Vmax and ΔV . Clinical data are presented as mean \pm SD, and compared using the unpaired student's t-test. Statistical significance was always set at a 2-tailed probability of $p < 0.05$. All statistics were performed using SAS JMP Pro (version 11.2 for Windows).

Results

In vitro coefficient of contraction

Average Cc was 0.71 ± 0.08 , 0.87 ± 0.03 and 0.87 ± 0.03 for the straight, tapered and semi-tapered LVOT profiles respectively ($p < 0.001$ for difference between straight and (semi-)tapered profiles). Within the straight LVOT profile, a decrease in diameter resulted in significantly higher Cc (0.63 ± 0.04 , 0.71 ± 0.03 and 0.80 ± 0.02 for the 25mm, 20mm and 15mm diameter profile respectively, $p < 0.001$). In contrast, in the (semi-)tapered profiles a decrease in diameter resulted in a small yet statistically significant decrease in Cc (Table 7.1).

Table 7.1 – In vitro measured coefficient of flow contraction (Cc) for the different LVOT profiles and the 25mm diameter ascending aorta profile tract diameter.

Similar results were observed with the 37.5mm aorta profile and with no aorta profile.

	25mm	20mm	15mm	ANOVA <i>p</i> -value
	0.65	0.75	0.80	<i><0.001</i>
	0.86	0.85	0.84	<i>0.2</i>
	0.87	0.86	0.84	<i>0.004</i>

Pressure gradients at similar flow rate and for the same geometric orifice of 1cm² were therefore significantly different among LVOT sizes and geometries (Figure 7.4). At 15L/min steady state flow (i.e. 250mL/s mean transaortic flow rate), the maximal pressure gradient ΔP_{\max} across the 1cm² orifice was 65±7mmHg, 50±6mmHg and 38±2mmHg for the straight 25mm, 20mm and 15mm diameter LVOT profile respectively ($p < 0.001$, Figure 7.4-A). ΔP_{\max} was lower in the tapered and semi-tapered profiles, without relevant impact of size in these geometries (Figures 7.4-B and 7.4-D). Similar differences were observed in terms of net pressure loss ΔP_{net} (Figure 7.4-C), albeit at lower absolute values due to the pressure recovery phenomenon.

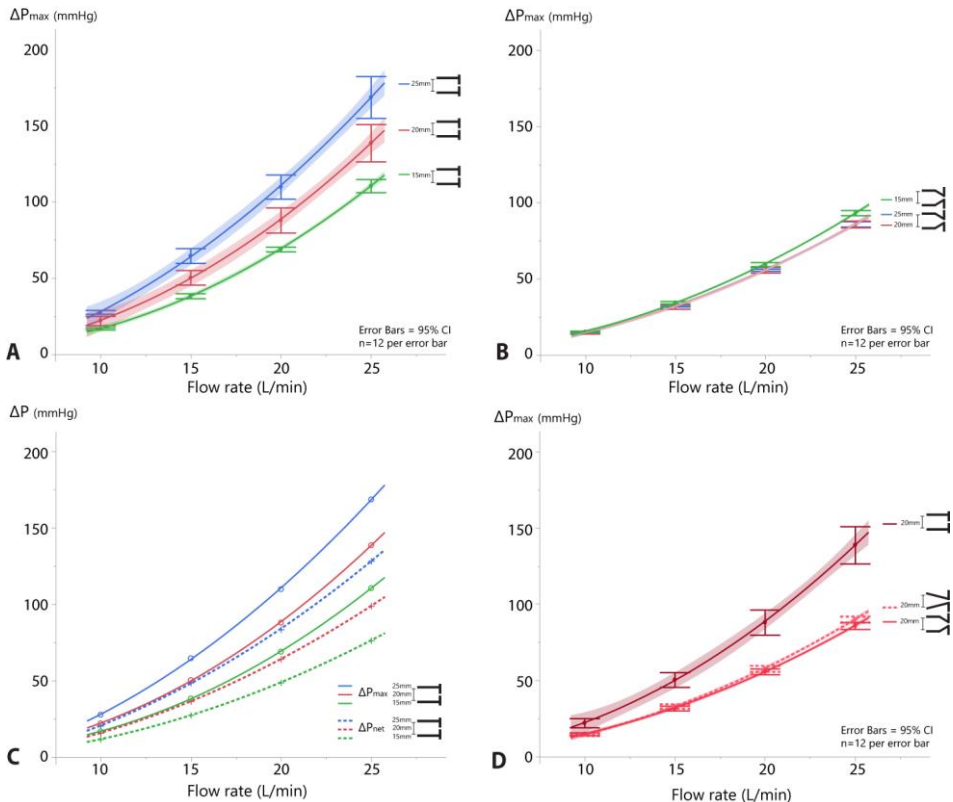
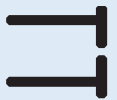


Figure 7.4 – Impact of LVOT size and geometry on pressure gradients for same geometric orifice of 1cm². CI, confidence interval;

In vitro pressure recovery

ΔP_{net} was $26 \pm 11\%$ smaller than ΔP_{max} , due to recovery of pressure at 10cm distal to the stenosis. C_p was 0.28 ± 0.10 , 0.25 ± 0.13 and 0.25 ± 0.11 for the straight, tapered and semi-tapered LVOT profile respectively (p =not significant). The size of the ascending aorta profile had a profound impact on C_p (0.12 ± 0.03 , 0.27 ± 0.02 and 0.39 ± 0.03 for no profile, the 37.5mm diameter tube, and the 25mm diameter tube respectively, $p < 0.001$). The size of the LVOT profile had a similar impact on C_p as was seen for C_c (i.e. a decrease in LVOT size led to increased C_p for straight profiles, whereas in the tapered profiles the opposite was observed), although the absolute changes in C_p due to LVOT size variation were small (Table 7.2).

Table 7.2 – Net pressure recovery coefficient (C_p) for the 25mm diameter outflow tube.

	25mm	20mm	15mm	ANOVA p -value
	0.35	0.39	0.40	0.006
	0.40	0.39	0.38	<0.001
	0.40	0.39	0.38	0.006

In vitro Doppler echocardiography

Echocardiographic V_{\max} showed an excellent correlation with the invasive ΔV_{\max} ($R^2=0.99$, $y=0.93x + 5.73$, Figure 7.5), justifying the neglecting of the proximal velocities in the invasive EOA calculations. EOA_{doppler} showed a similarly strong correlation with the invasively measured EOA at the vena contracta ($R^2=0.90$, $y=0.94x+0.09$).

The calculated Gorlin GOA based on the net pressure difference ΔP_{net} was $1.10 \pm 0.13 \text{cm}^2$ overall, and correlated moderately to the invasive EOA ($R^2=0.57$, $y=1.14x+0.15$). Figure 7.6 displays the relationship between EOA and Gorlin GOA for the different LVOT and ascending aorta profiles and 'true' GOA of 1cm^2 .

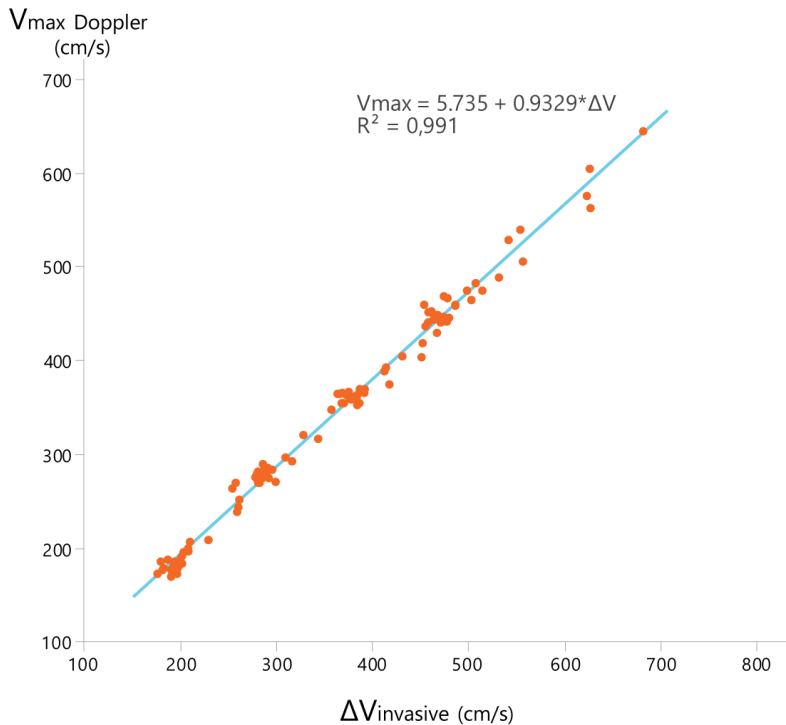


Figure 7.5 – Echo Doppler V_{\max} versus invasively measured ΔV

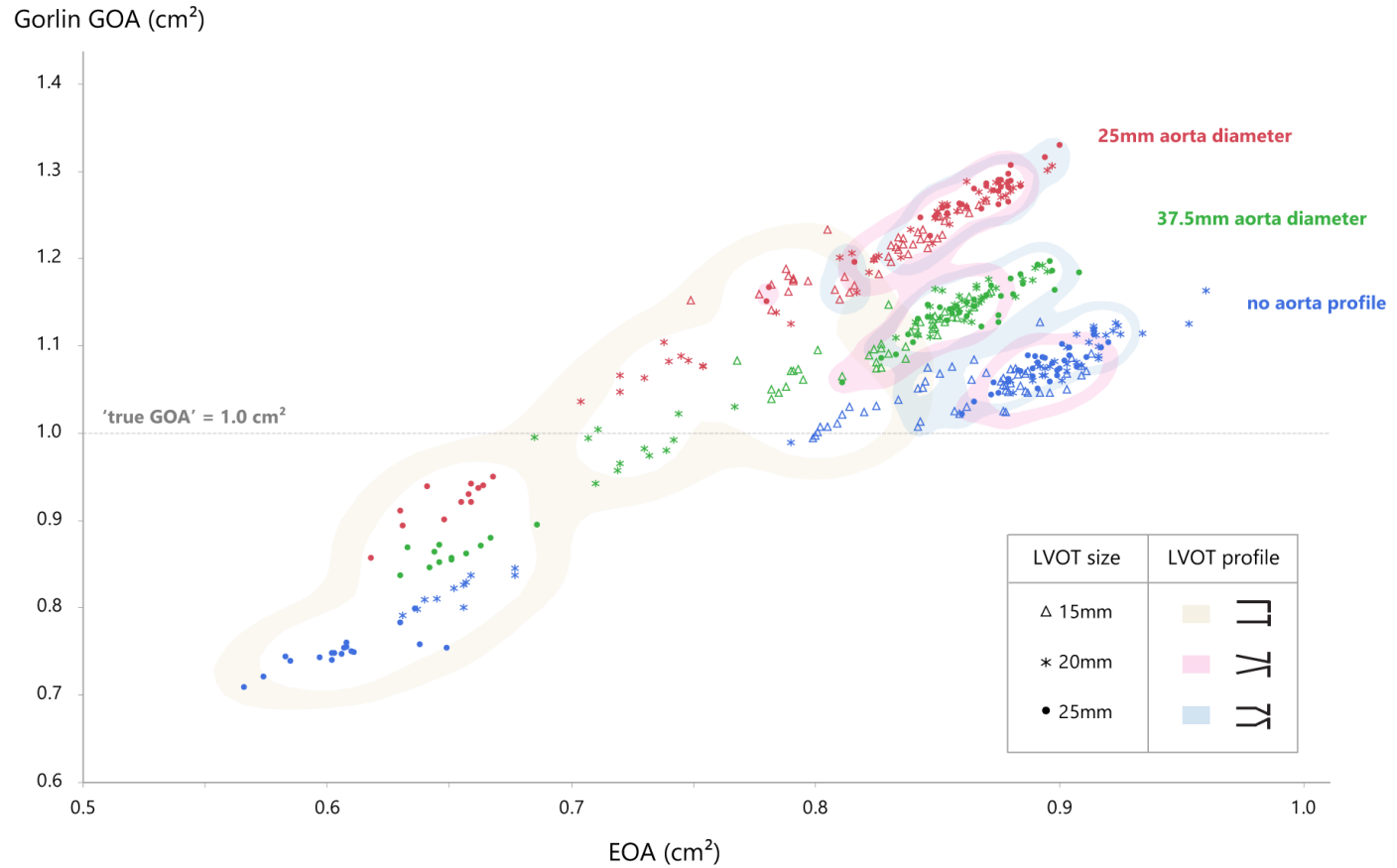


Figure 7.6 – Geometric orifice area (GOA) as calculated by the Gorlin equation versus the effective orifice area (EOA) measured in the vena contracta for the different left ventricular outflow tract profiles and ascending aorta diameters.

Clinical data

The study population consisted of 42 patients referred for TAVR. Median LVOT diameter was 20.0 mm (range 16.6–25.0 mm). Table 7.3 summarizes clinical and echocardiographic parameters for patients with small LVOT diameter (<20mm, n=21) versus large LVOT diameter (≥20mm, n=21). Patients with small LVOT size were typically female and with small body size. Septal wall hypertrophy was more pronounced in the small LVOT group (p=0.008, clinical example in Figure 7.7), and LVOT size indexed for body size was lower than in the large LVOT group. In the small LVOT patients, Cc was higher than in patients with large LVOT (0.88±0.10 versus 0.80±0.13, p=0.03). Aortic valves were more severely obstructed (AVA 0.63±0.13 versus 0.78±0.13, p<0.001) in small versus large LVOT patients for the same Doppler hemodynamics and EOA, even after correction for body size.

Table 7.3 – Comparison of clinical and Doppler echocardiographic parameters in the patient population undergoing transcatheter aortic valve replacement with respect to the size of the left ventricular outflow tract.

Parameters	LVOTd <20mm	LVOTd ≥20mm	p-value
n	21	21	1.0
age, yrs	84±6	83±6	0.64
male	5 (24%)	13 (62%)	0.01
BSA, m ²	1.67±0.18	1.85±0.22	0.009
Echocardiographic dimensions			
LVOTd, mm	18.3±1.0	21.6±1.3	<0.001
LVOTd index, mm/m ²	10.9±1.4	11.8±1.4	0.053
Basal septum thickness, mm	18±3	15±4	0.008
Ascending aorta diameter, mm	31±4	32±4	0.21
Doppler measurements			
LVOT VTI, cm	21.8±4.5	18.5±5.9	0.057
SV, mL	59±11	67±19	0.027
SV index, ml/m ²	34±6	36±9	0.25
AV mean gradient, mmHg	47±15	49.5	0.65
AV peak gradient, mmHg	79±21	80.7	0.73
AV Vmax	4.3±0.6	4.4±0.6	0.71
Coefficient of contraction			
EOA, cm ²	0.55±0.11	0.62±0.12	0.065
EOA index, cm ² /m ²	0.33±0.06	0.34±0.07	0.57
GOA planimetry, cm ²	0.63±0.13	0.78±0.13	<0.001
GOA planimetry index, cm ² /m ²	0.38±0.08	0.43±0.08	0.04
Cc	0.88±0.10	0.80±0.13	0.03

LVOTd, left ventricular outflow tract diameter; VTI, velocity time integral; SV, stroke volume; AV, aortic valve; EOA, effective orifice area; AVA, aortic valve area; Cc, coefficient of contraction;

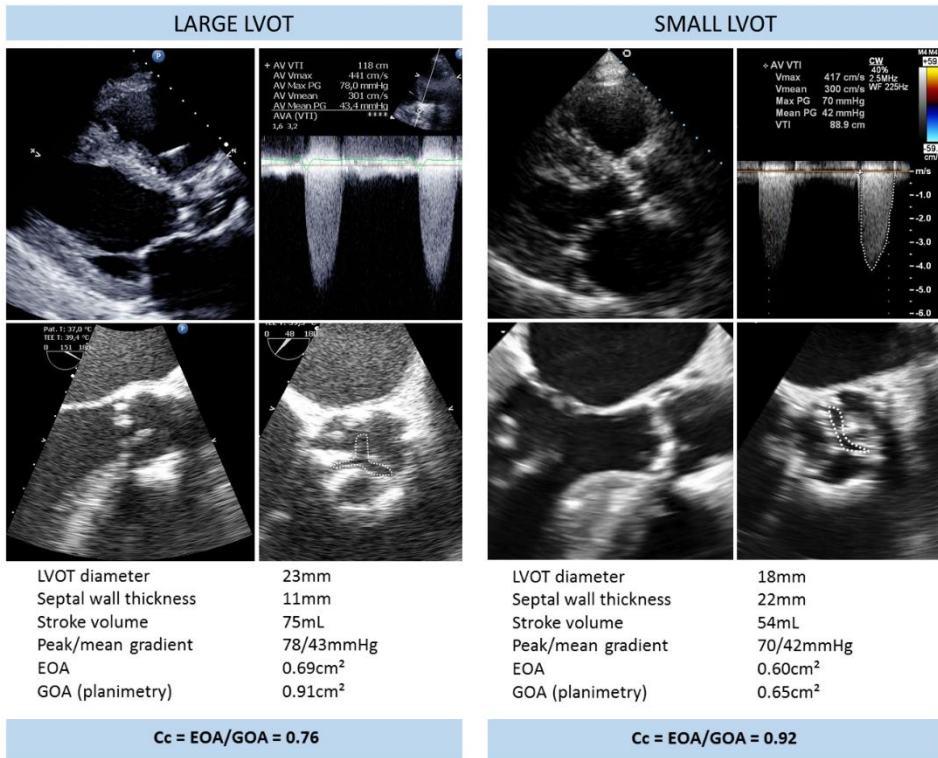


Figure 7.7 – Clinical comparison of a patient with large versus small left ventricular outflow tract, and the respective impact on aortic stenosis hemodynamics and grading.

Discussion

This study demonstrated that LVOT size influences the fluid dynamics of rigid AS, and plays a role in the discrepancies between EOA, Gorlin GOA and the 'true' anatomic AVA. In vitro steady-state flow simulations showed a lower pressure gradient over the same geometric orifice in small versus large (straight) LVOT profiles due to better flow convergence (higher Cc). In the clinical setting as well, small LVOT sizes were associated with higher Cc, and thus a closer concordance between anatomic AVA and the EOA was observed. In these small LVOT patients, by the time Doppler gradients and/or symptoms reached levels warranting referral for intervention, anatomic AVA was smaller than in patients with large LVOT sizes. Hypothetically, due to this better flow convergence, small LVOT patients are diagnosed with severe AS only at a further stage of the disease, which might (in part) explain the less favorable outcome previously observed in this subset of patients ^{254, 255}.

The role of the LVOT in the contraction of flow

Fluid dynamic studies for both aortic and mitral valve stenosis have previously shown that the valve inflow shape is an important determinant of the way flow 'contracts' through an orifice, and determines the ratio (Cc) of 'effective' use of the area (EOA) to actual area (GOA)^{174, 193, 252}. In flat abrupt orifices without funneling of flow, such as severely calcified (tricuspid) aortic valves, flow contraction is most pronounced and EOA least effective. In such flat orifices, the proximal inlet area A_{prox} has an impact on the contraction of flow, with smaller area (with respect to GOA) offering a more favorable flow contraction, and hence higher Cc (Figure 7.8). Mathematically, for a long and constant inlet profile approaching an abrupt flat stenosis in ideal fluid flow conditions, the relationship between EOA, GOA and A_{prox} was deduced by Garcia et al ¹⁹³ from basic hydrodynamic research and expressed as:

$$EOA = GOA \cdot \left(1 + \frac{\sqrt{2}}{2} \sqrt{1 - \frac{GOA}{A_{prox}}} \right)^{-1} \quad (6)$$

Based on this theoretical formula, C_c was expected to be 0.61, 0.63 and 0.68 for the straight 25mm, 20mm and 15mm diameter inlet profile respectively. The C_c values were 0.63, 0.71 and 0.80 respectively in our in vitro set-up and even higher C_c values were observed in the clinical population. LVOT profiles in our study, however, had a finite length of 40mm proximal to the stenosis, and some degree of flow convergence already occurred at the entrance of the LVOT profile in the smaller profiles. Therefore, the velocity profile and flow characteristics within the LVOT profiles were potentially different from the ideal flow conditions within long tubes represented in equation 6. Furthermore, the length of the LVOT in clinical practice is even shorter (range 5-25mm in our patient cohort) and similar flow convergence is expected to occur during ejection of blood from the larger ventricle into the small LVOT trajectory (Figure 7.7). We hypothesize that the LVOT acts as conduit that 'guides' the ejected volume towards and through the aortic valve, thereby optimizing flow convergence in case of smaller LVOT sizes (Figure 7.8).

Intriguingly, in the tapered and semi-tapered profiles, the small 15mm diameter profile tended to exert a lower C_c than the larger diameters. This is likely the result of a similar flow convergence at the entrance of the profile, that caused the small tapered profile to be less efficient. These differences in C_c however were small; therefore it is fair to conclude that in patients with leaflet 'doming' such as bicuspid valves or less calcified moderately stenotic valves, LVOT size has far less impact on flow contraction and on the difference between EOA, GOA and planimetry. Such patients were excluded from the clinical population to avoid confounding factors.

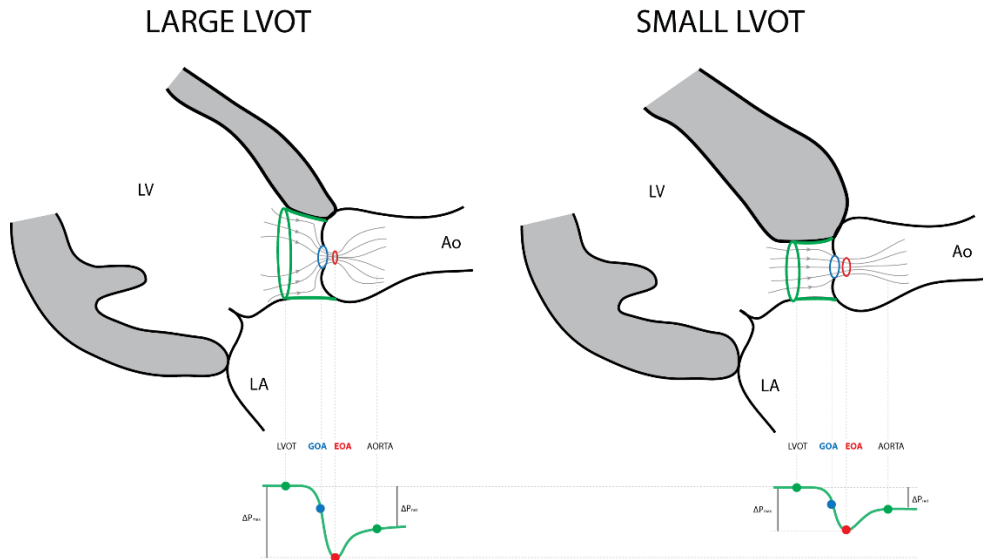


Figure 7.8 – Schematic representation of the difference between small and large LVOT with respect to flow contraction and effective orifice area in aortic stenosis.

Doppler echocardiography versus planimetry versus Gorlin area

Discrepant findings between Doppler echocardiography (EOA) and planimetry (GOA) are related to issues of flow contraction. Therefore, underestimation of valve area by Doppler of 37%, 29% and 20% respectively was observed for the 25mm, 20mm and 15mm straight LVOT profile in the in vitro study. Discrepant findings between Doppler echocardiography and invasive catheter measurements are generally related to pressure recovery²⁵⁶, since Doppler echocardiography measures ΔP_{\max} , as opposed to the invasive measurement of ΔP_{net} (Figure 7.3). The present study showed that the influence of LVOT size on discrepancies between Doppler and catheter gradients is limited (Table 7.2). Pressure recovery is dictated by the geometry of the 'post-stenotic' aortic outlet, and by its size with respect to the size of EOA^{192, 253}. Increases in EOA (i.e. Cc) for the same ascending aorta diameter will increase the amount of pressure recovery, yet this effect is small (Table 7.2).

The Gorlin formula: a one-size-fits-all coefficient of contraction

The Gorlin formula (equation 5) estimates the GOA, which was 1cm² in the in vitro study. Figure 7.6 however shows that the variance of estimated GOA is large, and that LVOT size and geometry has a significant impact on the discrepancy between estimated and true GOA. The Gorlin formula assumes an identical Cc for all situations (Cc=0.879), based on invasive measurements in a small sample size¹⁷². The present study shows that this assumption is most valid in tapered valve orifices, irrespective of LVOT size, but that in non-tapered, fixed orifices significant errors in GOA estimation occur. In such cases, modified Gorlin coefficients should be considered and investigated.

Clinical implications

In patients, apart from the discrepancies in AS grading, the influence of LVOT size on the pressure gradient and EOA deserves attention. Patients with small LVOT had more severely obstructed valve area for the same Doppler and catheter gradients and EOA, even after correction for body size. Small LVOT size in these patients was mediated by more profound basal septal wall hypertrophy. Our findings might in part explain why such patients with typically concentric (and septal wall) hypertrophy have less favorable outcome²⁵⁴: by the time of 'severe AS' diagnosis these patients are likely already at a further stage of valve degeneration and disease. Our findings warrant further exploration whether in these patients with smallest LVOT size (discrepant with respect to body size, i.e. due to septal hypertrophy or other anatomic factors) other thresholds for AS grading should be adopted, and whether earlier referral towards intervention would be desirable. This becomes increasingly relevant in the current era of transcatheter interventions at low procedural risk and mortality, and at low risk of postoperative patient-prosthesis mismatch (a particular concern in the small LVOT population)²⁵⁵.

Study limitations

The in vitro flow simulations occurred only at steady-state flow conditions to enable accurate pressure registrations during pullback. Flow rates were specifically chosen to encompass the mean (200mL/s = 12L/min steady state flow) and peak (400mL/s = 24L/min) transaortic flow rate observed in pulsatile clinical conditions. The clinical data originated from a single center retrospective cohort with dedicated echocardiographic data. The present clinical results therefore should be considered hypothesis-generating and need confirmation from larger independent study.

Conclusions

LVOT size plays a role in the contraction of flow through a stenotic orifice, with smaller LVOT sizes exerting a lower pressure gradient and higher effective orifice area for the same stenotic aortic valve area. Hypothetically, patients with small LVOT are at a more advanced stage of disease when symptoms develop and/or hemodynamic thresholds for intervention are reached.

GENERAL DISCUSSION

The main focus of this PhD thesis was to obtain a more thorough understanding of the individual dynamics of secondary MR, and to establish a framework towards a patient-tailored evaluation and approach.

Exercise dynamics in secondary MR

Part I has shed more light on the exercise (hemo)dynamics in secondary MR, and importantly, on how the current treatment approaches affect the dynamic lesion and exercise hemodynamics in general. An elaborate state-of-the art overview of the current knowledge (chapter 1) highlighted the paucity of exercise data in the current evidence on secondary MR. Nevertheless, the prognostic and functional impact of dynamic aggravation of secondary MR has been demonstrated convincingly. Our efforts in characterizing the post-operative exercise hemodynamics after the three most common treatments for secondary MR, i.e. restrictive mitral annuloplasty (chapters 2 and 3), mitral valve replacement (chapter 4) and percutaneous valve repair using MitraClip (chapter 5), therefore provide a welcome and relevant expansion of the current knowledge and insights.

Restrictive mitral annuloplasty has demonstrated an adequate reduction in secondary MR during exercise in one prior study¹³³ and in our study cohort. However, the potential negative impact of increased transmitral pressure gradients on exercise capacity after a too stringent ring undersizing was a cause of concern in prior studies³⁰⁻³². The general reflex in the cardiology and cardiac surgery community was to consider a mean gradient <5mmHg as a good surgical result, while a mean gradient ≥ 5 mmHg after surgery was to be avoided. The pressure gradient however is characteristically flow-dependent; therefore, for the same degree of stenosis differences in pressure gradient can be observed due to differences in forward flow rate (Figure 1-A). This is particularly relevant in a heart failure population

comprising a wide range of left ventricular ejection fraction and flow rate. As a result, in our patient cohort, patients with the highest gradient paradoxically achieved the highest workload and had the best exercise capacity because of better cardiac performance. Risk-stratification using a flow-independent parameter such as the mitral valve area (or effective orifice area) therefore would make more sense than the pressure gradient. Intriguingly and surprisingly however, the effective orifice area after restrictive annuloplasty appeared to be flow-dependent as well, and demonstrated a significant increase in area during dynamic exercise (Chapter 3). In contrast, in patients following mechanical valve replacement, such increase in effective orifice area could not be demonstrated during exercise (Chapter 4). Transmitral pressure gradients during exercise are therefore higher in the latter patient group for the same effective orifice area at rest (Figure 1-B); a finding that should be taken into consideration when selecting the optimal approach for an individual patient.

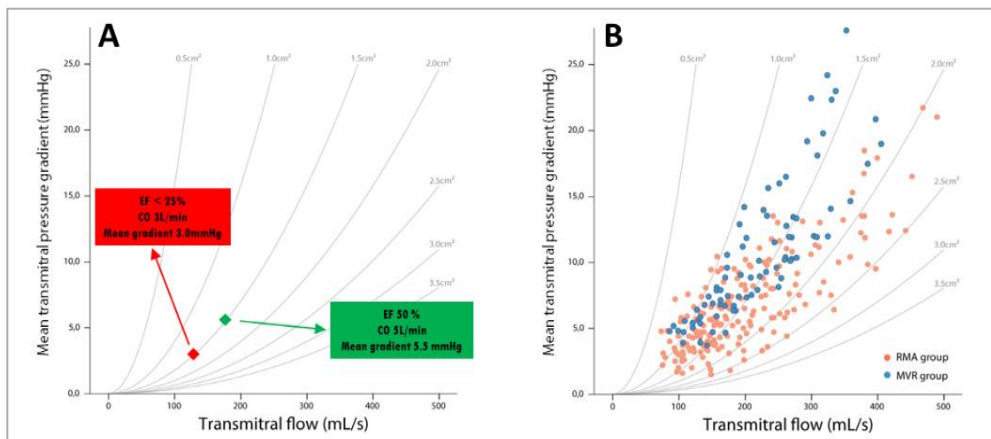


Figure 1 – Flow-rate dependency of the transmitral pressure gradient. Panel A shows a hypothetical example of two heart failure patients with similar effective orifice area of 1.5cm² but different ejection fraction. The patient with the worst ejection fraction (i.e. low flow rate) will have the lowest mean gradient, whereas the patient with normal ejection fraction will be diagnosed with a mean gradient >5mmHg. Panel B compares the pressure-flow relationship of restrictive mitral annuloplasty (RMA) group studied in Chapter 3 with the mechanical valve replacement group (MVR) studied in Chapter 4. Since effective orifice area is fixed in the MVR group, the transmitral gradients at peak exercise are significantly higher compared to RMA patients for the same effective orifice area at rest.

Furthermore, the demonstration of a dynamic valve area following restrictive annuloplasty revealed important new insights in the pathophysiology of the post-annuloplasty mitral stenosis: not the restrictive ring size (which is fixed) but a restricted opening angle of the anterior mitral leaflet was found to be the cause of increased pressure gradients after surgery. Restricted anterior leaflet opening was dictated by diastolic subvalvular tethering. As such, our findings strongly support further research of concomitant subvalvular procedures for secondary MR patients in order to relieve leaflet tethering. Relieving tethering might increase repair durability^{36, 179}, reduce the degree of undersizing needed to obtain the target coaptation length and reduce the functional stenosis observed after surgery. This should certainly be subject to further study, and could ideally also be evaluated in our patient-specific numerical mitral valve model.

In secondary MR patients percutaneously treated with MitraClip, three interesting observations could be made when comparing exercise hemodynamics before the procedure with the respective hemodynamics at 6 months after the procedure (Chapter 5). First, besides the MR reduction observed at rest, MitraClip therapy was able to reduce the dynamic component of secondary MR during exercise as well. Our prospective multicentre exercise echocardiography study was the first study to provide this important evidence. Second, the improvement in hemodynamic profile (systolic pulmonary artery pressures corrected for flow rate) that is observed at rest and during exercise, despite an increase in transmitral pressure gradient after MitraClip, suggests that the reduction in secondary MR outweighs the impact of reduced valve area with respect to exercise hemodynamics. Third, approximately 30% of patients showed no symptomatic benefit after 6 months, and had higher transmitral pressure gradients and less MR reduction during exercise after MitraClip. In our striving towards a patient-tailored approach, more insights into the mechanisms and predictors of exercise 'response' after MitraClip are needed in order to further improve the efficacy of the therapy and to target the most adequate patient population.

Finally, the fact that our letter-to-the-editor, pointing at the importance of exercise hemodynamics in the evaluation of secondary MR patients, was published by the New England Journal of Medicine further supports the considerable and timely clinical relevance of the present research and of the insights gained in this thesis.

Numerical mitral valve modeling

Undoubtedly the most important, advanced and clinically-relevant accomplishment of this thesis work has been the development and clinical validation of a numerical (finite element) mitral valve model based on the patient's specific anatomic data from 3D echocardiography (Part II, Chapter 6). Although several efforts had already been made by other groups to characterize the mechanical properties of mitral leaflet tissue and chordae tendineae for finite element modeling purposes²²²⁻²²⁵, and a number of models had been established based on ex vivo porcine MV data^{226, 227}, the clinical validity of these models remained to be proven. The developed model in this thesis builds upon the knowledge and insights from prior ex-vivo and autopsy studies, and incorporates a maximum amount of patient-specific features. The clinical validity of this individualized model was evaluated in 5 normal mitral valve datasets, demonstrating realistic dynamic valve closure and opening prediction, and accurate (mean distance error $1.32 \pm 0.30 \text{mm}$) prediction of the mid-systolic leaflet configuration. In addition, 5 secondary MR patients were modelled within the developed framework, with equally good (mean distance error $1.53 \pm 0.49 \text{mm}$) leaflet configuration prediction and importantly, a realistic prediction of the amount of leaflet tenting (i.e. tenting volume).

The clinical potential of the developed numerical model therefore is promising, particularly for secondary MR patients. This could already be appreciated in the first part of this thesis. As ongoing leaflet tethering (i.e. tenting) is the primary cause of MR recurrence³⁶ after standard interventions, and has been shown to cause impaired leaflet opening¹³⁹ after

surgery, additional approaches addressing the subvalvular apparatus (papillary muscle relocation³⁹, strut chordal cutting⁴¹, external constraint devices⁴³) are being proposed. However, because the underlying mechanisms causing the tenting differ greatly from individual to individual, a “one-size-fits-all” therapy is unlikely to exist. Therefore, a patient-specific 3D evaluation of the individual valve dynamics and leaflet tenting, as enabled by our developed numerical model, could provide a major clinical benefit, and might even allow pre-intervention simulation of different approaches to evaluate in advance what the optimal approach would be for the individual patient.

In vitro steady state flow model

An in vitro steady state flow model was specifically designed and manufactured to evaluate patterns of flow contraction when flow passes through different geometries (Part III, Chapter 7). The model was equipped with a hydraulic pump, flow sensor, multiple pressure sensors, a computerized feedback loop with frequency-controller and the ability of pressure catheter pullback within the set-up. As demonstrated in Chapter 7, the size and geometry of an inflow profile before a geometric stenosis has a profound impact on the flow contraction through the stenosis, and hence on the flow velocities and the respective pressure gradient. This is not only relevant for the aortic stenosis case studied here, but can be extrapolated towards hemodynamic considerations in secondary MR as well. Furthermore, the model showed excellent repeatability and reproducibility in the simplified aortic stenosis set-up, and therefore allows exploration towards more challenging geometries in the near future.

In the future, this set-up can be particularly relevant for the clinical practice, since clinically measured flow velocities and pressure gradients relate more to the way flow contracts through an orifice than to the orifice itself. In secondary MR patients treated with restrictive annuloplasty, we have demonstrated an increase in effective orifice area during exercise because of increased opening angle of the anterior mitral leaflet (Chapter 3). Whether this

increase in effective area corresponds to a true increase in geometric orifice area, or merely corresponds to improved coefficient of flow contraction for the same geometric orifice, remains to be determined. In addition, in mitral valve replacement patients, less than 50% of the geometric orifice area is effectively used by flow in the mitral position. Whether the geometry of the left atrium plays a role in this inefficient flow contraction, and importantly, whether the efficiency could improve with certain design alterations, remains to be determined. Furthermore, the relationship between Doppler gradients and the true anatomic orifice area following MitraClip therapy for secondary MR should still be explored. The in vitro steady state model with catheter pullback and simultaneous Doppler echocardiography interrogation therefore provides a powerful research tool.

Future work

This PhD thesis was able to initiate a framework and lay the preliminary foundations towards an individualized approach of the secondary MR patient. However, the work is far from over, and a lot of interesting pathways have opened up that deserve further exploration in future research endeavors and ongoing collaboration.

Further improvements in the modeling process will be evaluated and validated for the clinical practice, thereby gradually eliminating the assumptions that are currently inherent in the modeling process. Assessing the number and location of the chordae tendineae (possibly using multimodality fusion imaging), incorporating the exact number and location of the papillary muscles, implementing and evaluating the impact of active contractile tissue in the leaflet belly are among a few of the next steps towards a robust and clinically indispensable tool that allows an individualized patient care.

A time-consuming and cumbersome aspect in the current numerical modeling workflow is the fully manual segmentation of annulus, papillary muscles and leaflets within the 3D

echocardiography datasets. Steps towards a (semi-)automated segmentation of the mitral annulus have already been made within our research collaboration, as displayed in Figure 2, and were presented at an international conference. This work will hopefully continue to be explored in future projects, and expand towards the papillary muscles and leaflets as well.

Finally, as described above, a number of research questions remain to be explored within the steady state in vitro flow model, and new research questions emerge from within the clinical practice on a regular basis. Now that development of the model is completed, and the repeatability and validity of the measurements within the model have been demonstrated for the simplified inflow-outflow geometry study in Chapter 7, more advanced geometries and clinical situations can finally be evaluated within the fluid flow model. Such geometries can be custom-made designs, 3D printed true anatomic geometries, or even biological tissue. As a proof-of-concept (Figure 3) we have already evaluated the incorporation of explanted ovine mitral valves (3 in total), and explored changes in hemodynamics after simulation of specific interventions onto the leaflets and/or papillary muscles.

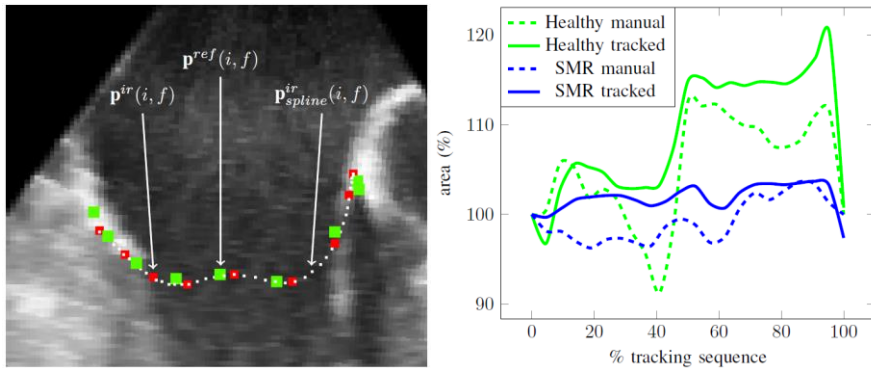


Figure 2 – Semi-automated annular tracking algorithm as evaluated in the Master Thesis work of Henri De Veene in collaboration with the Medical Image Research Center (KULeuven). Starting from one segmented annular geometry, the algorithm used non-rigid image registration to ‘track’ the annulus throughout the cardiac cycle. The difference between the tracked prediction (red) versus the manually segmented true situation (green) is shown in the left panel. Relative annular area change during the cardiac cycle was adequately predicted by the tracking method, both in the 5 healthy (green, large area change) and in 5 secondary mitral regurgitation (blue, small area change) patient data sets. Results were presented at the Engineering in Medicine and Biology Conference in Milan 2015 and published in full in proceedings (De Veene H, Bertrand PB, et al²⁵⁷)

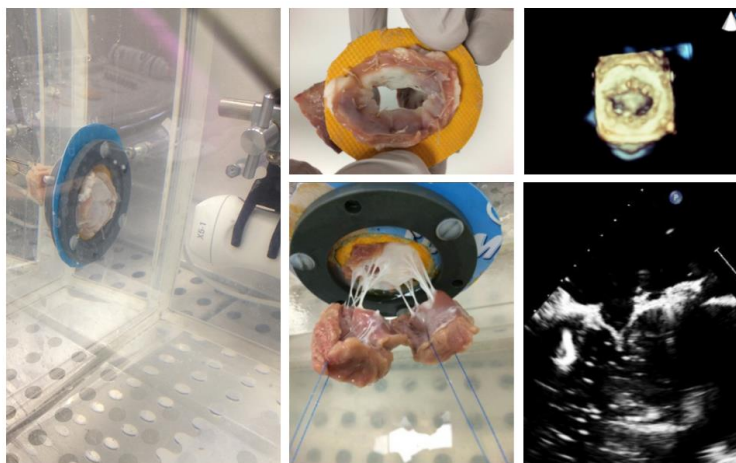


Figure 3 – Proof of concept study incorporating an explanted ovine mitral valve in the *in vitro* steady state flow model, with simultaneous pressure recording and Doppler echocardiography.

CURRICULUM VITAE

BERTRAND Philippe Bernard

Date of birth: 02 May 1984 (Tongeren, Belgium)

Nationality: Belgian

Married to: Laura Ceyskens

Father to: Juliette Bertrand (°27 April 2014)

Address: Pater Valentinuslaan 11 (bus 1)
3500 Hasselt

E-mail: philippe.pb.bertrand@gmail.com

Education

2003 – 2010: Master in Medicine (M.D.) *Magna cum laude*
Medical Doctor, KULeuven

2001 – 2006 Master in Civil Engineering *Magna cum laude*
Biomechanical Engineering, KULeuven

1995 – 2001 Secondary education *Summa cum laude*
Science – Mathematics, OLV Humaniora, Tongeren

Professional experience

2012 – 2016 PhD research, Hasselt University, Ziekenhuis Oost-Limburg

2010 – 2012 Residency in Internal Medicine - Cardiology

2011-2012: Ziekenhuis Oost Limburg, Genk, Belgium

2010-2011: UZ Gasthuisberg, Leuven, Belgium

2007 – 2008 Consultant – Research & Development (50%)
Clijmans & Gelaude bvba, Medisch-technisch adviesbureau

2006 – 2007 Research fellow (50%), IOF project
KULeuven, Department of Biomechanical Engineering (BME)
OF-HB/06/008: 'Integration of biomechanical expertise in planning of
cranio-maxillo-facial surgery'

Scientific achievements

Papers published in international peer-reviewed journals

1. Mechanism of symptomatic improvement after MitraClip therapy for secondary mitral regurgitation: the role of improved resting and exercise hemodynamics
Van De Heyning CM*, Bertrand PB*, Debonnaire P, De Maeyer C, Vandervoort PM, Coussement P, Paelinck B, De Bock D, Vrints C, Claeys MJ
J Am Coll Cardiol 2016 (Accepted)
2. Fact or Artifact in Two-Dimensional Echoardiography: Avoiding Misdiagnosis and Missed Diagnosis.
Bertrand PB, Levine RA, Isselbacher EM, Vandervoort PM.
J Am Soc Echocardiogr. 2016 Mar 8 (Epub). Review. (IF 4.1)
3. Mirror artifacts in two-dimensional echocardiography: Don't forget the third dimension.
Bertrand PB, Verhaert D, Vandervoort PM.
J Am Soc Echocardiogr. 2015 Nov;28(11):1376-7. (IF 4.1)
4. Surgical treatment of moderate ischemic mitral regurgitation.
Bertrand PB, Vandervoort PM, Dion RA.
N Engl J Med. 2015 Apr 30;372(18):1771. (IF 54.5)
5. Mitral Valve Area During Exercise After Restrictive Mitral Valve Annuloplasty: Importance of Diastolic Anterior Leaflet Tethering.
Bertrand PB, Verbrugge FH, Verhaert D, Smeets CJ, Grieten L, Mullens W, Gutermann H, Dion RA, Levine RA, Vandervoort PM.
J Am Coll Cardiol. 2015;65(5):452-461. (IF 16.5)
6. The figure-of-eight artifact in the echocardiographic assessment of percutaneous disc occluders: impact of imaging depth and device type.
Bertrand PB, Grieten L, Smeets CJ, Verbrugge FH, Mullens W, Vrolix M, Rivero-Ayerza M, Verhaert D, Vandervoort PM.
Echocardiography. 2015 Mar;32(3):557-64. (IF 1.2)
7. Functional impact of transmitral gradients at rest and during exercise after restrictive annuloplasty for ischemic mitral regurgitation.
Bertrand PB, Gutermann H, Smeets C, Van Kerrebroeck C, Verhaert D, Vandervoort P, Dion RA.
J Thorac Cardiovasc Surg. 2014 Jul;148(1):183-7. (IF 4.0)

8. Tricuspid annuloplasty concomitant with mitral valve surgery: effects on right ventricular remodeling.
Bertrand PB, Koppers G, Verbrugge FH, Mullens W, Vandervoort P, Dion R, Verhaert D. *J Thorac Cardiovasc Surg*. 2014 Apr;147(4):1256-64. (IF 4.0)
9. Etiology and relevance of the figure-of-8 artifact on echocardiography after percutaneous left atrial appendage closure with the Amplatzer™ Cardiac Plug.
Bertrand PB, Grieten L, De Meester P, Verbrugge FH, Mullens W, Verhaert D, Rivero-Ayerza M, Budts W, Vandervoort PM. *J Am Soc Echocardiogr*. 2014 Mar;27(3):323-8.e1. (IF 4.1)
10. Altered mitral inflow orifice in severe aortic regurgitation: real time three-dimensional echocardiographic findings.
Bertrand PB, Verhaert D, Vandervoort P. *Echocardiography*. 2014;31(1):E30-2. (IF 1.2)
11. Detection of subclinical transient fluid accumulation during pregnancy in a patient with an implantable cardioverter defibrillator and OptiVol® fluid monitoring algorithm.
Smeets CJ, Lanssens D, Gyselaers W, Bertrand PB, Grieten L, Vandervoort P. *Int J Cardiol*. 2016 Mar. (IF 4.0)
12. Papillary fibro-elastoma as a rare cause of rate-dependent angina: importance of diastolic coronary perfusion.
Hendrickx I, Bertrand PB, Vrolix M, Ferdinande B, Cruysberghs Y. *Eur Heart J Cardiovasc Imaging*. 2016 Mar 16. (IF 4.1)
13. Natriuretic Response to Diuretic Therapy in Decompensated Heart Failure with Reduced Ejection Fraction and Volume Overload.
Verbrugge FH, Dupont M, Bertrand PB, Nijst P, Penders J, Dens J, Verhaert D, Vandervoort P, Tang WH, Mullens W. *Acta Cardiol*. 2015 Jun;70(3):265-73.
14. Non-invasive methods for maternal cardiac output monitoring.
Staelens AS, Bertrand PB, Vonck S, Malbrain M, Gyselaers W. *Fetal and Maternal Medicine Review*. June 2015, p1-17.
15. Pulmonary vascular response to exercise in symptomatic heart failure with reduced ejection fraction and pulmonary hypertension.
Verbrugge FH, Dupont M, Bertrand PB, Nijst P, Grieten L, Dens J, Verhaert D, Janssens

S, Tang WH, Mullens W.

Eur J Heart Fail. 2015 Mar;17(3):320-8. doi: 10.1002/ejhf.217. (IF 6.57)

16. Pulmonary homograft endocarditis and aortic autograft failure after Ross procedure: a double stentless bioprosthesis approach.

Smeets C, Bertrand PB, Spadaccio C, Beran M, Verhaert D, Vandervoort PM, Gutermann H, Dion RA. *J Heart Valve Dis.* 2014 May;23(3):360-3. (IF 1.07)

17. Uptitration of Neurohumoral Blockers in Hospitalized Heart Failure Patients with Reduced versus Preserved Ejection Fraction.

Verbrugge FH, Duchenne J, Bertrand PB, Dupont M, Tang WH, Mullens W. *Am J Cardiol.* 2013 Dec 15;112(12):1913-20. (IF 3.209)

18. Symptomatic tibial vein aneurysm - a diagnostic challenge.

T'Seyen S, Bertrand P, Goosens V, Stas M, Verhamme P, Maleux G.

Vasa. 2013 Jan;42(1):72-6. doi: 10.1024/0301-1526/a000239. (IF 1.308)

Papers at international conferences, published in full in proceedings

19. Automatic Mitral Annulus Tracking in Volumetric Ultrasound Using Non-Rigid Image Registration.

De Veene H, Bertrand PB, Popovic N, Vandervoort PM, Claus P, De Beule M, Heyde B, *Conf Proc IEEE Eng Med Biol Soc.* 2015;2015:1985-8

20. Waving at the heart: implementation of a Kinect based real-time interactive control system for viewing cineangiogram loops during cardiac catheterisation procedures.

Suelze B, Agten R, Bertrand PB, Vandenberg T, Thoelen R, Vandervoort P, Grieten L. *Comput Cardiol* 2013. (IEEE proceedings)

21. Assessment of joint contact areas using a CT-based distance criterion: cross-validation with a cadaver study.

Bartels W, Bertrand P, Gelaude F, Moens P, Fabry G, Van der Perre G and Vander Sloten J, 2007. *Proceedings of the International Society for Computer Assisted Orthopaedic Surgery (CAOS 2007), Heidelberg, Germany, June 20-23, 2007*, pp. 540-543.

22. Inter-subject variability of hip moment arms.

Gelaude F, Bartels W, Bertrand P, Broos PL, Lauwers B, Van der Perre G and Vander Sloten J. 2007. *HipHub symposium 2007 'Prediction and evaluation of THR performance: can we plan success', Leuven, Belgium, June 22-23, 2007*, pp. 37-38.

Other articles

23. Profylactische tricuspidalisklepplastiek tijdens mitralisklepheelkunde: invloed op rechterventrikelgrootte, -functie en -geometrie. Bloedvaten-Hart-Longen: BHL Vol. 19 Nr 4 (06-2014)
24. More than pretty pictures: Clinical indications and how to use advanced imaging. Tijdschrift voor Cardiologie. Jaargang 27, Nr. 2, april 2015, p.77-80.

Awards

- 2016 Best Imaging Abstract – Belgian Society of Cardiology
- 2015 Young Investigator Award – BGWNICI, Brugge, Belgium
- 2015 Congress Highlight in 3D echocardiography, EuroEcho 2015, Sevilla
- 2015 Best Poster Award – Belgian Society of Cardiology, 2015
- 2013 High Score Abstract – EACVI – EuroEcho 2013 (Istanbul)
- 2007 Shortlisted for de Altran Foundation for Innovation 2007 Award
“Mending the human body through technological innovation”.
- 2001 Finalist of the 13th Flemish Physics Olympiad

Grants

- 2015 FWO aspirant grant renewal
- 2014 FWO travel grant, K225614N, Massachussets General Hospital, Harvard Medical School, Boston (1 week Research Visit, R.A. Levine)
- FWO travel grant, K1G9114N, AHA conference, Chicago
- 2013 FWO aspirant grant
- 2012 BOF/DOC research grant, Hasselt University

REFERENCES

1. Silverman ME and Hurst JW. The mitral complex. Interaction of the anatomy, physiology, and pathology of the mitral annulus, mitral valve leaflets, chordae tendineae, and papillary muscles. *Am Heart J*. 1968;76:399-418.
2. Ranganathan N, Lam JH, Wigle ED and Silver MD. Morphology of the human mitral valve. II. The valve leaflets. *Circulation*. 1970;41:459-67.
3. Lam JH, Ranganathan N, Wigle ED and Silver MD. Morphology of the human mitral valve. I. Chordae tendineae: a new classification. *Circulation*. 1970;41:449-58.
4. Roberts WC and Cohen LS. Left Ventricular Papillary Muscles: Description of the Normal and a Survey of Conditions Causing them to be Abnormal. *Circulation*. 1972;46:138-154.
5. Silbiger JJ and Bazaz R. Contemporary insights into the functional anatomy of the mitral valve. *Am Heart J*. 2009;158:887-95.
6. Perloff JK and Roberts WC. The mitral apparatus. Functional anatomy of mitral regurgitation. *Circulation*. 1972;46:227-39.
7. Enriquez-Sarano M, Akins CW and Vahanian A. Mitral regurgitation. *Lancet*. 2009;373:1382-94.
8. Dal-Bianco JP, Beaudoin J, Handschumacher MD and Levine RA. Basic mechanisms of mitral regurgitation. *Can J Cardiol*. 2014;30:971-81.
9. Di Mauro M, Gallina S, D'Amico MA, Izzicupo P, Lanuti P, Bascelli A, Di Fonso A, Bartoloni G, Calafiore AM, Di Baldassarre A and Italian Group of Study for Heart Valve D. Functional mitral regurgitation: from normal to pathological anatomy of mitral valve. *Int J Cardiol*. 2013;163:242-8.
10. Levine RA. Dynamic mitral regurgitation--more than meets the eye. *N Engl J Med*. 2004;351:1681-4.
11. Lamas GA, Mitchell GF, Flaker GC, Smith SC, Jr., Gersh BJ, Basta L, Moye L, Braunwald E and Pfeffer MA. Clinical significance of mitral regurgitation after acute myocardial infarction. Survival and Ventricular Enlargement Investigators. *Circulation*. 1997;96:827-33.
12. Lehmann KG, Francis CK and Dodge HT. Mitral regurgitation in early myocardial infarction. Incidence, clinical detection, and prognostic implications. TIMI Study Group. *Ann Intern Med*. 1992;117:10-7.
13. Bursi F, Enriquez-Sarano M, Nkomo VT, Jacobsen SJ, Weston SA, Meverden RA and Roger VL. Heart failure and death after myocardial infarction in the community: the emerging role of mitral regurgitation. *Circulation*. 2005;111:295-301.
14. Bursi F, Enriquez-Sarano M, Jacobsen SJ and Roger VL. Mitral regurgitation after myocardial infarction: a review. *Am J Med*. 2006;119:103-12.
15. Koelling TM, Aaronson KD, Cody RJ, Bach DS and Armstrong WF. Prognostic significance of mitral regurgitation and tricuspid regurgitation in patients with left ventricular systolic dysfunction. *American Heart Journal*. 2002;144:524-529.
16. Trichon BH, Felker GM, Shaw LK, Cabell CH and O'Connor CM. Relation of frequency and severity of mitral regurgitation to survival among patients with left ventricular systolic dysfunction and heart failure. *The American Journal of Cardiology*. 2003;91:538-543.
17. Rossi A, Dini FL, Faggiano P, Agricola E, Ciccoira M, Frattini S, Simioniuc A, Gullace M, Ghio S, Enriquez-Sarano M and Temporelli PL. Independent prognostic value of functional mitral regurgitation in patients with heart failure. A quantitative analysis of

- 1256 patients with ischaemic and non-ischaemic dilated cardiomyopathy. *Heart*. 2011;97:1675-80.
18. Grigioni F, Enriquez-Sarano M, Zehr KJ, Bailey KR and Tajik AJ. Ischemic mitral regurgitation: long-term outcome and prognostic implications with quantitative Doppler assessment. *Circulation*. 2001;103:1759-64.
 19. Lapu-Bula R. Contribution of Exercise-Induced Mitral Regurgitation to Exercise Stroke Volume and Exercise Capacity in Patients With Left Ventricular Systolic Dysfunction. *Circulation*. 2002;106:1342-1348.
 20. Carabello BA. The current therapy for mitral regurgitation. *J Am Coll Cardiol*. 2008;52:319-26.
 21. Nishimura RA, Otto CM, Bonow RO, Carabello BA, Erwin JP, 3rd, Guyton RA, O'Gara PT, Ruiz CE, Skubas NJ, Sorajja P, Sundt TM, 3rd, Thomas JD and American College of Cardiology/American Heart Association Task Force on Practice G. 2014 AHA/ACC guideline for the management of patients with valvular heart disease: executive summary: a report of the American College of Cardiology/American Heart Association Task Force on Practice Guidelines. *J Am Coll Cardiol*. 2014;63:2438-88.
 22. Vahanian A, Alfieri O, Andreotti F, Antunes MJ, Baron-Esquivias G, Baumgartner H, Borger MA, Carrel TP, De Bonis M, Evangelista A, Falk V, Jung B, Lancellotti P, Pierard L, Price S, Schafers HJ, Schuler G, Stepinska J, Swedberg K, Takkenberg J, Von Oppell UO, Windecker S, Zamorano JL and Zembala M. Guidelines on the management of valvular heart disease (version 2012). *Eur Heart J*. 2012;33:2451-96.
 23. Levine RA and Schwammenthal E. Ischemic mitral regurgitation on the threshold of a solution: from paradoxes to unifying concepts. *Circulation*. 2005;112:745-58.
 24. Asgar AW, Mack MJ and Stone GW. Secondary Mitral Regurgitation in Heart Failure: Pathophysiology, Prognosis, and Therapeutic Considerations. *J Am Coll Cardiol*. 2015;65:1231-1248.
 25. Di Salvo TG, Acker MA, Dec GW and Byrne JG. Mitral valve surgery in advanced heart failure. *J Am Coll Cardiol*. 2010;55:271-82.
 26. Bax JJ, Braun J, Somer ST, Klautz R, Holman ER, Versteegh MI, Boersma E, Schalij MJ, van der Wall EE and Dion RA. Restrictive annuloplasty and coronary revascularization in ischemic mitral regurgitation results in reverse left ventricular remodeling. *Circulation*. 2004;110:II103-8.
 27. Bolling SF, Pagani FD, Deeb GM and Bach DS. Intermediate-term outcome of mitral reconstruction in cardiomyopathy. *J Thorac Cardiovasc Surg*. 1998;115:381-6; discussion 387-8.
 28. Wu AH, Aaronson KD, Bolling SF, Pagani FD, Welch K and Koelling TM. Impact of mitral valve annuloplasty on mortality risk in patients with mitral regurgitation and left ventricular systolic dysfunction. *J Am Coll Cardiol*. 2005;45:381-7.
 29. Mihaljevic T, Lam BK, Rajeswaran J, Takagaki M, Lauer MS, Gillinov AM, Blackstone EH and Lytle BW. Impact of mitral valve annuloplasty combined with revascularization in patients with functional ischemic mitral regurgitation. *J Am Coll Cardiol*. 2007;49:2191-201.
 30. Magne J, Senechal M, Mathieu P, Dumesnil JG, Dagenais F and Pibarot P. Restrictive annuloplasty for ischemic mitral regurgitation may induce functional mitral stenosis. *J Am Coll Cardiol*. 2008;51:1692-701.
 31. Kainuma S, Taniguchi K, Daimon T, Sakaguchi T, Funatsu T, Kondoh H, Miyagawa S, Takeda K, Shudo Y, Masai T, Fujita S, Nishino M, Sawa Y and Osaka Cardiovascular Surgery Research G. Does stringent restrictive annuloplasty for functional mitral regurgitation cause functional mitral stenosis and pulmonary hypertension? *Circulation*. 2011;124:S97-106.

32. Williams ML, Daneshmand MA, Jollis JG, Horton JR, Shaw LK, Swaminathan M, Davis RD, Glower DD, Smith PK and Milano CA. Mitral gradients and frequency of recurrence of mitral regurgitation after ring annuloplasty for ischemic mitral regurgitation. *Ann Thorac Surg.* 2009;88:1197-201.
33. Kubota K, Otsuji Y, Ueno T, Koriyama C, Levine RA, Sakata R and Tei C. Functional mitral stenosis after surgical annuloplasty for ischemic mitral regurgitation: importance of subvalvular tethering in the mechanism and dynamic deterioration during exertion. *J Thorac Cardiovasc Surg.* 2010;140:617-23.
34. McGee EC, Gillinov AM, Blackstone EH, Rajeswaran J, Cohen G, Najam F, Shiota T, Sabik JF, Lytle BW, McCarthy PM and Cosgrove DM. Recurrent mitral regurgitation after annuloplasty for functional ischemic mitral regurgitation. *J Thorac Cardiovasc Surg.* 2004;128:916-24.
35. Acker MA, Parides MK, Perrault LP, Moskowitz AJ, Gelijns AC, Voisine P, Smith PK, Hung JW, Blackstone EH, Puskas JD, Argenziano M, Gammie JS, Mack M, Ascheim DD, Bagiella E, Moquete EG, Ferguson TB, Horvath KA, Geller NL, Miller MA, Woo YJ, D'Alessandro DA, Ailawadi G, Dagenais F, Gardner TJ, O'Gara PT, Michler RE and Kron IL. Mitral-Valve Repair versus Replacement for Severe Ischemic Mitral Regurgitation. *N Engl J Med.* 2014;370:23-32.
36. Hung J, Papakostas L, Tahta SA, Hardy BG, Bollen BA, Duran CM and Levine RA. Mechanism of recurrent ischemic mitral regurgitation after annuloplasty: continued LV remodeling as a moving target. *Circulation.* 2004;110:II85-90.
37. Ciarka A, Braun J, Delgado V, Versteegh M, Boersma E, Klautz R, Dion R, Bax JJ and Van de Veire N. Predictors of mitral regurgitation recurrence in patients with heart failure undergoing mitral valve annuloplasty. *Am J Cardiol.* 2010;106:395-401.
38. Kron IL, Hung J, Overbey JR, Bouchard D, Gelijns AC, Moskowitz AJ, Voisine P, O'Gara PT, Argenziano M, Michler RE, Gillinov M, Puskas JD, Gammie JS, Mack MJ, Smith PK, Sai-Sudhakar C, Gardner TJ, Ailawadi G, Zeng X, O'Sullivan K, Parides MK, Swayze R, Thourani V, Rose EA, Perrault LP, Acker MA and Investigators C. Predicting recurrent mitral regurgitation after mitral valve repair for severe ischemic mitral regurgitation. *J Thorac Cardiovasc Surg.* 2015;149:752-61 e1.
39. Kron IL, Green GR and Cope JT. Surgical relocation of the posterior papillary muscle in chronic ischemic mitral regurgitation. *Ann Thorac Surg.* 2002;74:600-1.
40. Fattouch K, Lancellotti P, Castrovinci S, Murana G, Sampognaro R, Corrado E, Caruso M, Speziale G, Novo S and Ruvolo G. Papillary muscle relocation in conjunction with valve annuloplasty improve repair results in severe ischemic mitral regurgitation. *J Thorac Cardiovasc Surg.* 2012;143:1352-5.
41. Messas E, Guerrero JL, Handschumacher MD, Conrad C, Chow CM, Sullivan S, Yoganathan AP and Levine RA. Chordal cutting: a new therapeutic approach for ischemic mitral regurgitation. *Circulation.* 2001;104:1958-63.
42. Hvass U and Joudinaud T. The papillary muscle sling for ischemic mitral regurgitation. *J Thorac Cardiovasc Surg.* 2010;139:418-23.
43. Grossi EA, Patel N, Woo YJ, Goldberg JD, Schwartz CF, Subramanian V, Feldman T, Bourge R, Baumgartner N, Genco C, Goldman S, Zenati M, Wolfe JA, Mishra YK, Trehan N, Mittal S, Shang S, Mortier TJ, Schweich CJ, Jr. and Group R-MS. Outcomes of the RESTOR-MV Trial (Randomized Evaluation of a Surgical Treatment for Off-Pump Repair of the Mitral Valve). *J Am Coll Cardiol.* 2010;56:1984-93.
44. Acker MA, Bolling S, Shemin R, Kirklin J, Oh JK, Mann DL, Jessup M, Sabbah HN, Starling RC, Kubo SH, Acorn Trial Principal I and Study C. Mitral valve surgery in heart failure: insights from the Acorn Clinical Trial. *J Thorac Cardiovasc Surg.* 2006;132:568-77, 577 e1-4.

45. Borger MA. Chronic ischemic mitral regurgitation: insights into Pandora's box. *Circulation*. 2012;126:2674-6.
46. Wagner CE and Kron IL. Subvalvular techniques to optimize surgical repair of ischemic mitral regurgitation. *Curr Opin Cardiol*. 2014;29:140-4.
47. Nishimura RA, Otto CM, Bonow RO, Carabello BA, Erwin JP, 3rd, Guyton RA, O'Gara PT, Ruiz CE, Skubas NJ, Sorajja P, Sundt TM, 3rd, Thomas JD and American College of Cardiology/American Heart Association Task Force on Practice G. 2014 AHA/ACC guideline for the management of patients with valvular heart disease: a report of the American College of Cardiology/American Heart Association Task Force on Practice Guidelines. *J Am Coll Cardiol*. 2014;63:e57-185.
48. Lancellotti P, Gerard PL and Pierard LA. Long-term outcome of patients with heart failure and dynamic functional mitral regurgitation. *Eur Heart J*. 2005;26:1528-32.
49. Feinberg MS, Schwammenthal E, Shlizerman L, Porter A, Hod H, Friemark D, Mateszky S, Boyko V, Mandelzweig L, Vered Z, Behar S and Sagie A. Prognostic significance of mild mitral regurgitation by color Doppler echocardiography in acute myocardial infarction. *Am J Cardiol*. 2000;86:903-7.
50. Szymanski C, Levine RA, Tribouilloy C, Zheng H, Handschumacher MD, Tawakol A and Hung J. Impact of mitral regurgitation on exercise capacity and clinical outcomes in patients with ischemic left ventricular dysfunction. *Am J Cardiol*. 2011;108:1714-20.
51. Levine RA and Hung J. Ischemic mitral regurgitation, the dynamic lesion: clues to the cure. *J Am Coll Cardiol*. 2003;42:1929-32.
52. Schwammenthal E, Chen C, Benning F, Block M, Breithardt G and Levine RA. Dynamics of mitral regurgitant flow and orifice area. Physiologic application of the proximal flow convergence method: clinical data and experimental testing. *Circulation*. 1994;90:307-22.
53. Hung J, Otsuji Y, Handschumacher MD, Schwammenthal E and Levine RA. Mechanism of dynamic regurgitant orifice area variation in functional mitral regurgitation: physiologic insights from the proximal flow convergence technique. *J Am Coll Cardiol*. 1999;33:538-45.
54. Breithardt OA, Sinha AM, Schwammenthal E, Bidaoui N, Markus KU, Franke A and Stellbrink C. Acute effects of cardiac resynchronization therapy on functional mitral regurgitation in advanced systolic heart failure. *Journal of the American College of Cardiology*. 2003;41:765-770.
55. He S, Fontaine AA, Schwammenthal E, Yoganathan AP and Levine RA. Integrated mechanism for functional mitral regurgitation: leaflet restriction versus coapting force: in vitro studies. *Circulation*. 1997;96:1826-34.
56. Otsuji Y, Handschumacher MD, Schwammenthal E, Jiang L, Song JK, Guerrero JL, Vlahakes GJ and Levine RA. Insights from three-dimensional echocardiography into the mechanism of functional mitral regurgitation: direct in vivo demonstration of altered leaflet tethering geometry. *Circulation*. 1997;96:1999-2008.
57. Kono T, Sabbah HN, Rosman H, Alam M, Jafri S and Goldstein S. Left ventricular shape is the primary determinant of functional mitral regurgitation in heart failure. *J Am Coll Cardiol*. 1992;20:1594-8.
58. Otsuji Y, Levine RA, Takeuchi M, Sakata R and Tei C. Mechanism of ischemic mitral regurgitation. *J Cardiol*. 2008;51:145-56.
59. Kim K, Kaji S, An Y, Nishino T, Tani T, Kitai T and Furukawa Y. Interpapillary muscle distance independently affects severity of functional mitral regurgitation in patients with systolic left ventricular dysfunction. *J Thorac Cardiovasc Surg*. 2014;148:434-40 e1.
60. Kalra K, Wang Q, McIver BV, Shi W, Guyton RA, Sun W, Sarin EL, Thourani VH and Padala M. Temporal changes in interpapillary muscle dynamics as an active indicator

- of mitral valve and left ventricular interaction in ischemic mitral regurgitation. *J Am Coll Cardiol*. 2014;64:1867-79.
61. Topilsky Y, Vaturi O, Watanabe N, Bichara V, Nkomo VT, Michelena H, Le Tourneau T, Mankad SV, Park S, Capps MA, Suri R, Pislaru SV, Maalouf J, Yoshida K and Enriquez-Sarano M. Real-time 3-dimensional dynamics of functional mitral regurgitation: a prospective quantitative and mechanistic study. *J Am Heart Assoc*. 2013;2:e000039.
 62. Tigen K, Karaahmet T, Dundar C, Guler A, Cevik C, Basaran O, Kirma C and Basaran Y. The importance of papillary muscle dyssynchrony in predicting the severity of functional mitral regurgitation in patients with non-ischaemic dilated cardiomyopathy: a two-dimensional speckle-tracking echocardiography study. *Eur J Echocardiogr*. 2010;11:671-6.
 63. Liang YJ, Zhang Q, Fang F, Lee AP, Liu M, Yan BP, Lam YY, Chan GC and Yu CM. Incremental value of global systolic dyssynchrony in determining the occurrence of functional mitral regurgitation in patients with left ventricular systolic dysfunction. *Eur Heart J*. 2013;34:767-74.
 64. Otsuji Y, Kumanohoso T, Yoshifuku S, Matsukida K, Koriyama C, Kisanuki A, Minagoe S, Levine RA and Tei C. Isolated annular dilation does not usually cause important functional mitral regurgitation: comparison between patients with lone atrial fibrillation and those with idiopathic or ischemic cardiomyopathy. *J Am Coll Cardiol*. 2002;39:1651-6.
 65. Song JM, Kim JJ, Ha TY, Lee JW, Jung SH, Hwang IS, Lee I, Sun BJ, Kim DH, Kang DH and Song JK. Basal chordae sites on the mitral valve determine the severity of secondary mitral regurgitation. *Heart*. 2015, 10.1136/heartjnl-2014-306854.
 66. Laughlin MH. Cardiovascular response to exercise. *Am J Physiol*. 1999;277:S244-59.
 67. Manou-Stathopoulou V, Goodwin CD, Patterson T, Redwood SR, Marber MS and Williams RP. The effects of cold and exercise on the cardiovascular system. *Heart*. 2015;101:808-20.
 68. Slutsky R, Karliner J, Ricci D, Schuler G, Pfisterer M, Peterson K and Ashburn W. Response of left ventricular volume to exercise in man assessed by radionuclide equilibrium angiography. *Circulation*. 1979;60:565-71.
 69. Iskandrian AS, Hakki AH, DePace NL, Manno B and Segal BL. Evaluation of left ventricular function by radionuclide angiography during exercise in normal subjects and in patients with chronic coronary heart disease. *J Am Coll Cardiol*. 1983;1:1518-29.
 70. Tomai F, Ciavolella M, Crea F, Gaspardone A, Versaci F, Giannitti C, Scali D, Chiariello L and Gioffre PA. Left ventricular volumes during exercise in normal subjects and patients with dilated cardiomyopathy assessed by first-pass radionuclide angiography. *Am J Cardiol*. 1993;72:1167-71.
 71. Furukawa K, Nishida K, Yamada C, Niki S, Sugihara H, Kohno Y, Katsume H, Ijichi H, Kitamura H and Kunishige H. Left ventricular size and performance during graded supine exercise in normal subjects. *Jpn Heart J*. 1983;24:503-14.
 72. Crawford MH, Petru MA and Rabinowitz C. Effect of isotonic exercise training on left ventricular volume during upright exercise. *Circulation*. 1985;72:1237-43.
 73. La Gerche A, Claessen G, Van de Bruaene A, Pattyn N, Van Cleemput J, Gewillig M, Bogaert J, Dymarkowski S, Claus P and Heidbuchel H. Cardiac MRI: a new gold standard for ventricular volume quantification during high-intensity exercise. *Circ Cardiovasc Imaging*. 2013;6:329-38.
 74. Paulsen WJ, Boughner DR, Friesen A and Persaud JA. Ventricular response to isometric and isotonic exercise. Echocardiographic assessment. *Br Heart J*. 1979;42:521-7.
 75. Stefadouros MA, Grossman W, el-Shahawy M and Witham C. The effect of isometric exercise on the left ventricular volume in normal man. *Circulation*. 1974;49:1185-9.

76. Shen WF, Roubin GS, Hirasawa K, Choong CY, Hutton BF, Harris PJ, Fletcher PJ and Kelly DT. Left ventricular volume and ejection fraction response to exercise in chronic congestive heart failure: difference between dilated cardiomyopathy and previous myocardial infarction. *Am J Cardiol.* 1985;55:1027-31.
77. Keren G, Katz S, Gage J, Strom J, Sonnenblick EH and LeJemtel TH. Effect of isometric exercise on cardiac performance and mitral regurgitation in patients with severe congestive heart failure. *Am Heart J.* 1989;118:973-9.
78. Mann DL, Scharf J, Ahnve S and Gilpin E. Left ventricular volume during supine exercise: importance of myocardial scar in patients with coronary heart disease. *J Am Coll Cardiol.* 1987;9:26-34.
79. Lafitte S, Bordachar P, Lafitte M, Garrigue S, Reuter S, Reant P, Serri K, Lebouffos V, Berrhouet M, Jais P, Haissaguerre M, Clementy J, Roudaut R and DeMaria AN. Dynamic ventricular dyssynchrony: an exercise-echocardiography study. *J Am Coll Cardiol.* 2006;47:2253-9.
80. Sullivan MJ, Knight JD, Higginbotham MB and Cobb FR. Relation between central and peripheral hemodynamics during exercise in patients with chronic heart failure. Muscle blood flow is reduced with maintenance of arterial perfusion pressure. *Circulation.* 1989;80:769-81.
81. Pina IL. Exercise and Heart Failure: A Statement From the American Heart Association Committee on Exercise, Rehabilitation, and Prevention. *Circulation.* 2003;107:1210-1225.
82. Lancellotti P, Lebrun F and Pierard LA. Determinants of exercise-induced changes in mitral regurgitation in patients with coronary artery disease and left ventricular dysfunction. *J Am Coll Cardiol.* 2003;42:1921-8.
83. Giga V, Ostojic M, Vujisic-Tesic B, Djordjevic-Dikic A, Stepanovic J, Beleslin B, Petrovic M, Nedeljkovic M, Nedeljkovic I and Milic N. Exercise-induced changes in mitral regurgitation in patients with prior myocardial infarction and left ventricular dysfunction: relation to mitral deformation and left ventricular function and shape. *Eur Heart J.* 2005;26:1860-5.
84. Lancellotti P, Stainier PY, Lebois F and Pierard LA. Effect of dynamic left ventricular dyssynchrony on dynamic mitral regurgitation in patients with heart failure due to coronary artery disease. *Am J Cardiol.* 2005;96:1304-7.
85. D'Andrea A, Caso P, Cuomo S, Scarafile R, Salerno G, Limongelli G, Di Salvo G, Severino S, Ascione L, Calabro P, Romano M, Romano G, Santangelo L, Maiello C, Cotrufo M and Calabro R. Effect of dynamic myocardial dyssynchrony on mitral regurgitation during supine bicycle exercise stress echocardiography in patients with idiopathic dilated cardiomyopathy and 'narrow' QRS. *Eur Heart J.* 2007;28:1004-11.
86. Takano H, Adachi H, Ohshima S, Taniguchi K and Kurabayashi M. Functional mitral regurgitation during exercise in patients with heart failure. *Circ J.* 2006;70:1563-7.
87. Izumo M, Lancellotti P, Suzuki K, Kou S, Shimozaoto T, Hayashi A, Akashi YJ, Osada N, Omiya K, Nobuoka S, Ohtaki E and Miyake F. Three-dimensional echocardiographic assessments of exercise-induced changes in left ventricular shape and dyssynchrony in patients with dynamic functional mitral regurgitation. *Eur J Echocardiogr.* 2009;10:961-7.
88. Ennezat PV, Marechaux S, Le Tourneau T, Lamblin N, Bauters C, Van Belle E, Gal B, Kacet S, Asseman P, Deklunder G, LeJemtel TH and de Groote P. Myocardial asynchronism is a determinant of changes in functional mitral regurgitation severity during dynamic exercise in patients with chronic heart failure due to severe left ventricular systolic dysfunction. *Eur Heart J.* 2006;27:679-83.
89. Madaric J, Vanderheyden M, Van Laethem C, Verhamme K, Feys A, Goethals M, Verstreken S, Geelen P, Penicka M, De Bruyne B and Bartunek J. Early and late effects

- of cardiac resynchronization therapy on exercise-induced mitral regurgitation: relationship with left ventricular dyssynchrony, remodelling and cardiopulmonary performance. *Eur Heart J*. 2007;28:2134-41.
90. Peteiro J, Freire E, Montserrat L and Castro-Beiras A. The effect of exercise on ischemic mitral regurgitation. *Chest*. 1998;114:1075-82.
 91. Peteiro J, Monserrat L, Bouzas A, Piñon P, Mariñas J, Piñeiro M and Castro-Beiras A. Prognostic Value of Mitral Regurgitation Assessment During Exercise Echocardiography in Patients with Known or Suspected Coronary Artery Disease. *Journal of the American Society of Echocardiography*. 2006;19:1229-1237.
 92. Schwammenthal E and Levine RA. The non-ischaemic dynamics of ischaemic mitral regurgitation: solving the paradox. *Eur Heart J*. 2005;26:1454-5.
 93. Yamano T, Nakatani S, Kanzaki H, Toh N, Amaki M, Tanaka J, Abe H, Hasegawa T, Sawada T, Matsubara H and Kitakaze M. Exercise-induced changes of functional mitral regurgitation in asymptomatic or mildly symptomatic patients with idiopathic dilated cardiomyopathy. *Am J Cardiol*. 2008;102:481-5.
 94. Tada H, Tamai J, Takaki H, Ohnishi E, Okano Y and Yoshioka T. Mild mitral regurgitation reduces exercise capacity in patients with idiopathic dilated cardiomyopathy. *Int J Cardiol*. 1997;58:41-5.
 95. Izumo M, Suzuki K, Moonen M, Kou S, Shimozato T, Hayashi A, Akashi YJ, Osada N, Omiya K, Miyake F, Ohtaki E and Lancellotti P. Changes in mitral regurgitation and left ventricular geometry during exercise affect exercise capacity in patients with systolic heart failure. *Eur J Echocardiogr*. 2011;12:54-60.
 96. Lancellotti P, Troisfontaines P, Toussaint AC and Pierard LA. Prognostic importance of exercise-induced changes in mitral regurgitation in patients with chronic ischemic left ventricular dysfunction. *Circulation*. 2003;108:1713-7.
 97. Lancellotti P, Magne J, Dulgheru R, Ancion A, Martinez C and Pierard LA. Clinical Significance of Exercise Pulmonary Hypertension in Secondary Mitral Regurgitation. *Am J Cardiol*. 2015, 10.1016/j.amjcard.2015.02.028.
 98. Pierard LA and Lancellotti P. The role of ischemic mitral regurgitation in the pathogenesis of acute pulmonary edema. *N Engl J Med*. 2004;351:1627-34.
 99. Yancy CW, Jessup M, Bozkurt B, Butler J, Casey DE, Jr., Drazner MH, Fonarow GC, Geraci SA, Horwich T, Januzzi JL, Johnson MR, Kasper EK, Levy WC, Masoudi FA, McBride PE, McMurray JJ, Mitchell JE, Peterson PN, Riegel B, Sam F, Stevenson LW, Tang WH, Tsai EJ, Wilkoff BL and American College of Cardiology Foundation/American Heart Association Task Force on Practice G. 2013 ACCF/AHA guideline for the management of heart failure: a report of the American College of Cardiology Foundation/American Heart Association Task Force on practice guidelines. *Circulation*. 2013;128:e240-327.
 100. St John Sutton M, Pfeffer MA, Moye L, Plappert T, Rouleau JL, Lamas G, Rouleau J, Parker JO, Arnold MO, Sussex B and Braunwald E. Cardiovascular death and left ventricular remodeling two years after myocardial infarction: baseline predictors and impact of long-term use of captopril: information from the Survival and Ventricular Enlargement (SAVE) trial. *Circulation*. 1997;96:3294-9.
 101. Greenberg B, Quinones MA, Koilpillai C, Limacher M, Shindler D, Benedict C and Shelton B. Effects of long-term enalapril therapy on cardiac structure and function in patients with left ventricular dysfunction. Results of the SOLVD echocardiography substudy. *Circulation*. 1995;91:2573-81.
 102. Doughty RN, Whalley GA, Walsh HA, Gamble GD, Lopez-Sendon J, Sharpe N and Investigators CES. Effects of carvedilol on left ventricular remodeling after acute myocardial infarction: the CAPRICORN Echo Substudy. *Circulation*. 2004;109:201-6.

103. Remme WJ, Riegger G, Hildebrandt P, Komajda M, Jaarsma W, Bobbio M, Soler-Soler J, Scherhag A, Lutiger B and Ryden L. The benefits of early combination treatment of carvedilol and an ACE-inhibitor in mild heart failure and left ventricular systolic dysfunction. The carvedilol and ACE-inhibitor remodelling mild heart failure evaluation trial (CARMEN). *Cardiovasc Drugs Ther.* 2004;18:57-66.
104. Capomolla S, Febo O, Gnemmi M, Riccardi G, Opasich C, Caporotondi A, Mortara A, Pinna GD and Cobelli F. Beta-blockade therapy in chronic heart failure: diastolic function and mitral regurgitation improvement by carvedilol. *Am Heart J.* 2000;139:596-608.
105. Lowes BD, Gill EA, Abraham WT, Larrain JR, Robertson AD, Bristow MR and Gilbert EM. Effects of carvedilol on left ventricular mass, chamber geometry, and mitral regurgitation in chronic heart failure. *Am J Cardiol.* 1999;83:1201-5.
106. Seneviratne B, Moore GA and West PD. Effect of captopril on functional mitral regurgitation in dilated heart failure: a randomised double blind placebo controlled trial. *Br Heart J.* 1994;72:63-8.
107. Slutsky R, Battler A, Gerber K, Gordon D, Froelicher V, Karliner J and Ashburn W. Effect of nitrates on left ventricular size and function during exercise: comparison of sublingual nitroglycerin and nitroglycerin paste. *Am J Cardiol.* 1980;45:831-40.
108. Hecht HS, Karahalios SE, Schnugg SJ, Ormiston JA, Hopkins JM, Rose JG and Singh BN. Improvement in supine bicycle exercise performance in refractory congestive heart failure after isosorbide dinitrate: radionuclide and hemodynamic evaluation of acute effects. *Am J Cardiol.* 1982;49:133-40.
109. Keren G, Katz S, Strom J, Sonnenblick EH and LeJemtel TH. Dynamic mitral regurgitation. An important determinant of the hemodynamic response to load alterations and inotropic therapy in severe heart failure. *Circulation.* 1989;80:306-13.
110. Stevenson LW, Brunken RC, Belil D, Grover-McKay M, Schwaiger M, Schelbert HR and Tillisch JH. Afterload reduction with vasodilators and diuretics decreases mitral regurgitation during upright exercise in advanced heart failure. *J Am Coll Cardiol.* 1990;15:174-80.
111. Roth A, Shotan A and Elkayam U. A randomized comparison between the hemodynamic effects of hydralazine and nitroglycerin alone and in combination at rest and during isometric exercise in patients with chronic mitral regurgitation. *Am Heart J.* 1993;125:155-63.
112. Mullens W, Borowski AG, Curtin R, Grimm RA, Thomas JD and Tang WHW. Mechanical dyssynchrony in advanced decompensated heart failure: Relation to hemodynamic responses to intensive medical therapy. *Heart Rhythm.* 2008;5:1105-1110.
113. St John Sutton MG, Plappert T, Hilpisch KE, Abraham WT, Hayes DL and Chinchoy E. Sustained reverse left ventricular structural remodeling with cardiac resynchronization at one year is a function of etiology: quantitative Doppler echocardiographic evidence from the Multicenter InSync Randomized Clinical Evaluation (MIRACLE). *Circulation.* 2006;113:266-72.
114. Abraham WT, Fisher WG, Smith AL, Delurgio DB, Leon AR, Loh E, Kocovic DZ, Packer M, Clavell AL, Hayes DL, Ellestad M, Trupp RJ, Underwood J, Pickering F, Truex C, McAtee P, Messenger J and Evaluation MSGMIRC. Cardiac resynchronization in chronic heart failure. *N Engl J Med.* 2002;346:1845-53.
115. Cleland JG, Daubert JC, Erdmann E, Freemantle N, Gras D, Kappenberger L, Tavazzi L and Cardiac Resynchronization-Heart Failure Study I. The effect of cardiac resynchronization on morbidity and mortality in heart failure. *N Engl J Med.* 2005;352:1539-49.
116. Solis J, McCarty D, Levine RA, Handschumacher MD, Fernandez-Friera L, Chen-Tournoux A, Mont L, Vidal B, Singh JP, Brugada J, Picard MH, Sitges M and Hung J.

- Mechanism of decrease in mitral regurgitation after cardiac resynchronization therapy: optimization of the force-balance relationship. *Circ Cardiovasc Imaging*. 2009;2:444-50.
117. Mullens W, Bartunek J, Tang WH, Delrue L, Herbots L, Willems R, De Bruyne B, Goethals M, Verstreken S and Vanderheyden M. Early and late effects of cardiac resynchronization therapy on force-frequency relation and contractility regulating gene expression in heart failure patients. *Heart Rhythm*. 2008;5:52-9.
 118. Kanzaki H, Bazaz R, Schwartzman D, Dohi K, Sade LE and Gorcsan J, 3rd. A mechanism for immediate reduction in mitral regurgitation after cardiac resynchronization therapy: insights from mechanical activation strain mapping. *J Am Coll Cardiol*. 2004;44:1619-25.
 119. Ypenburg C, Lancellotti P, Tops LF, Bleeker GB, Holman ER, Pierard LA, Schalij MJ and Bax JJ. Acute effects of initiation and withdrawal of cardiac resynchronization therapy on papillary muscle dyssynchrony and mitral regurgitation. *J Am Coll Cardiol*. 2007;50:2071-7.
 120. Ypenburg C, Lancellotti P, Tops LF, Boersma E, Bleeker GB, Holman ER, Thomas JD, Schalij MJ, Pierard LA and Bax JJ. Mechanism of improvement in mitral regurgitation after cardiac resynchronization therapy. *Eur Heart J*. 2008;29:757-65.
 121. Sitges M, Vidal B, Delgado V, Mont L, Garcia-Alvarez A, Tolosana JM, Castel A, Berrueto A, Azqueta M, Pare C and Brugada J. Long-term effect of cardiac resynchronization therapy on functional mitral valve regurgitation. *Am J Cardiol*. 2009;104:383-8.
 122. Lancellotti P, Melon P, Sakalihan N, Waleffe A, Dubois C, Bertholet M and Pierard LA. Effect of cardiac resynchronization therapy on functional mitral regurgitation in heart failure. *Am J Cardiol*. 2004;94:1462-5.
 123. Bordachar P, Lafitte S, Reuter S, Serri K, Garrigue S, Laborderie J, Reant P, Jais P, Haissaguerre M, Roudaut R and Clementy J. Echocardiographic assessment during exercise of heart failure patients with cardiac resynchronization therapy. *Am J Cardiol*. 2006;97:1622-5.
 124. Marechaux S, Pincon C, Gal B, Kouakam C, Marquie C, Lacroix D, de Groote P, Mouquet F, Le Tourneau T, Dennetiere S, Guyomar Y, Solal AC, Logeart D, Asseman P, Le Jemtel TH and Ennezat PV. Functional mitral regurgitation at rest determines the acute hemodynamic response to cardiac resynchronization therapy during exercise: an acute exercise echocardiographic study. *J Am Soc Echocardiogr*. 2009;22:464-71.
 125. Parthenakis FI, Patrianakos AP, Simantirakis EN and Vardas PE. CRT and exercise capacity in heart failure: the impact of mitral valve regurgitation. *Europace*. 2008;10 Suppl 3:iii96-100.
 126. Pierard LA and Lancellotti P. When and how does cardiac resynchronization therapy reduce dynamic mitral regurgitation? *Eur Heart J*. 2007;28:2055-6.
 127. Brandt RR, Reiner C, Arnold R, Sperzel J, Pitschner HF and Hamm CW. Contractile response and mitral regurgitation after temporary interruption of long-term cardiac resynchronization therapy. *Eur Heart J*. 2006;27:187-92.
 128. van Bommel RJ, Marsan NA, Delgado V, Borleffs CJ, van Rijnsoever EP, Schalij MJ and Bax JJ. Cardiac resynchronization therapy as a therapeutic option in patients with moderate-severe functional mitral regurgitation and high operative risk. *Circulation*. 2011;124:912-9.
 129. Verhaert D, Popovic ZB, De S, Puntawangkoon C, Wolski K, Wilkoff BL, Starling RC, Tang WH, Thomas JD, Griffin BP and Grimm RA. Impact of mitral regurgitation on reverse remodeling and outcome in patients undergoing cardiac resynchronization therapy. *Circ Cardiovasc Imaging*. 2012;5:21-6.
 130. D'Andrea A, Mele D, Nistri S, Riegler L, Galderisi M, Agricola E, Losi MA, Ballo P, Mondillo S, Badano LP and Working Group Nucleus on Echocardiography of Italian Society of C.

- The prognostic impact of dynamic ventricular dyssynchrony in patients with idiopathic dilated cardiomyopathy and narrow QRS. *Eur Heart J Cardiovasc Imaging*. 2013;14:183-9.
131. Smith PK, Puskas JD, Ascheim DD, Voisine P, Gelijns AC, Moskowitz AJ, Hung JW, Parides MK, Ailawadi G, Perrault LP, Acker MA, Argenziano M, Thourani V, Gammie JS, Miller MA, Page P, Overbey JR, Bagiella E, Dagenais F, Blackstone EH, Kron IL, Goldstein DJ, Rose EA, Moquete EG, Jeffries N, Gardner TJ, O'Gara PT, Alexander JH, Michler RE and Cardiothoracic Surgical Trials Network I. Surgical treatment of moderate ischemic mitral regurgitation. *N Engl J Med*. 2014;371:2178-88.
 132. Penicka M, Linkova H, Lang O, Fojt R, Kocka V, Vanderheyden M and Bartunek J. Predictors of improvement of unrepaired moderate ischemic mitral regurgitation in patients undergoing elective isolated coronary artery bypass graft surgery. *Circulation*. 2009;120:1474-81.
 133. Fattouch K, Guccione F, Sampognaro R, Panzarella G, Corrado E, Navarra E, Calvaruso D and Ruvolo G. POINT: Efficacy of adding mitral valve restrictive annuloplasty to coronary artery bypass grafting in patients with moderate ischemic mitral valve regurgitation: a randomized trial. *J Thorac Cardiovasc Surg*. 2009;138:278-85.
 134. Chan KM, Punjabi PP, Flather M, Wage R, Symmonds K, Roussin I, Rahman-Haley S, Pennell DJ, Kilner PJ, Dreyfus GD, Pepper JR and Investigators R. Coronary artery bypass surgery with or without mitral valve annuloplasty in moderate functional ischemic mitral regurgitation: final results of the Randomized Ischemic Mitral Evaluation (RIME) trial. *Circulation*. 2012;126:2502-10.
 135. Bertrand PB, Vandervoort PM and Dion RA. Surgical treatment of moderate ischemic mitral regurgitation. *N Engl J Med*. 2015;372:1771.
 136. Grayburn PA, Carabello B, Hung J, Gillam LD, Liang D, Mack MJ, McCarthy PM, Miller DC, Trento A and Siegel RJ. Defining "severe" secondary mitral regurgitation: emphasizing an integrated approach. *J Am Coll Cardiol*. 2014;64:2792-801.
 137. Marwick TH, Zoghbi WA and Narula J. Redrawing the borders: considering guideline revision in functional mitral regurgitation. *JACC Cardiovasc Imaging*. 2014;7:333-5.
 138. Acker MA, Gelijns AC and Kron IL. Surgery for severe ischemic mitral regurgitation. *N Engl J Med*. 2014;370:1463.
 139. Bertrand PB, Verbrugge FH, Verhaert D, Smeets CJ, Grieten L, Mullens W, Gutermann H, Dion RA, Levine RA and Vandervoort PM. Mitral valve area during exercise after restrictive mitral valve annuloplasty: importance of diastolic anterior leaflet tethering. *J Am Coll Cardiol*. 2015;65:452-61.
 140. Fino C, Iacovoni A, Ferrero P, Merlo M, Bellavia D, D'Elia E, Miceli A, Senni M, Caputo M, Ferrazzi P, Galletti L and Magne J. Determinants of functional capacity after mitral valve annuloplasty or replacement for ischemic mitral regurgitation. *J Thorac Cardiovasc Surg*. 2015;149:1595-603.
 141. Pibarot P and Dumesnil JG. Prosthesis-patient mismatch: definition, clinical impact, and prevention. *Heart*. 2006;92:1022-9.
 142. Li M, Dumesnil JG, Mathieu P and Pibarot P. Impact of valve prosthesis-patient mismatch on pulmonary arterial pressure after mitral valve replacement. *J Am Coll Cardiol*. 2005;45:1034-40.
 143. Fino C, Iacovoni A, Ferrero P, Senni M, Merlo M, Cugola D, Ferrazzi P, Caputo M, Miceli A and Magne J. Restrictive mitral valve annuloplasty versus mitral valve replacement for functional ischemic mitral regurgitation: An exercise echocardiographic study. *J Thorac Cardiovasc Surg*. 2014;148:447-453 e2.
 144. Jones RH, Velazquez EJ, Michler RE, Sopko G, Oh JK, O'Connor CM, Hill JA, Menicanti L, Sadowski Z, Desvigne-Nickens P, Rouleau JL, Lee KL and Investigators SH. Coronary

- bypass surgery with or without surgical ventricular reconstruction. *N Engl J Med*. 2009;360:1705-17.
145. Mihos CG and Santana O. Is an adjunctive subvalvular repair during mitral annuloplasty for secondary mitral regurgitation effective in preventing recurrent regurgitation? *Interact Cardiovasc Thorac Surg*. 2015, 10.1093/icvts/ivv328.
 146. Kincaid EH, Riley RD, Hines MH, Hammon JW and Kon ND. Anterior leaflet augmentation for ischemic mitral regurgitation. *Ann Thorac Surg*. 2004;78:564-8; discussion 568.
 147. Borger MA, Murphy PM, Alam A, Fazel S, Maganti M, Armstrong S, Rao V and David TE. Initial results of the chordal-cutting operation for ischemic mitral regurgitation. *J Thorac Cardiovasc Surg*. 2007;133:1483-92.
 148. Szymanski C, Bel A, Cohen I, Touchot B, Handschumacher MD, Desnos M, Carpentier A, Menasche P, Hagege AA, Levine RA, Messas E and Leducq Foundation MTN. Comprehensive annular and subvalvular repair of chronic ischemic mitral regurgitation improves long-term results with the least ventricular remodeling. *Circulation*. 2012;126:2720-7.
 149. Langer F, Kunihara T, Hell K, Schramm R, Schmidt KI, Aicher D, Kindermann M and Schafers HJ. RING+STRING: Successful repair technique for ischemic mitral regurgitation with severe leaflet tethering. *Circulation*. 2009;120:S85-91.
 150. Feldman T, Foster E, Glower DD, Kar S, Rinaldi MJ, Fail PS, Smalling RW, Siegel R, Rose GA, Engeron E, Loghini C, Trento A, Skipper ER, Fudge T, Letsou GV, Massaro JM, Mauri L and Investigators EI. Percutaneous repair or surgery for mitral regurgitation. *N Engl J Med*. 2011;364:1395-406.
 151. Maisano F, Franzen O, Baldus S, Schafer U, Hausleiter J, Butter C, Ussia GP, Sievert H, Richardt G, Widder JD, Moccetti T and Schillinger W. Percutaneous mitral valve interventions in the real world: early and 1-year results from the ACCESS-EU, a prospective, multicenter, nonrandomized post-approval study of the MitraClip therapy in Europe. *J Am Coll Cardiol*. 2013;62:1052-61.
 152. Al Amri I, Debonnaire P, Witkowski T, van der Kley F, Palmen M, de Weger A, Klautz RJ, Bax JJ, Schalij MJ, Ajmone Marsan N and Delgado V. Mitral valve geometry and hemodynamics after surgical mitral valve annuloplasty and implications for percutaneous treatment of patients with recurrent mitral regurgitation. *Am J Cardiol*. 2013;112:714-9.
 153. Schmidt FP, von Bardeleben RS, Nikolai P, Jabs A, Wunderlich N, Munzel T, Hink U and Warnholtz A. Immediate effect of the MitraClip procedure on mitral ring geometry in primary and secondary mitral regurgitation. *Eur Heart J Cardiovasc Imaging*. 2013;14:851-7.
 154. Grayburn PA, Foster E, Sangli C, Weissman NJ, Massaro J, Glower DG, Feldman T and Mauri L. Relationship between the magnitude of reduction in mitral regurgitation severity and left ventricular and left atrial reverse remodeling after MitraClip therapy. *Circulation*. 2013;128:1667-74.
 155. Auricchio A, Schillinger W, Meyer S, Maisano F, Hoffmann R, Ussia GP, Pedrazzini GB, van der Heyden J, Fratini S, Klersy C, Komtebedde J, Franzen O and Investigators P-C. Correction of mitral regurgitation in nonresponders to cardiac resynchronization therapy by MitraClip improves symptoms and promotes reverse remodeling. *J Am Coll Cardiol*. 2011;58:2183-9.
 156. Herrmann HC, Rohatgi S, Wasserman HS, Block P, Gray W, Hamilton A, Zunamon A, Homma S, Di Tullio MR, Kraybill K, Merlino J, Martin R, Rodriguez L, Stewart WJ, Whitlow P, Wieggers SE, Silvestry FE, Foster E and Feldman T. Mitral valve hemodynamic effects of percutaneous edge-to-edge repair with the MitraClip device for mitral regurgitation. *Catheter Cardiovasc Interv*. 2006;68:821-8.

157. Boerlage-van Dijk K, van Riel AC, de Bruin-Bon RH, Wiegerinck EM, Koch KT, Vis MM, Meregalli PG, Bindraban NR, Mulder BJ, Piek JJ, Bouma BJ and Baan J, Jr. Mitral inflow patterns after MitraClip implantation at rest and during exercise. *J Am Soc Echocardiogr.* 2014;27:24-31 e1.
158. Herrmann HC and Maisano F. Transcatheter therapy of mitral regurgitation. *Circulation.* 2014;130:1712-22.
159. Rim Y, Laing ST, Kee P, McPherson DD and Kim H. Evaluation of mitral valve dynamics. *JACC Cardiovasc Imaging.* 2013;6:263-8.
160. Braun J, van de Veire NR, Klautz RJ, Versteegh MI, Holman ER, Westenberg JJ, Boersma E, van der Wall EE, Bax JJ and Dion RA. Restrictive mitral annuloplasty cures ischemic mitral regurgitation and heart failure. *Ann Thorac Surg.* 2008;85:430-6; discussion 436-7.
161. Rubino AS, Onorati F, Santarpia G, Achille F, Lorusso R, Santini F and Renzulli A. Impact of increased transmitral gradients after undersized annuloplasty for chronic ischemic mitral regurgitation. *Int J Cardiol.* 2012;158:71-7.
162. Martin CE, Castano M, Gomez-Plana J, Gualis J, Comendador JM and Iglesias I. Mitral stenosis after IMR ETlogix ring annuloplasty for ischemic regurgitation. *Asian Cardiovasc Thorac Ann.* 2012;20:534-8.
163. Pepi M, Tamborini G, Galli C, Barbier P, Doria E, Berti M, Guazzi M and Fiorentini C. A new formula for echo-Doppler estimation of right ventricular systolic pressure. *J Am Soc Echocardiogr.* 1994;7:20-6.
164. Nishimura RA, Otto CM, Bonow RO, Carabello BA, Erwin JP, 3rd, Guyton RA, O'Gara PT, Ruiz CE, Skubas NJ, Sorajja P, Sundt TM, 3rd and Thomas JD. 2014 AHA/ACC Guideline for the Management of Patients With Valvular Heart Disease: A Report of the American College of Cardiology/American Heart Association Task Force on Practice Guidelines. *J Am Coll Cardiol.* 2014, 10.1016/j.jacc.2014.02.536.
165. De Bonis M, Ferrara D, Taramasso M, Calabrese MC, Verzini A, Buzzatti N and Alfieri O. Mitral replacement or repair for functional mitral regurgitation in dilated and ischemic cardiomyopathy: is it really the same? *Ann Thorac Surg.* 2012;94:44-51.
166. Magne J, Girerd N, Senechal M, Mathieu P, Dagenais F, Dumesnil JG, Charbonneau E, Voisine P and Pibarot P. Mitral repair versus replacement for ischemic mitral regurgitation: comparison of short-term and long-term survival. *Circulation.* 2009;120:S104-11.
167. Kouris N, Ikonomidis I, Kontogianni D, Smith P and Nihoyannopoulos P. Mitral valve repair versus replacement for isolated non-ischemic mitral regurgitation in patients with preoperative left ventricular dysfunction. A long-term follow-up echocardiography study. *Eur J Echocardiogr.* 2005;6:435-42.
168. Bertrand PB, Gutermann H, Smeets CJ, Van Kerrebroeck C, Verhaert D, Vandervoort P and Dion R. Functional impact of transmitral gradients at rest and during exercise after restrictive annuloplasty for ischemic mitral regurgitation. *J Thorac Cardiovasc Surg.* 2014;148:183-7.
169. Grimaldi A, De Bonis M, Pappalardo F, Taramasso M, Verzini A, Calabrese MC, Maisano F and Alfieri O. Undersized annuloplasty for functional mitral regurgitation: is it responsible for clinically relevant mitral stenosis during exercise? *J Heart Valve Dis.* 2012;21:446-53.
170. Lang RM, Bierig M, Devereux RB, Flachskampf FA, Foster E, Pellikka PA, Picard MH, Roman MJ, Seward J, Shanewise JS, Solomon SD, Spencer KT, Sutton MS, Stewart WJ, Chamber Quantification Writing G, American Society of Echocardiography's G, Standards C and European Association of E. Recommendations for chamber quantification: a report from the American Society of Echocardiography's Guidelines and Standards Committee and the Chamber Quantification Writing Group, developed

- in conjunction with the European Association of Echocardiography, a branch of the European Society of Cardiology. *J Am Soc Echocardiogr*. 2005;18:1440-63.
171. Karp K, Teien D and Eriksson P. Doppler echocardiographic assessment of the valve area in patients with atrioventricular valve stenosis by application of the continuity equation. *J Intern Med*. 1989;225:261-6.
 172. Gorlin R and Gorlin SG. Hydraulic formula for calculation of the area of the stenotic mitral valve, other cardiac valves, and central circulatory shunts. I. *Am Heart J*. 1951;41:1-29.
 173. Flachskampf FA, Weyman AE, Guerrero JL and Thomas JD. Influence of orifice geometry and flow rate on effective valve area: an in vitro study. *J Am Coll Cardiol*. 1990;15:1173-80.
 174. Gilon D, Cape EG, Handschumacher MD, Jiang L, Sears C, Solheim J, Morris E, Strobel JT, Miller-Jones SM, Weyman AE and Levine RA. Insights from three-dimensional echocardiographic laser stereolithography. Effect of leaflet funnel geometry on the coefficient of orifice contraction, pressure loss, and the Gorlin formula in mitral stenosis. *Circulation*. 1996;94:452-9.
 175. Magne J, Mathieu P, Dumesnil JG, Tanne D, Dagenais F, Doyle D and Pibarot P. Impact of prosthesis-patient mismatch on survival after mitral valve replacement. *Circulation*. 2007;115:1417-25.
 176. Braverman AC, Thomas JD and Lee RT. Doppler echocardiographic estimation of mitral valve area during changing hemodynamic conditions. *Am J Cardiol*. 1991;68:1485-90.
 177. Voelker W, Berner A, Regele B, Schmid M, Dittmann H, Stotzer T, Haase KK, Baumbach A and Karsch KR. Effect of exercise on valvular resistance in patients with mitral stenosis. *J Am Coll Cardiol*. 1993;22:777-82.
 178. Leavitt JI, Coats MH and Falk RH. Effects of exercise on transmitral gradient and pulmonary artery pressure in patients with mitral stenosis or a prosthetic mitral valve: a Doppler echocardiographic study. *J Am Coll Cardiol*. 1991;17:1520-6.
 179. Zhu F, Otsuji Y, Yotsumoto G, Yuasa T, Ueno T, Yu B, Koriyama C, Hamasaki S, Biro S, Kisanuki A, Minagoe S, Levine RA, Sakata R and Tei C. Mechanism of persistent ischemic mitral regurgitation after annuloplasty: importance of augmented posterior mitral leaflet tethering. *Circulation*. 2005;112:I396-401.
 180. Nishimura RA, Otto CM, Bonow RO, Carabello BA, Erwin JP, 3rd, Guyton RA, O'Gara PT, Ruiz CE, Skubas NJ, Sorajja P, Sundt TM, 3rd and Thomas JD. 2014 AHA/ACC Guideline for the Management of Patients With Valvular Heart Disease: A Report of the American College of Cardiology/American Heart Association Task Force on Practice Guidelines. *Circulation*. 2014, 10.1161/CIR.0000000000000031.
 181. Pibarot P and Dumesnil JG. Prosthetic heart valves: selection of the optimal prosthesis and long-term management. *Circulation*. 2009;119:1034-48.
 182. Blauwet LA, Malouf JF, Connolly HM, Hodge DO, Herges RM, Suri RM and Miller FA, Jr. Comprehensive hemodynamic assessment of 368 normal St. Jude Medical mechanical mitral valve prostheses based on early postimplantation echocardiographic studies. *J Am Soc Echocardiogr*. 2013;26:381-9.
 183. Rosenhek R, Binder T, Maurer G and Baumgartner H. Normal values for Doppler echocardiographic assessment of heart valve prostheses. *J Am Soc Echocardiogr*. 2003;16:1116-27.
 184. Bech-Hanssen O, Caidahl K, Wallentin I, Ask P and Wranne B. Assessment of effective orifice area of prosthetic aortic valves with Doppler echocardiography: an in vivo and in vitro study. *J Thorac Cardiovasc Surg*. 2001;122:287-95.
 185. Verdonck PR, Van Nooten GJ and Van Belleghem Y. Pulse duplicator hydrodynamics of four different bileaflet valves in the mitral position. *Cardiovasc Surg*. 1997;5:593-603.

186. Baumgartner H, Khan SS, DeRobertis M, Czer LS and Maurer G. Doppler assessment of prosthetic valve orifice area. An in vitro study. *Circulation*. 1992;85:2275-83.
187. Silberman S, Shaheen J, Merin O, Fink D, Shapira N, Liviatan-Strauss N and Bitran D. Exercise hemodynamics of aortic prostheses: comparison between stentless bioprostheses and mechanical valves. *Ann Thorac Surg*. 2001;72:1217-21.
188. Izzat MB, Birdi I, Wilde P, Bryan AJ and Angelini GD. Comparison of hemodynamic performances of St. Jude Medical and CarboMedics 21 mm aortic prostheses by means of dobutamine stress echocardiography. *J Thorac Cardiovasc Surg*. 1996;111:408-15.
189. Hobson NA, Wilkinson GA, Cooper GJ, Wheeldon NM and Lynch J. Hemodynamic assessment of mitral mechanical prostheses under high flow conditions: comparison between dynamic exercise and dobutamine stress. *J Heart Valve Dis*. 2006;15:87-91.
190. Thormann J, Gottwik M, Schleppe M and Hehrlein F. Hemodynamics alterations induced by isoproterenol and pacing after aortic valve replacement with the Bjork-Shiley or St. Jude medical prosthesis. *Circulation*. 1981;63:895-904.
191. Vandervoort PM, Greenberg NL, Powell KA, Cosgrove DM and Thomas JD. Pressure recovery in bileaflet heart valve prostheses. Localized high velocities and gradients in central and side orifices with implications for Doppler-catheter gradient relation in aortic and mitral position. *Circulation*. 1995;92:3464-72.
192. Baumgartner H, Schima H, Tulzer G and Kuhn P. Effect of stenosis geometry on the Doppler-catheter gradient relation in vitro: a manifestation of pressure recovery. *J Am Coll Cardiol*. 1993;21:1018-25.
193. Garcia D, Pibarot P, Landry C, Allard A, Chayer B, Dumesnil JG and Durand LG. Estimation of aortic valve effective orifice area by Doppler echocardiography: effects of valve inflow shape and flow rate. *J Am Soc Echocardiogr*. 2004;17:756-65.
194. Bitar JN, Lechin ME, Salazar G and Zoghbi WA. Doppler echocardiographic assessment with the continuity equation of St. Jude Medical mechanical prostheses in the mitral valve position. *Am J Cardiol*. 1995;76:287-93.
195. Eriksson MJ, Rosfors S, Radegran K and Brodin LA. Effects of exercise on Doppler-derived pressure difference, valve resistance, and effective orifice area in different aortic valve prostheses of similar size. *Am J Cardiol*. 1999;83:619-22, A10.
196. Minardi G, Manzara C, Creazzo V, Maselli D, Casali G, Pulignano G and Musumeci F. Evaluation of 17-mm St. Jude Medical Regent prosthetic aortic heart valves by rest and dobutamine stress echocardiography. *J Cardiothorac Surg*. 2006;1:27.
197. Chambers J, Deverall P, Jackson G and Sowton E. The Hatle orifice area formula tested in normal bileaflet mechanical mitral prostheses. *Int J Cardiol*. 1992;35:397-404.
198. Pibarot P and Dumesnil JG. Doppler echocardiographic evaluation of prosthetic valve function. *Heart*. 2012;98:69-78.
199. Shigenobu M and Sano S. Evaluation of St. Jude Medical mitral valve function by exercise Doppler echocardiography. *J Card Surg*. 1995;10:161-8.
200. Pibarot P, Dumesnil JG, Jobin J, Lemieux M, Honos G and Durand LG. Usefulness of the indexed effective orifice area at rest in predicting an increase in gradient during maximum exercise in patients with a bioprosthesis in the aortic valve position. *Am J Cardiol*. 1999;83:542-6.
201. Nickenig G, Estevez-Loureiro R, Franzen O, Tamburino C, Vanderheyden M, Luscher TF, Moat N, Price S, Dall'Ara G, Winter R, Corti R, Grasso C, Snow TM, Jeger R, Blankenberg S, Settergren M, Tiroch K, Balzer J, Petronio AS, Buttner HJ, Etti F, Sievert H, Fiorino MG, Claeys M, Ussia GP, Baumgartner H, Scandura S, Alamgir F, Keshavarzi F, Colombo A, Maisano F, Ebelt H, Aruta P, Lubos E, Plicht B, Schueler R, Pighi M, Di Mario C and Transcatheter Valve Treatment Sentinel Registry Investigators of the ERPotESoC. Percutaneous mitral valve edge-to-edge repair: in-hospital results

- and 1-year follow-up of 628 patients of the 2011-2012 Pilot European Sentinel Registry. *J Am Coll Cardiol*. 2014;64:875-84.
202. Siegel RJ, Biner S, Rafique AM, Rinaldi M, Lim S, Fail P, Hermiller J, Smalling R, Whitlow PL, Herrmann HC, Foster E, Feldman T, Glower D, Kar S and Investigators E. The acute hemodynamic effects of MitraClip therapy. *J Am Coll Cardiol*. 2011;57:1658-65.
 203. Herrmann HC, Kar S, Siegel R, Fail P, Loghini C, Lim S, Hahn R, Rogers JH, Bommer WJ, Wang A, Berke A, Lerakis S, Kramer P, Wong SC, Foster E, Glower D, Feldman T and Investigators E. Effect of percutaneous mitral repair with the MitraClip device on mitral valve area and gradient. *EuroIntervention*. 2009;4:437-42.
 204. D'Ascenzo F, Moretti C, Marra WG, Montefusco A, Omede P, Taha S, Castagno D, Gaemperli O, Taramasso M, Frea S, Pidello S, Rudolph V, Franzen O, Braun D, Giannini C, Ince H, Perl L, Zoccai G, Marra S, D'Amico M, Maisano F, Rinaldi M and Gaita F. Meta-analysis of the usefulness of Mitraclip in patients with functional mitral regurgitation. *Am J Cardiol*. 2015;116:325-31.
 205. Lancellotti P, Tribouilloy C, Hagendorff A, Popescu BA, Edvardsen T, Pierard LA, Badano L, Zamorano JL and Scientific Document Committee of the European Association of Cardiovascular I. Recommendations for the echocardiographic assessment of native valvular regurgitation: an executive summary from the European Association of Cardiovascular Imaging. *Eur Heart J Cardiovasc Imaging*. 2013;14:611-44.
 206. Vandendriessche T, Kotrc M, Tijskens M, Bartunek J, Delesie M, Paelinck BP, De Bock D, Penicka M, Stockman B, De Maeyer C, Vrints C, Vanderheyden M and Claeys MJ. Percutaneous mitral valve repair in high-risk patients: initial experience with the Mitraclip system in Belgium. *Acta Cardiol*. 2014;69:265-70.
 207. Lang RM, Badano LP, Mor-Avi V, Afilalo J, Armstrong A, Ernande L, Flachskampf FA, Foster E, Goldstein SA, Kuznetsova T, Lancellotti P, Muraru D, Picard MH, Rietzschel ER, Rudski L, Spencer KT, Tsang W and Voigt JU. Recommendations for cardiac chamber quantification by echocardiography in adults: an update from the American Society of Echocardiography and the European Association of Cardiovascular Imaging. *J Am Soc Echocardiogr*. 2015;28:1-39 e14.
 208. Zamorano JL, Badano LP, Bruce C, Chan KL, Goncalves A, Hahn RT, Keane MG, La Canna G, Monaghan MJ, Nihoyannopoulos P, Silvestry FE, Vanoverschelde JL and Gillam LD. EAE/ASE recommendations for the use of echocardiography in new transcatheter interventions for valvular heart disease. *J Am Soc Echocardiogr*. 2011;24:937-65.
 209. Helmcke F, Nanda NC, Hsiung MC, Soto B, Adey CK, Goyal RG and Gatewood RP, Jr. Color Doppler assessment of mitral regurgitation with orthogonal planes. *Circulation*. 1987;75:175-83.
 210. Baumgartner H, Hung J, Bermejo J, Chambers JB, Evangelista A, Griffin BP, Iung B, Otto CM, Pellikka PA, Quinones M, American Society of E and European Association of E. Echocardiographic assessment of valve stenosis: EAE/ASE recommendations for clinical practice. *J Am Soc Echocardiogr*. 2009;22:1-23; quiz 101-2.
 211. Rudski LG, Lai WW, Afilalo J, Hua L, Handschumacher MD, Chandrasekaran K, Solomon SD, Louie EK and Schiller NB. Guidelines for the echocardiographic assessment of the right heart in adults: a report from the American Society of Echocardiography endorsed by the European Association of Echocardiography, a registered branch of the European Society of Cardiology, and the Canadian Society of Echocardiography. *J Am Soc Echocardiogr*. 2010;23:685-713; quiz 786-8.
 212. Puls M, Lubos E, Boekstegers P, von Bardeleben RS, Ouarrak T, Butter C, Zuern CS, Bekeredjian R, Sievert H, Nickenig G, Eggebrecht H, Seneges J and Schillinger W. One-year outcomes and predictors of mortality after MitraClip therapy in contemporary

- clinical practice: results from the German transcatheter mitral valve interventions registry. *Eur Heart J*. 2016;37:703-12.
213. Giannini C, Petronio AS, De Carlo M, Guarracino F, Conte L, Fiorelli F, Pieroni A and Di Bello V. Integrated reverse left and right ventricular remodelling after MitraClip implantation in functional mitral regurgitation: an echocardiographic study. *Eur Heart J Cardiovasc Imaging*. 2014;15:95-103.
 214. Lewis GD, Bossone E, Naeije R, Grunig E, Saggari R, Lancellotti P, Ghio S, Varga J, Rajagopalan S, Oudiz R and Rubenfire M. Pulmonary vascular hemodynamic response to exercise in cardiopulmonary diseases. *Circulation*. 2013;128:1470-9.
 215. van Riel AC, Boerlage-van Dijk K, de Bruin-Bon RH, Araki M, Koch KT, Vis MM, Meregalli PG, van den Brink RB, Piek JJ, Mulder BJ, Baan J, Jr. and Bouma BJ. Percutaneous mitral valve repair preserves right ventricular function. *J Am Soc Echocardiogr*. 2014;27:1098-106.
 216. Surder D, Pedrazzini G, Gaemperli O, Biaggi P, Felix C, Rufibach K, der Maur CA, Jeger R, Buser P, Kaufmann BA, Moccetti M, Hurlimann D, Buhler I, Bettex D, Scherman J, Pasotti E, Faletra FF, Zuber M, Moccetti T, Luscher TF, Erne P, Grunenfelder J and Corti R. Predictors for efficacy of percutaneous mitral valve repair using the MitraClip system: the results of the MitraSwiss registry. *Heart*. 2013;99:1034-40.
 217. Foster E, Wasserman HS, Gray W, Homma S, Di Tullio MR, Rodriguez L, Stewart WJ, Whitlow P, Block P, Martin R, Merlino J, Herrmann HC, Wiegers SE, Silvestry FE, Hamilton A, Zunamon A, Kraybill K, Gerber IL, Weeks SG, Zhang Y and Feldman T. Quantitative assessment of severity of mitral regurgitation by serial echocardiography in a multicenter clinical trial of percutaneous mitral valve repair. *Am J Cardiol*. 2007;100:1577-83.
 218. Hamilton-Craig C, Strugnelli W, Gaikwad N, Ischenko M, Speranza V, Chan J, Neill J, Platts D, Scalia GM, Burstow DJ and Walters DL. Quantitation of mitral regurgitation after percutaneous MitraClip repair: comparison of Doppler echocardiography and cardiac magnetic resonance imaging. *Ann Cardiothorac Surg*. 2015;4:341-51.
 219. Raphael C, Briscoe C, Davies J, Ian Whinnett Z, Manisty C, Sutton R, Mayet J and Francis DP. Limitations of the New York Heart Association functional classification system and self-reported walking distances in chronic heart failure. *Heart*. 2007;93:476-82.
 220. Kron IL, Perrault LP and Acker MA. We need a better way to repair ischemic mitral regurgitation. *J Thorac Cardiovasc Surg*. 2015;150:428.
 221. Votta E, Le TB, Stevanella M, Fusini L, Caiani EG, Redaelli A and Sotiropoulos F. Toward patient-specific simulations of cardiac valves: state-of-the-art and future directions. *J Biomech*. 2013;46:217-28.
 222. May-Newman K and Yin FC. A constitutive law for mitral valve tissue. *J Biomech Eng*. 1998;120:38-47.
 223. Kunzelman KS and Cochran RP. Mechanical properties of basal and marginal mitral valve chordae tendineae. *ASAIO Trans*. 1990;36:M405-8.
 224. Kunzelman KS, Cochran RP, Chuong C, Ring WS, Verrier ED and Eberhart RD. Finite element analysis of the mitral valve. *J Heart Valve Dis*. 1993;2:326-40.
 225. Prot V, Skallerud B and Holzapfel GA. Transversely isotropic membrane shells with application to mitral valve mechanics. Constitutive modelling and finite element implementation. *International Journal for Numerical Methods in Engineering*. 2007;71:987-1008.
 226. Lim KH, Yeo JH and Duran CM. Three-dimensional asymmetrical modeling of the mitral valve: a finite element study with dynamic boundaries. *J Heart Valve Dis*. 2005;14:386-92.

227. Prot V, Haaverstad R and Skallerud B. Finite element analysis of the mitral apparatus: annulus shape effect and chordal force distribution. *Biomech Model Mechanobiol.* 2009;8:43-55.
228. Heyde B, Cygan S, Choi HF, Lesniak-Plewinska B, Barbosa D, Elen A, Claus P, Loeckx D, Kaluzynski K and D'Hooge J. Regional cardiac motion and strain estimation in three-dimensional echocardiography: a validation study in thick-walled univentricular phantoms. *IEEE Trans Ultrason Ferroelectr Freq Control.* 2012;59:668-82.
229. Kunzelman KS, Reimink MS and Cochran RP. Annular dilatation increases stress in the mitral valve and delays coaptation: a finite element computer model. *Cardiovasc Surg.* 1997;5:427-34.
230. Zuo K. Characterization of Biomechanical Properties of Mitral Valve Chordae Tendineae. *Master's Thesis.* 2014; Paper 568. http://digitalcommons.uconn.edu/gs_theses/568
231. Grande-Allen KJ, Barber JE, Klatka KM, Houghtaling PL, Vesely I, Moravec CS and McCarthy PM. Mitral valve stiffening in end-stage heart failure: evidence of an organic contribution to functional mitral regurgitation. *J Thorac Cardiovasc Surg.* 2005;130:783-90.
232. Saito K, Okura H, Watanabe N, Obase K, Tamada T, Koyama T, Hayashida A, Neishi Y, Kawamoto T and Yoshida K. Influence of chronic tethering of the mitral valve on mitral leaflet size and coaptation in functional mitral regurgitation. *JACC Cardiovasc Imaging.* 2012;5:337-45.
233. Mansi T, Voigt I, Georgescu B, Zheng X, Mengue EA, Hackl M, Ionasec RI, Noack T, Seeburger J and Comaniciu D. An integrated framework for finite-element modeling of mitral valve biomechanics from medical images: application to MitralClip intervention planning. *Med Image Anal.* 2012;16:1330-46.
234. Burlina P, Sprouse C, Mukherjee R, DeMenthon D and Abraham T. Patient-specific mitral valve closure prediction using 3D echocardiography. *Ultrasound Med Biol.* 2013;39:769-83.
235. Wang Q and Sun W. Finite element modeling of mitral valve dynamic deformation using patient-specific multi-slices computed tomography scans. *Ann Biomed Eng.* 2013;41:142-53.
236. Prot V, Skallerud B, Sommer G and Holzapfel GA. On modelling and analysis of healthy and pathological human mitral valves: two case studies. *J Mech Behav Biomed Mater.* 2010;3:167-77.
237. Votta E, Caiani E, Veronesi F, Soncini M, Montevecchi FM and Redaelli A. Mitral valve finite-element modelling from ultrasound data: a pilot study for a new approach to understand mitral function and clinical scenarios. *Philos Transact A Math Phys Eng Sci.* 2008;366:3411-34.
238. Prot V and Skallerud B. Nonlinear solid finite element analysis of mitral valves with heterogeneous leaflet layers. *Computational Mechanics.* 2008;43:353-368.
239. Krishnamurthy G, Itoh A, Swanson JC, Bothe W, Karlsson M, Kuhl E, Craig Miller D and Ingels NB, Jr. Regional stiffening of the mitral valve anterior leaflet in the beating ovine heart. *J Biomech.* 2009;42:2697-701.
240. Grande-Allen KJ, Borowski AG, Troughton RW, Houghtaling PL, Dipaola NR, Moravec CS, Vesely I and Griffin BP. Apparently normal mitral valves in patients with heart failure demonstrate biochemical and structural derangements: an extracellular matrix and echocardiographic study. *J Am Coll Cardiol.* 2005;45:54-61.
241. Goldstein D, Moskowitz AJ, Gelijns AC, Ailawadi G, Parides MK, Perrault LP, Hung JW, Voisine P, Dagenais F, Gillinov AM, Thourani V, Argenziano M, Gammie JS, Mack M, Demers P, Atluri P, Rose EA, O'Sullivan K, Williams DL, Bagiella E, Michler RE, Weisel RD, Miller MA, Geller NL, Taddei-Peters WC, Smith PK, Moquete E, Overbey JR, Kron

- IL, O'Gara PT, Acker MA and Ctsn. Two-Year Outcomes of Surgical Treatment of Severe Ischemic Mitral Regurgitation. *N Engl J Med*. 2016;374:344-53.
242. de Jaegere P, De Santis G, Rodriguez-Olivares R, Bosmans J, Bruining N, Dezutter T, Rahhab Z, El Faquir N, Collas V, Bosmans B, Verhegghe B, Ren C, Geleirse M, Schultz C, van Mieghem N, De Beule M and Mortier P. Patient-Specific Computer Modeling to Predict Aortic Regurgitation After Transcatheter Aortic Valve Replacement. *JACC Cardiovasc Interv*. 2016;9:508-12.
243. Schultz C, Rodriguez-Olivares R, Bosmans J, Lefevre T, De Santis G, Bruining N, Collas V, Dezutter T, Bosmans B, Rahhab Z, El Faquir N, Watanabe Y, Segers P, Verhegghe B, Chevalier B, van Mieghem N, De Beule M, Mortier P and de Jaegere P. Patient-specific image-based computer simulation for the prediction of valve morphology and calcium displacement after TAVI with the Medtronic CoreValve and the Edwards SAPIEN valve. *EuroIntervention*. 2016;11:1044-52.
244. Otto CM and Prendergast B. Aortic-valve stenosis--from patients at risk to severe valve obstruction. *N Engl J Med*. 2014;371:744-56.
245. Makkar RR, Fontana GP, Jilaihawi H, Kapadia S, Pichard AD, Douglas PS, Thourani VH, Babaliaros VC, Webb JG, Herrmann HC, Bavaria JE, Kodali S, Brown DL, Bowers B, Dewey TM, Svensson LG, Tuzcu M, Moses JW, Williams MR, Siegel RJ, Akin JJ, Anderson WN, Pocock S, Smith CR, Leon MB and Investigators PT. Transcatheter aortic-valve replacement for inoperable severe aortic stenosis. *N Engl J Med*. 2012;366:1696-704.
246. Osnabrugge RL, Mylotte D, Head SJ, Van Mieghem NM, Nkomo VT, LeReun CM, Bogers AJ, Piazza N and Kappetein AP. Aortic stenosis in the elderly: disease prevalence and number of candidates for transcatheter aortic valve replacement: a meta-analysis and modeling study. *J Am Coll Cardiol*. 2013;62:1002-12.
247. Minners J, Allgeier M, Gohlke-Baerwolf C, Kienzle RP, Neumann FJ and Jander N. Inconsistencies of echocardiographic criteria for the grading of aortic valve stenosis. *Eur Heart J*. 2008;29:1043-8.
248. Minners J, Allgeier M, Gohlke-Baerwolf C, Kienzle RP, Neumann FJ and Jander N. Inconsistent grading of aortic valve stenosis by current guidelines: haemodynamic studies in patients with apparently normal left ventricular function. *Heart*. 2010;96:1463-8.
249. Michelena HI, Margaryan E, Miller FA, Eleid M, Maalouf J, Suri R, Messika-Zeitoun D, Pellikka PA and Enriquez-Sarano M. Inconsistent echocardiographic grading of aortic stenosis: is the left ventricular outflow tract important? *Heart*. 2013;99:921-31.
250. Dumesnil JG and Yoganathan AP. Theoretical and practical differences between the Gorlin formula and the continuity equation for calculating aortic and mitral valve areas. *Am J Cardiol*. 1991;67:1268-72.
251. Fischer JL, Haberer T, Dickson D and Henselmann L. Comparison of Doppler echocardiographic methods with heart catheterisation in assessing aortic valve area in 100 patients with aortic stenosis. *Br Heart J*. 1995;73:293-8.
252. Gilon D, Cape EG, Handschumacher MD, Song JK, Solheim J, VanAuker M, King ME and Levine RA. Effect of three-dimensional valve shape on the hemodynamics of aortic stenosis: three-dimensional echocardiographic stereolithography and patient studies. *J Am Coll Cardiol*. 2002;40:1479-86.
253. Clark C. The fluid mechanics of aortic stenosis--I. Theory and steady flow experiments. *J Biomech*. 1976;9:521-8.
254. Clavel MA, Dumesnil JG, Capoulade R, Mathieu P, Senechal M and Pibarot P. Outcome of patients with aortic stenosis, small valve area, and low-flow, low-gradient despite preserved left ventricular ejection fraction. *J Am Coll Cardiol*. 2012;60:1259-67.

255. Pibarot P and Dumesnil JG. Low-flow, low-gradient aortic stenosis with normal and depressed left ventricular ejection fraction. *J Am Coll Cardiol.* 2012;60:1845-53.
256. Garcia D, Dumesnil JG, Durand L-G, Kadem L and Pibarot P. Discrepancies between catheter and Doppler estimates of valve effective orifice area can be predicted from the pressure recovery phenomenon. *Journal of the American College of Cardiology.* 2003;41:435-442.
257. De Veene H, Bertrand PB, Popovic N, Vandervoort PM, Claus P, De Beule M and Heyde B. Automatic mitral annulus tracking in volumetric ultrasound using non-rigid image registration. *Conf Proc IEEE Eng Med Biol Soc.* 2015;2015:1985-8.